Dear Ugo Nanni and Slawek Tulaczyk,

We appreciate your constructive comments to our manuscript tc-2020-94 entitled "Monitoring the seasonal changes of an englacial conduit network using repeated ground penetrating radar measurements". On the following pages we have provided a point-by-point response to your comments.

If you have any further questions, we would happily answer them, and we look forward to hearing back from you regarding your decision.

Best regards,
Gregory Church and the co-authors.

List of substantial changes/comments:

Introduction: the introduction has been reworked such that there is now a clear focus on what is missing from previous GPR studies and why this GPR study is unique. We have used a previously proposed reflectivity extraction methodology but with application to a glacioradar dataset in order to investigate the seasonal englacial conduit changes.

Methodology: In order to provide a manuscript that flows, we feel that the numerical modelling needs to be placed after the results section. Therefore, we have altered the names of the sections. The methods section has been relabelled as 'Field Data and Processing' this includes all relevant information regarding the field acquisition and processing. We have moved parts from the results section that were related to the GPR processing to the Field Data and Processing part.

We feel that the numerical modelling section still needs to remain after the results section, because we can only justify the use of the numerical modelling knowing the fact that we have a thin englacial conduit. The thin water layer conduit GPR forward modelling is now in a separate section after the results and before the discussion. The numerical modelling has been split into two parts: Methodology and Results.

Uncertainties: A lack of uncertainties in both the reflectivity and the conduit geometry was brought to our attention from both reviewers. Significant effort has been made addressing this and the manuscript has been updated accordingly. A separate section in the discussion has been added for the uncertainties in the EM wave-propagation velocities (CMP Analysis), Channel Reflectivity, Channel Thickness and Channel Spatial Extent (Horizontal Resolution).

Conduit Geometry:

1. Lateral resolution/Channel Spatial Extent: The horizontal resolution is defined as the first Fresnel zone prior to migration however, post-migration the horizontal resolution is collapsed to the bin size. The GPR data have been 2D migrated and therefore along the profile the resolution is the bin size of the migration (0.5 m). Across the profile the horizontal resolution is the first Fresnel zone, this is 17 m for a 90 m deep reflector @ 0.1689 m/ns with a 25 MHz antenna. This is within the vicinity of the conduit width. In order to offset having a large across-profile Fresnel zone the acquisition grid was set-up such that perpendicular GPR profiles were acquired. Therefore, within the cross profiles we have a horizontal resolution of 0.5 m. An issue of the lateral resolution comes from the interpolation of the reflectivity, and therefore we estimate this to be around 6 m (half profile spacing) due to the spacing of profiles ~12m. We have added a section in the discussion regarding the horizontal resolution. A true 3D data acquisition and migration would reduce the Fresnel zone to the bin size which is beyond the scope of this manuscript.

2. Conduit Thickness: We have addressed the uncertainty based upon three different potential errors:

    1. Picking error

2. Incorrect EM-propagation velocity
3. Error obtained from the numerical modelling (see next section)

These three errors have been discussed in the revised manuscript. In summary there exist a large uncertainty on the thickness, within the range of ± 90%. However, even with such a large thickness range we are able to state that the conduit network is still thin and remains less than the wavelength of the GPR signal.

Channel Reflectivity: In order to evaluate the reflectivity uncertainty of the field data, we acquired 4 coincident profiles in a single day and compared the reflectivity output. There exists some variation in the reflectivity, likely caused by not being in exactly the same position. We have produced an additional figure and included it in an additional document (supplement figures) that highlights the variability and have updated the manuscript to describe the uncertainties.

a) GPR Data Example
b) Reflectivity extracted along profile – red bar is the mean of the four coincident profiles. Grey area represents the variability (minimum and maximum reflectivity values). The uncertainty is ±0.15.

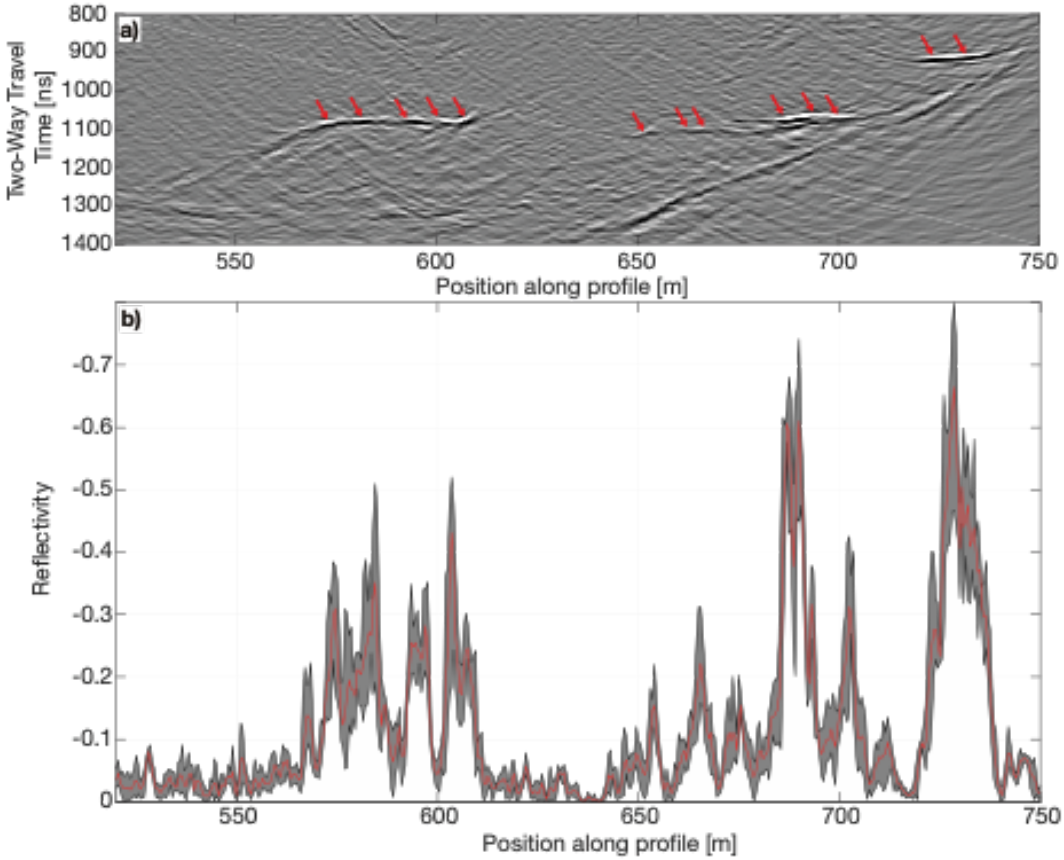

Figure: Uncertainty results from repeated GPR profiles undertaken in July 2018. a) GPR imaging result for repeated profile. b) Apparent reflectivity extracted from the GPR field data. The grey filled area represents the minimum and maximum reflectivity range from the four repeated profiles. The red line is the mean of the four profiles.

Numerical Modelling Uncertainties:
In addition to the uncertainties directly from the field data, we can use the synthetic data to provide some statistical analysis of the uncertainties by introducing noise to mimic the field data. There are two main types of noise for glacio-radar:

1. Random noise (background EM). Our GPR data does not suffer from a high level of random noise. We investigated this by looking at the amplitude spectrum at the end of the GPR record (where no coherent reflections or diffractions are present) and compared it to the beginning of the GPR record, where reflections and diffractions are present. The random noise was 40 dB below the coherent noise and we therefore neglected this from our forward modelling routine.

2. Coherent noise generated by diffractions either from englacial water pockets or surface streams can cause constructive or deconstructive interference with the conduit reflection. In order to add coherent noise to the synthetic data, we selected coherent noise from a field dataset acquired in 2018 and added this directly to the synthetic data (prior to migration). A total of 48 different coherent noise datasets were generated. Using the standard deviation of the extracted reflectivity and thickness we are able to provide uncertainties to the forward modelling and indirectly apply these uncertainties to the field data observations. The uncertainties from the numerical modelling have been included in the discussion relating to the conduit reflectivity values.

Ugo Nanni Review:

The study of Church and colleagues provides unique observations on the annual and seasonal evolution of an englacial drainage system geometry. With the use of repeated GPR measurements they are capable to estimate both size and spatial of an englacial conduit and monitor its evolution through time. I find the observations presented in this study of great importance for the glacial hydrology community. However, I find that the study focus much on the methodological aspect and on the observation with a limited discussion of the possible implications for englacial hydrology and glacier dynamics processes. I found the structure of the paper sometime confusing, with methodology description in the Results section, and results being discussed in the Results section. I suggest to rearrange the concerned sections (see below and in-text comments).

Detailed comments can be found in the attached pdf and here are my general comments.

We have provided replies to your comments in the supplied PDF.

Introduction: The section present general aspects of GPR measurements and glacial hydrology observations, but I found that it is difficult to understand which problem the authors aims to tackle. The problematics of the study and the limitations of previous ones are not well defined. In my opinion, the introduction should be re-worked with that in mind. I suggest the authors to consider widening their Introduction on glacial hydrology and including recent works on such environment for temperate glaciers.

See response in the list of substantial changes to the manuscript.

Methodology: I am not familiar with GPR measurements, but I find difficult to know is this study propose an innovative GPR analysis or not. I would like to have more information on what are the current limitations of GPR measurements. The authors devote large part of the manuscript to their approaches and I found difficult to follow such descriptions if we do not know why it is important beyond their study. In the results section you present several new methodologies. That renders the sections very difficult to follow. I suggest to move the methodological description in the Methodology section when possible, and try to reduce the description when possible.

No such GPR reflectivity analysis has been completed on temperate glaciers or over englacial conduits. See reply in the list of substantial changes regarding the reworked Methodology/Field Data section.

Results: There is a general lack of quantitative uncertainties when presenting the results and the conduits geometry. Some of the results are quite speculative and I suggest to be more precise on this particular aspect and better describe the observations without jumping to your own interpretation. Care should be taken to do not already discuss your results in this section.

Discussion: This section contains numerous very short-sub-sections that I suggest to collapse. The discussion on englacial hydrology mechanism and spatial extent is very short and I do not find enough evidences for the author to propose such mechanism. I suggest to add more details on these section. The discussion on the methodological aspect lacks of a wider context and on how their approach really improve their observations. As previously said, I find that the authors do not discuss enough the measurements uncertainties.

There is a section added into the discussion regarding the uncertainties for the EM wave-propagating velocities, conduit reflectivity, conduit thickness and lateral extent. See the reply in the list of substantial changes.

Figures/Tables: There are a lot of figure and Tables and I suggest to try reduce the number of tables as it renders the reading difficult.

We feel that having 11 figures and 4 tables for a publication in the Cryosphere is not excessive. All figures and tables are cross-referenced in the text and are of importance to the manuscript.

I find the observation of particular importance but I find a general confusion throughout the manuscript that impeach the reader to capture the importance of such observations and the proposed methodology. I support the publication of this manuscript with the above suggested modifications.

Many thanks for the constructive review and we hope that the modifications are satisfactory to you.

Slawek Tulaczyk Review:

This manuscript reports on radar imaging of an englacial conduit located at ca. 100m below the surface of Rhongletscher. The authors image this conduit repeatedly over several years with a GPR using antennas with 25MHz center frequency. The radar data constrain the seasonal and interannual evolution of this conduit. The authors use the radar data to put constraints on conduit thickness, reflectivity, and width. They use full- waveform simulations to tackle the fact that the conduit represents a thin layer, which is at times near/below the vertical resolution of the radar data.

I found this manuscript to be interesting and insightful. For the most part, it is methodologically sound. I am particularly impressed with the fact that the authors recognized the need to tackle the thin-layer problem in a rigorous way. The investigation of the dependence of conduit reflectivity on conduit thickness, which is near the resolution limit, represents a valuable contribution to radioglaciology.

Many thanks for your positive review and providing constructive criticism in order to improve the quality of the manuscript.

There are, however, several aspects of this manuscript that, in my opinion, can be improved:

(1) For instance, I am uneasy about the fact that critical quantities such as the conduit reflectivity and thickness are reported without error bars, even though they are estimated from radar data that, naturally, contain noise. In all instances, uncertainties in quantities derived from data should be reported.

See reply in the list of substantial changes section – in summary we have used repeated GPR profiles acquired in July 2018 to show the variability in the extracted reflectivity and to provide uncertainties.

(2) I find the repeated references to 'dry' and 'wet' glaciological environments to be not salient to the interpretation of radar results presented in the manuscript. It is a somewhat artificial distinction that worked in Baelum and Benn, 2011, but seems to add little here. I think that the manuscript will improve if the use of this distinction will be limited or eliminated.

We have removed the reference to the dry and wet throughout and have stated where appropriate reflectivities indicate an ice-water or ice-wet sand interface or an ice-air interface. The table that was based upon Baelum and Benn has been updated to include uncertainties based upon zero-incidence reflectivity analysis using relative permittivity ranges from Reynolds (2001).

(3) Whereas I appreciate the insights from the full-waveform modeling of the thin-layer problem, I do not think that the model output can be used to fully quantify uncertainties on conduit thickness and reflectivity derived from GPR data. Their simulations do not include any noise, but the real GPR data do contain noise. If it is possible, the authors should run additional simulations with a realistic level of noise included in the model setup. If this is not feasible, at least a discussion of this limitation should be provided.

See reply in the list of substantial changes section – in summary we have reworked the modelling exercise to include coherent noise. By adding coherent noise into the modelling exercise we have been able to define uncertainties to both the thickness and the reflectivity.

(4) The authors invested a lot of effort into considering the impact of vertical resolution (range resolution) on their data interpretation. However, there is no consideration given to the effect of horizontal GPR resolution on their results. This impacts the mapping of the conduit width and shape in particular. But it is also possible that the calculated reflectivities result from the radar signal reflecting from a large area (the Fresnel zone) with a mixture of different real reflectivities. It is relatively straightforward to calculate the diameter of the Fresnel zone at any given depth. My quick estimate indicates that, in this case, the Fresnel zone may be almost as wide as the width of the conduit detected in this study. So, this could be a significant complication.

See reply in the list of substantial changes section. We have added in the discussion a section regarding uncertainties and this contains details of the horizontal resolution.

Specific Comments

Line 52 – 'in cold ice' rather than 'on cold ice.'
Changed

Line 60 – By definition of the word 'annual' (occurring once a year), the sequence 2012, 2016, 2017 is not a sequence of annual measurements.
Altered to say 'repeated GPR profiles from 2012, 2016 and 2017 and repeated GPR seasonal profiles during 2018 and 2019'

Line 121 – geometrical is misspelled.
Changed

Lines 130-132 – When expressed in terms of energy ratio, a reflection coefficient cannot have negative values. This is why the reflection coefficient defined as the ratio of the reflected wave energy to the incident wave energy is equal to the second power of the amplitude reflection coefficient. The latter is defined as the amplitude ratio of the reflected and the incident wave. As written currently, this passage violates energy conservation because reflection cannot result in negative energy. In reality, the authors are talking about the amplitude reflection coefficient, which can have negative values because of phase reversal. But they misrepresent this as the energy reflection coefficient.
Rephrased to state: "The amplitude reflection coefficient explains the proportions of energy…"

Line 132 – Strictly speaking, the way that the reflection coefficient is treated here (e.g., Table 3), it is only a function of the dielectric permittivity, not electrical properties such as electrical conductivity or electrical resistivity.

Table 3 – I appreciate that the authors are copying this table from a prior publication, but some specific assumptions underly calculations of these reflection coefficients by the

original authors (Baelum and Benn, 2011). These values of the reflection coefficient have been calculated with specific assumptions regarding the porosity of these materials (e.g., granite and sand). These values are not some generally applicable values for all granites or wet sand. The footnotes to this table should state the assumptions underlying these values. Also, it would be much more realistic to re-calculate a range of values for granite and wet sand making assumptions that span some reasonable range of porosities for these two materials.

Table 3 has been altered. Wet and dry environment labels have been removed and they have been removed from the body of the manuscript. Zero-offset reflection coefficients have been calculated for a range of electric permittivity using Reynolds (2011) and therefore uncertainties have been provided. Granite has been removed from the table as it was not required in the manuscript and provided confusion to the readers.

Line 152 – It does seem that there is at least a faint reflector on the right-hand side of the image for September 2012. The strength of these faint reflectors from September 2012 data appears about equal to the strength of reflectors from figure 3b.

We agree that there are hints of the beginning of an englacial conduit. However, we wanted to emphasis the fact that it's not as laterally continuous and well developed as in 2017. We have reworded such that it read: 'there is no obvious reflection spanning across the section in September 2012'.

Line 155 – I am not sure that this conclusion is well justified by observations (see my comment above for Line 152).

We have reworded such that it states: 'From these observations we conclude that this englacial feature has undergone significant evolution between 2012 and 2017.'

Line 187 – I must admit that I do not understand the logic of picking -0.11 as 'the boundary between dry and wet glacial reflection environment' in this study. Do the authors really expect that there may be 'granite' in the middle of the ice column? Undoubtedly, the only plausible materials in the conduit are either glacial meltwater, sediments, or air. The only 'dry' material that could be there is, then, air? This part of the discussion must be improved. The entire distinction of dry vs. wet seems artificial and unnecessary in the context of this paper. The authors are allowing themselves to be too influenced by Baelum and Benn, 2011.

This sentence has been removed as a result of removing the dry/wet reflectivity scenario table.

Line 190 - The reflectivity of zero means that there is no reflection. If the channel was dry (full of air), then according to Table 3 the reflection coefficient should be +0.28. Hence, the logical interpretation of reflection coefficient being zero is that the conduits either close entirely or become so thin that the radar wave passes through them without detectable reflection. This should be the conclusion from the observation of near zero reflection, not the relatively vague statement that 'the channel is not a wet environment.'

We agree that the original reads difficult and therefore we have updated the manuscript to read: "The reflectivity during the winter months (Fig. 5a-c & g-h) is around zero indicating that there is a lack of a reflection and the190conduit is neither filled with a dry or wet material."

Table 4 - I find this table confusing. For one, conductivity and magnetic loss are given the same symbol (Greek sigma). Are they the same thing? Rather not since they do not have the same values. They may be interrelated since I do not recall that magnetic loss is part of Maxwell's equations, whereas the three other parameters are (permittivity, conductivity, permeability). Since the governing equations for the related calculations are not shown, it is difficult to really envision how these parameters are used in the forward modeling. Finally, I am always bothered when such parameter values are given without uncertainty ranges. We rarely know, or can assume, specific parameter values without considering what range they can really have.

Fundamental electrical properties affecting the propagation of EM waves are (1) dielectric permittivity, (2) electrical resistivity, (3) magnetic loss and (4) the magnetic permeability. The modelling was complete using gprMax and the referenced papers provide an overview of the forward modelling algorithm (Warren, C., Giannopoulos, A. and Giannakis, I. 2016) and is beyond the scope of the paper. As both materials for modelling are non-magnetic, we assume the magnetic (relative) permeability to be 1 and we assume the magnetic loss is 0. We have modified the Greek symbol for the magnetic loss to be σ_*.

We understand the need for uncertainties for these parameters however these parameters are for the GPR forward modelling and for this purpose we take only a single value for such parameters. We have modified the table such that they provide a range but state that we are only using single values for the modelling exercise:

Material	***Relative permittivity***	***Conductivity (S m^{-1})***
Temperate ice	***3-4 / Modelling: 3.2***	***$5e^{-7}$-$5e^{-8}$ / Modelling: $5e^{-8}$***
Fresh water	***80-81 / Modelling: 80***	***Modelling: 0.0005***

Line 234 - Whereas I am impressed by the full-waveform modeling used to get around the thin-layer problem, the approach taken here has at least one shortcoming. Unlike synthetic data, real data are noisy. The authors contend that they can use their real, noisy data to determine the conduit thickness to within +-0.15 based on idealized, noiseless simulations. They make a similar claim about the reflectivity being within +-0.1. The noise-free simulations represent a useful end-member but they cannot be used to determine the uncertainty on conduit thickness and reflectivity based on real data. The authors should analyze the power spectrum of noise in their GPR data and then add this noise to their forward simulations. This approach will enable them to quantify more realistic ranges of uncertainties on conduit thickness and reflectivity.

See reply in the list of substantial changes.

Figure 9 and its discussion in text - I got utterly lost in keeping track of what thickness and what reflectivity the authors call 'true', 'apparent' 'calculated' and 'observed'. This needs to get streamlined. I think that the best approach is to use only two of these terms. 'Apparent' should be used when talking about conduit thickness and reflectivity derived from GPR data. 'True' should be used to describe the equivalent quantities obtained from forward simulations.

This has been streamlined. As the reviewer suggested, we have taken <u>apparent</u> reflectivities and thicknesses to be from the output of the modelling and <u>true</u> thicknesses to be from the modelling conduit input shape.

Line 287 - delete the unnecessary verb 'are'
Changed

Line 292 - 'Remnants' 'are' (not 'is')
Changed

Line 299 - This artificial distinction between 'wet' and dry' glacial environment is really an unnecessary oversimplification.
As in part (2) above, we have removed the wet/dry references. We have altered this line to state the it would indicate an englacial environment without the presence of water.

Line 319 - 'appears as a single specular reflection'
Changed

Line 325 - ' plotting the reflection normalized by the amplitude of the basal reflector'
Section 5.3 and Figures 10 and 11 - When discussing and plotting conduit shape, it would be useful for the authors to calculate the Fresnel zone's size for their radar at a depth of the englacial conduit. I made a quick and dirty calculation and I'm getting some dozens of meters. So, the Fresnel zone for this 25 MHz radar at 100m depth below the surface can be comparable to the conduit's width. Perhaps the conduit width appears artificially larger than it is because of this limit in horizontal radar resolution? In any event, the size of the Fresnel zone should be considered here. The authors have invested a lot of effort to investigate the limits of vertical resolution, but there is no effort to quantify the horizontal resolution.
See response in the list of substantial changes to the manuscript.

Monitoring the seasonal changes of an englacial conduit network using repeated ground penetrating radar measurements

Gregory Church[1,2], Melchior Grab[1,2], Cédric Schmelzbach[2], Andreas Bauder[1], and Hansruedi Maurer[2]

[1]Laboratory of Hydraulics, Hydrology and Glaciology (VAW), ETH Zurich, Zurich, Switzerland
[2]Institute of Geophysics, ETH Zurich, Zurich, Switzerland

Correspondence: Gregory Church (church@vaw.baug.ethz.ch)

Abstract. Englacial conduits act as water pathways to feed surface meltwater into the subglacial drainage system. A change of meltwater into the subglacial drainage system can alter the glacier's dynamics. Between 2012 and 2019, repeated 25 MHz ground penetrating radar (GPR) surveys were carried out over an active englacial conduit network within the ablation area of the temperate Rhonegletscher, Switzerland. In 2012, 2016 and 2017 GPR measurements were carried out only once a year, and an englacial conduit was detected in 2017. In 2018 and 2019 the repetition survey rate was increased to monitor seasonal variations of the detected englacial conduit. The resulting GPR data were processed using an impedance inversion workflow to compute GPR reflection coefficients and layer impedances, which are indicative of the conduit's infill material. The spatial and temporal evolution of the reflection coefficients also provided insights into the morphology of the Rhonegletscher's englacial conduit network. During the summer melt seasons, we observed an active, water-filled, sediment-transporting englacial conduit network that yielded large negative GPR reflection coefficients (<-0.2). ~~For all the~~ The GPR surveys conducted during the summer ~~,~~ provided evidence that the englacial conduit was 15-20 m ± 6 m wide, ~0.4 m ± 0.35 m thick, ~250 m ± 6 m long with a shallow inclination (2°) and having a sinusoidal shape from the GPR data. We speculate that ~~such a geometry is likely the result of extensional hydraulic fracturing~~extensional hydraulic fracturing is responsible for the formation of the conduit as a result of the conduit network geometry observed and from borehole observations. Synthetic GPR waveform modelling using a thin water-filled conduit showed that a conduit thickness larger than 0.4 m (0.3 × minimum wavelength) thick can be correctly identified using 25 MHz GPR data. During the winter periods, the englacial conduit ~~shuts down~~ no longer transports water and either physically closed or ~~becomes~~ became very thin (<0.1 m), thereby producing small negative reflection coefficients that are caused by either sediments lying within the closed conduit or water within the very thin conduit. Furthermore, the englacial conduit reactivated during the following melt season at an identical position as in the previous year.

1 Introduction

Surface meltwater is routed through the glacier's interior by englacial drainage systems, before it reaches subglacial drainage systems (Fountain and Walder, 1998; Cuffey and Paterson, 2010). Subglacial drainage systems play an important role on the dynamics of glaciers (Iken et al., 1996; Bingham et al., 2008). For example, ~~high subglacial water pressure can lubricate~~ water flowing along the base of a glacier can facilitate glacial sliding by lubricating the ice-bed interface ~~, which may result~~

(Hewitt, 2013). With an increase in subglacial water pressure, the ice-bed friction weakens, resulting in a faster sliding velocity (Iken and Bindschadler, 1986; Zwally et al., 2002). The subglacial water pressure can dramatically increase, ~~when the drainage system does~~ if either the englacial or subglacial drainage systems do not adapt quickly ~~enough, while surface meltwater is routed rapidly through the englacial~~ to an increased melt water input. Furthermore, the water pressure can increase depending on how water is routed through the glacier's drainage system. There is often a short time lag~~between the surface meltwater being present and the~~ , in the region of hours and days, between the start of surface melting and an increase in glacier velocity (Bingham et al., 2005). Englacial drainage systems often provide the meltwater pathways that can facilitate changes in subglacial water pressure, and as a result they can impact the glacier's dynamics. Furthermore, knowledge of the englacial conduit's seasonal evolution and geometry is important for a glacier's hydrological modelling. Therefore, studying the seasonal evolution of an englacial drainage system throughout the melt season is key to ~~understanding~~ understand how and when they transport water ~~to~~ into the subglacial drainage systems.

~~Depending on the temperature of the ice, there~~ There exist different mechanisms for ~~developing~~ the formation of englacial drainage networks and these are broadly dependent on the temperature of ice. Ice below the pressure melting point (cold ice) is impermeable and until recently (Vatne, 2001; Boon and Sharp, 2003), it was assumed that surface melt water has limited penetration within cold-ice glaciers. However, recent research has provided evidence that ~~surface-to-bed~~ englacial drainage networks are present in cold ice glaciers and they are formed by three distinct mechanisms (Benn et al., 2009; Gulley, 2009). The first mechanism includes surface melt water that creates incisions on the glacier's surface, and these surface streams can become englacial, if their upper levels becomes blocked or closes due to ice creep. Such englacial streams are known as 'cut-and-closure' conduits ~~(Gulley et al., 2009a)~~and first described by Fountain and Walder (1998) and later by (Vatne, 2001; Gulley et al., 2009a). The second mechanism for the formation of englacial conduits within cold ice, is hydraulically assisted fracture propagation (Boon and Sharp, 2003; van der Veen, 2007). Englacial conduits can develop from water filled crevasses where stressed ice and the water pressure within the fracture is large enough to overcome the fracture toughness of the surrounding ice. The third mechanism is related to the exploitation of permeable structures within the body of the glacier~~(Gulley et al., 2009a)~~, such as fractures (Fountain et al., 2005) or debris-filled crevasses (Gulley and Benn, 2007).

The englacial drainage network theory was originally developed for ice at the pressure melting point (temperate ice) (Shreve, 1972; Röthlisberger, 1972). Temperate ice was assumed to be permeable and this led to the theoretical model that englacial conduits form from water flowing between ice crystal boundaries within connected veins. ~~As~~ Lliboutry (1971) argued that englacial conduits have difficulty forming within connected veins as a result of ~~theoretical challenges by Lliboutry (1971) and~~ deformation and recrystallisation of the grains closing intergrannular channels. Furthermore, field observations by Gulley et al. (2009b) have resulted in the formation mechanisms of englacial conduits within temperate ice ~~has been~~ being questioned. As within cold ice, englacial conduits seem to form as a result of hydraulically assisted fracture propagation in temperate ice (Gulley, 2009). Additionally, englacial conduits can form from the exploitation of pre-existing fractures (Fountain et al., 2005; Gulley et al., 2009a).

There exist only a limited number of studies investigating englacial conduit conditions on temperate ice. Studies of glacier's drainage systems are based primarily on dye tracer experiments, speleology, borehole studies, geophysical measurements

or a combination of these techniques. Englacial drainage systems have been interpreted from dye tracer testing on temperate glaciers (Nienow et al., 1996, 1998; Hock et al., 1999), but difficulties arose, since tracer tests do not offer direct observations of englacial drainage networks. Direct observations have been made into inactive englacial channels using speleology techniques (Gulley, 2009; Naegeli et al., 2014; Temminghoff et al., 2019), but they were obviously conducted, only when the drainage system was dry and inactive. Therefore, such observations do not provide temporal information on the englacial conduit's seasonal evolution.

Geophysical experiments can provide observations on active englacial conduit networks covering a large spatial distribution, and they can be repeated, thereby providing information on the temporal evolution. Two geophysical methods have regularly been used for studying the glacier's hydrological systems, seismology (active and passive) and radar. Ground-penetrating-radar (GPR) has been used to detect englacial drainage systems ~~on~~ in cold ice (Moorman and Michel, 2000; Stuart, 2003; Catania et al., 2008; Catania and Neumann, 2010; Schaap et al., 2019; Hansen et al., 2020) and temperate ice (Arcone and Yankielun, 2000; Hart et al., 2015). There exist only a small number of studies that investigate seasonal changes within the englacial hydrological network and all of these have been undertaken on cold-ice glaciers. Across several years, GPR measurements were performed by Bælum and Benn (2011) over a small cold-ice valley glacier to investigate the glacier's thermal regime. Pettersson et al. (2003) used time-lapse GPR imaging, separated by 12 years, to detect changes to the cold-temperate ice transition surface and Irvine-Fynn et al. (2006) used repeated GPR measurements to investigate hydrological seasonal changes on a polythermal glacier. However, for these studies the GPR profiles were not repeated several times during a year and across a number of years. Therefore, very limited information is available on the seasonal evolution of englacial drainage systems ~~on~~ and there is little knowledge of these changes within temperate glaciers.

Reflectivity analysis is commonly employed on GPR data in order to provide subsurface properties and to identify subsurface materials. The strength of the reflected GPR signal is a function of media's electrical properties that form an interface and can therefore be used to determine subglacial environments. Such studies have been conducted with an impulse ice-penetrating radar system within a cold-ice environment (Macgregor et al., 2011; Christianson et al., 2016), however no such analysis have been performed using a commercial GPR within a temperate ice environment or to characterise an englacial conduit network. In order to extract the reflectivity from a commercial GPR system, an inversion workflow can be implemented (Schmelzbach et al., 2012). Within a glaciological such an inversion workflow can provide hydrological temporal and spatial changes. Temporal and spatial changes have be obtained using repeated GPR amplitude analysis and such studies have been completed on non-glaciological settings (Truss et al., 2007; Guo et al., 2014). Such investigations have not yet been conducted within a glaciological environment to detect hydrological changes.

Alongside GPR, passive seismology has been employed to identify and characterise the subglacial drainage network (Gimbert et al., 2016 Such an approach has recently been used to investigate subglacial conduits on temperate glacier (Vore et al., 2019; Lindner et al., 2019; Nan Passive seismology can be a complimentary tool to GPR reflectivity analysis in order to monitor seasonal evolution of the glacier's hydrological system. Our primary focus of our study is to use the GPR reflectivity analysis to detect seasonal changes within an englacial conduit network.

In this study, we use a comprehensive GPR dataset that includes ~~annual measurements~~ GPR profiles from 2012, 2016, 2017 and ~~seasonal measurements~~ repeated GPR seasonal profiles during 2018 and 2019. ~~This~~ GPR imaging and reflectivity analysis facilitates studying the temporal and spatial changes of an englacial conduit network on a temperate glacier. By repeating GPR measurements several times throughout the melt seasons, we can gain insights into how an englacial network changes and evolves in response to the meltwater supply. Additionally, by performing GPR measurements across subsequent melt seasons, we can ~~check~~verify, if these englacial networks were reactivated after the winter period in a similar location, or if they close down and become inactive the following melt season. We detect these seasonal and annual changes by extracting the GPR reflection strength (reflectivity) using a GPR impedance inversion scheme (Schmelzbach et al., 2012). The spatial extent of the reflectivity patterns allows potential englacial flow paths to be imaged. Alongside the GPR data, we were able to use direct observation into the englacial conduit network using a borehole camera in 2018. In brief, there are three main objectives of this research, namely

1. to implement a GPR processing routine to extract GPR reflection coefficients related to englacial structures,
2. to interpret the spatial reflection coefficients in order to gain an understanding of the temporal conduit morphology, and
3. to correlate the englacial conduit's dimensions to previous studies in order to understand the conduit's formation mechanisms.

Furthermore, ~~using a GPR modelling algorithm , we are able~~ we used a GPR data simulation algorithm using a variety of 3D englacial conduit models in order to quantify the spatial dimensions of an active englacial conduit network.

2 Study Site

This englacial network monitoring case study was conducted on the Rhonegletscher (Fig. 1), where an englacial conduit network was previously detected using active seismic reflection data (Church et al., 2019). The Rhonegletscher is the sixth largest glacier in the Swiss Alps (Farinotti et al., 2009), and it is the source of the Rhone river. The glacier has been well studied and documented due to the ease of access from the nearby Furka pass, with the first measurements from the beginning of the 17th century (Mercanton, 1916). The glacier flows southwards from 3600 down to 2200 m above sea level (asl) with a surface area of approximately 16 km^2 (Huss and Farinotti, 2012). In recent years, a proglacial lake formed as a result of the glacier retreating (Tsutaki et al., 2013; Church et al., 2018). This proglacial lake is dammed by a granite riegel, and there is likely a hydraulic interaction between the lake and the glacier's drainage network. The survey site was located within the lower ablation area between 2280 m and 2350 m asl, where the ice thickness in 2017 was approximately 100 m (Fig. 1).

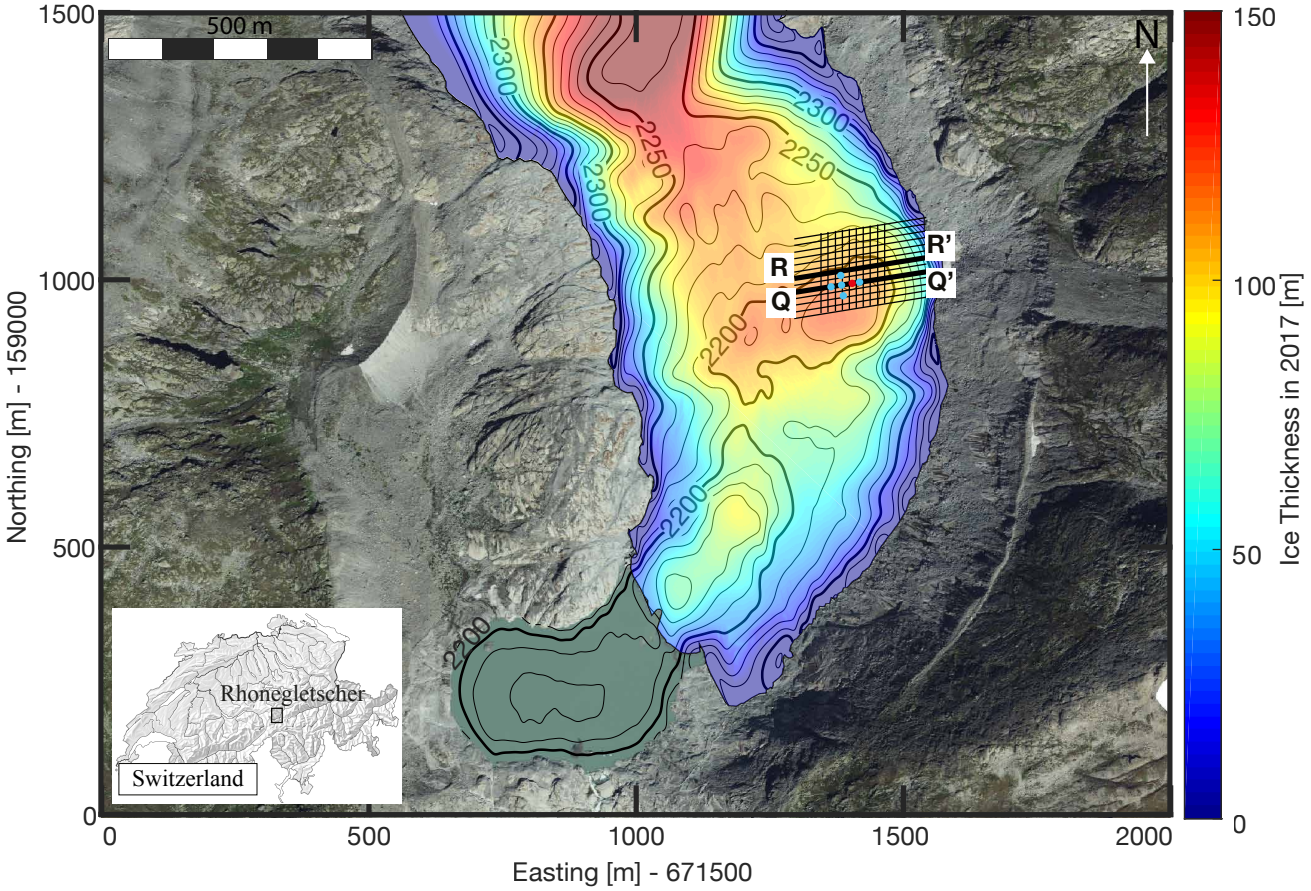

Figure 1. Map of the Rhonegletscher's lower ablation area, ice thickness (colour-coding), basal topography (black contour lines) updated from Church et al. (2018) and GPR repeated survey site (black grid). The two thicker GPR profile lines (R-R' and Q-Q') are displayed in Fig. 3 and Fig. 4. Five boreholes were drilled in August 2018 to provide ground-truths on the conduit and are marked as blue and red dots. The red dot represents the borehole where the borehole camera acquired a video.

3 ~~Methods~~Field Data and Processing

3.1 GPR Data Acquisition

To investigate seasonal englacial conduit variations, we performed ~~several~~ 13 GPR field campaigns from 2012 until 2019 (Table 1). Three GPR surveys, that covered a single profile across the survey site (Q-Q' in Fig. 1), were conducted over three different
125 years (2012, 2016 and 2017). Upon detection of ~~the englacial conduit network in 2017 (Church et al., 2019)~~an englacial GPR reflection, which was later identified as an englacial conduit network (details on the identification of the network can be found in Church et al. (2019)), we performed a dense GPR grid at different times of the year in 2018 and 2019 over the englacial

Table 1. Overview of the GPR surveys acquired over the englacial conduit network. Survey months in italic and bold represent winter (snow covered) and summer (snow free) acquisition respectively and the asterisk marks the months where common midpoint measurements were additionally acquired.

Year	No. of surveys	Time of Year	Survey Type
2012	1	**Sep**	Single Profile
2016	1	*Apr*	Single Profile
2017	1	**Sep**	Single Profile
2018	7	*Mar*, *Apr**, *May**, **Jul**, **Sep***, **Oct***, *Dec*	Grid
2019	3	*Feb*, *May*, **Aug**	Grid

conduit network (grids of black lines in Fig. 1). The GPR grid includes 13 profiles oriented east-west (average length: 250 m) and 10 profiles oriented north-south (average length: 150 m), with a spacing of 13 m between adjacent profiles.

All The majority of the field measurements were conducted as common offset (CO) surveys, and they were acquired using a Sensor & Software pulseEKKO Pro GPR system with 25 MHz antennas. CO measurements are acquired keeping the transmitting and receiving antenna at a constant distance apart (known as offset) and allows large quantities of data to be collected in a time-efficient manner. The GPR antennas were carried by hand during summer month acquisitions (snow-free, June-October) and during winter month acquisitions (snow covered, November-May), they were mounted and pulled on pulk sleds. The GPR antennas were positioned in a transverse electric (TE) broadside configuration and kept at a constant offset of 4 m between transmitting and receiving antennas. Additionally, the orientation of the antennas were perpendicular to the walking direction. For all GPR lines, a high precision global navigation satellite system (GNSS) continuously recorded the GPR antennas mid-point and the accuracy given by the GNSS was generally below 0.05 m.

In addition to the CO profiles, we acquired common midpoint (CMP) data in order to evaluate the electromagnetic (EM) wave velocity of the glacial ice. CMP's are acquired by incrementally increasing the offset between the transmitting and receiving antennas over a given central location such that we image a point in the subsurface with different offsets. These CMP measurements were performed in April, May, September and October 2018 over the englacial conduit in order to detect any seasonal changes to the EM-wave velocities. The location of the CMPs was directly over the englacial conduit (marked by the green line in Fig. 2c).

3.2 Borehole Data Acquisition

In 2018, six boreholes were drilled around the englacial conduit network (Fig. 1) using a hot water drill. Two boreholes were drilled directly into the conduit network, and we were able to lower a borehole camera (GeoVISION^{TM} Dual-Scan) within these boreholes to make direct observations within the englacial conduit network.

3.3 GPR Data Processing

The raw CO GPR data were processed using a combination of an in-house MATLAB based toolbox (GPRglaz Rutishauser et al. (2016); Langhammer et al. (2017); Grab et al. (2018)) and Seismic Unix. The processing scheme aims to recover the GPR reflection coefficients from the englacial conduit reflections by means of an impedance inversion scheme. This inversion scheme is based upon the seismic impedance inversion developed in the late 1970s and 1980s (Russell, 1988). The reflectivity is recovered by the inversion on pre-conditioned GPR data using the underlying assumption that the GPR reflectivity is represented by a series of sparsely distributed spikes, this inversion is known as a sparse-spiking deconvolution (Velis, 2008). The aim of the sparse-spiking deconvolution operator is to find the smallest number of spikes that, after convolution with the GPR source wavelet, matches the pre-conditioned GPR data within a small error. Within a glaciological setting, the spikes from the deconvolution would represent englacial reflectors or the glacier base. The workflow implemented was based upon the processing described in Schmelzbach et al. (2012).

An outline of the GPR CO processing is described in Table 2. It consists of the following major steps: (1-6) pre-processing by assigning the GNSS data with the GPR data, setting time zero and the record length, interpolating clipped data, bandpass filtering to remove noise, trace binning to account for varying walking speeds, elevation static correction, (7) deterministic amplitude correction to compensate for the amplitude decay due to ~~gemoetrical~~ geometrical spreading, absorption and transmission losses, (8) GPR deconvolution to remove the GPR source wavelet and increase the vertical resolution (Schmelzbach and Huber, 2015), (9) an amplitude preserving migration to re-position the reflections in their correct location and to increase the horizontal resolution, (10) identifying an amplitude matching scalar in order to match the amplitudes across all GPR surveys, (11-13) sparse-spike deconvolution to recover the reflectivity (Sacchi, 1997) and to calibrate the reflectivity and stretch the reflectivity to depth below glacier surface. In order to calibrate the reflectivity, ground truth data were used. The reflectivity within the vicinity of the borehole was calibrated to be the ice-water reflectivity as direct observations provided a flowing water-filled conduit (Church et al., 2019). The outcome of this workflow after migration (9) is shown in Fig. 2 and Fig. 3a-e. The final output (13), including the reflection coefficients, are displayed in Fig. 3f-i.

The spatial and temporal distribution of the reflection coefficients is the primary outcome of the processing workflow. The amplitude reflection coefficient explains the proportions of energy that are reflected from a given interface. Its values range between -1 and 1. Their magnitudes and polarities are indicative for the electrical material properties adjacent to an interface. ~~Bælum and Benn (2011) divided the~~ For zero-offset (vertical incidence) example reflection coefficients for ~~glaciological environments into dry and wet groups (Table 3)~~englacial environments are provided in Table 3 using relative permittivity ranges from Reynolds (2011).

The GPR reflection coefficient has previously been used in order to determine the presence of water or bed conditions on Matanuska Glacier in Alaska, USA (Arcone et al., 1995). In the Rhonegletscher case study, we will make use of the reflection coefficient for imaging the spatial extent and the temporal evolution of the englacial conduit, and it will also provide information, ~~as to whether the conduit is dry or wet. Since the GPR antennas were constantly separated by 4 m, and the target~~

Table 2. Common offset GPR processing workflow

	Processing Step	Comments
1.	Merge GPR and GNSS data	
2.	Set time zero and record length	2000 ns (~170 m depth of penetration in ice)
3.	Interpolate clipped GPR data	
4.	Butterworth bandpass filter	10-75 MHz
5.	Trace Binning along profile	Binned to 0.5 m spacing
6.	Elevation static correction	
7.	Amplitude corrections	Summer α = 0.0007, winter α = 0.0004 (see Schmelzbach et al. (2012) for details)
8.	GPR deconvolution	Schmelzbach and Huber (2015)
9.	Phase Shift Migration	Seismic Unix migration and constant velocity of 0.1689 m ns^{-1}
10.	Amplitude matching between all GPR datasets	
11.	Sparse deconvolution to recover reflectivity	Described in Sacchi (1997)
12.	Calibrate the reflectivity	Setting the reflectivity to be the ice-water reflectivity at the borehole site in 2018
13.	Time to depth conversion	Constant velocity 0.1689 m ns^{-1}

Table 3. GPR reflection coefficients from typical ~~glaciological~~ englacial conduit environments using zero-offset measurements~~(Bælum and Benn, 2011).Wet and dry environments are highlighted by dark grey and light grey cell shading respectively.~~

		Upper Medium	
		Ice	Water
Lower Medium	Ice	-	+0.67±0.01
	Air	+0.28 ±0.02	-
	~~Granite~~ Wet Sand/Gravel	~~-0.11~~ -0.39 ±0.03	~~+0.6Wet Sand-0.47~~ -
	Water	-0.67±0.01	-

~~was around 80-100 m below the glacier surface, the angle of incidence is less than 1 degree, and vertically incident waves can be assumed~~on the filling material within the conduit.

The GPR reflectivity workflow provides both the englacial conduit top and bottom reflection time (thickness if the filling material is known) and the englacial channel reflectivity. To provide details on seasonal evolution, both the extracted reflectivity and conduit thickness from the field data were interpolated and smoothed for each seasonal GPR acquisition.

The CMP measurements were also processed using GPRglaz, but SeisSpace ProMAX 2-D was used for the EM wave-propagation velocity analysis. The pre-processing included assigning the geometry and amplitude correction for geometrical spreading. As described by Booth et al. (2010), we applied a static shift prior to picking the velocities in ProMAX in order to remove the systematic error in semblance analysis of GPR CMP data. The ~~velocity determined from the CMP measurements (Fig. 4a and d) were~~ EM wave-propagation velocities were picked on the englacial reflection using a second order normal moveout correction this velocity was used for the migration velocity in the workflow indicated in Table 2.

4 Field Data Results

4.1 GPR Imaging Results

For studying the general evolution of the englacial conduit network we analysed all GPR profiles, however we consider profile Q-Q' (Fig. 1) as an example for the annual evolution. In Fig. 2, the GPR sections acquired during the summer months are displayed. Due to the increased presence of water during the summer melt season (average daily discharge in Figure S4), the signature of a potential englacial conduit is expected to be most pronounced during this time of the year as a result of water filling the conduit. As shown in Fig. 2a, in September 2012 there is no ~~clear englacial reflection visible in September 2012~~obvious englacial reflection spanning across the section, but in September 2017, we observe a ~~conspicuous~~ strong englacial reflection pattern at about 2210 m asl (Fig. 2b). This feature is also visible in the GPR sections acquired in summer 2018 and 2019 (Figs. 2c and 2d), although its shape and strengths exhibits some minor variations. From these observations we conclude that this englacial feature ~~is recent, and it must have formed~~ has undergone significant evolution between 2012 and 2017.

Besides the ~~general appearance~~ annual changes of this englacial feature, it is also interesting to study its seasonal variability. We analysed all GPR profiles within the grid between 2018 and 2019, however, we consider profile R-R' (Fig. 1) as an example for the seasonal imaging results. In Fig. 3, the GPR sections, acquired in 2018 and 2019, are displayed. Additionally, the spatial distribution of the reflectivity (reflection coefficients) is provided. The single continuous englacial reflector is present across the majority of the acquired profile during the summer months (Fig. 3c and e), whereas in April 2018 (winter) it is almost absent (Fig. 3b), and its reflection strength is also reduced in May 2019 (winter) (Fig. 3d). The reflectivity (Fig. 3f-i) emphasises the contrasting englacial environment between summer and winter. Similar observations were also made in profile Q-Q' (~~not shown~~Fig. S2) and across the majority of GPR profiles acquired, but in profile R-R' they are slightly more pronounced.

4.2 GPR Common Midpoint (CMP) Results

~~The CMPs were acquired in order to determine the EM wave propagation velocity through glacial ice for the CO phase shift migrations and to determine, if any seasonal variation exist. Four CMPs were acquired at different times of the year (Table 1), and the velocities were picked using semblance analysis from SeisSpace ProMAX 2-D. The location of the CMPs was directly over the englacial conduit (marked by the green line in Fig. 2c), where the conduit was a specular reflector showing~~

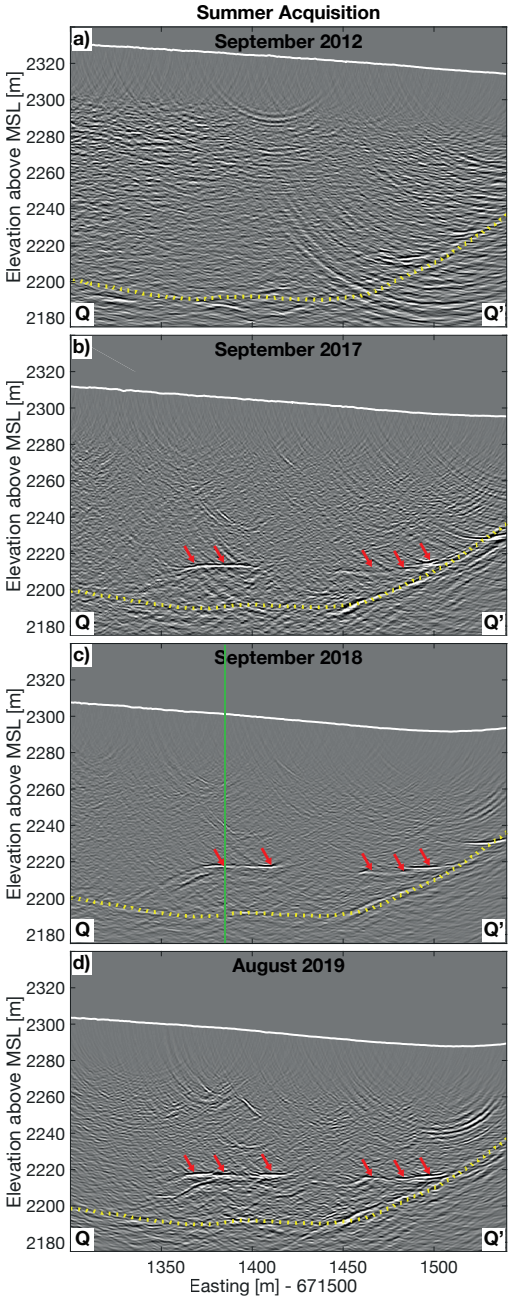

Figure 2. GPR imaging results from a repeated profile (Q-Q' in Fig. 1) over a single line after migration from 2012 until 2019. The yellow line represents the ice-bedrock interface and the red arrows represent the englacial conduit network reflection appearing from summer 2017. The green line in c) marks the location of the CMP acquired. Zoomed GPR profile images are available in Fig. S1.

f

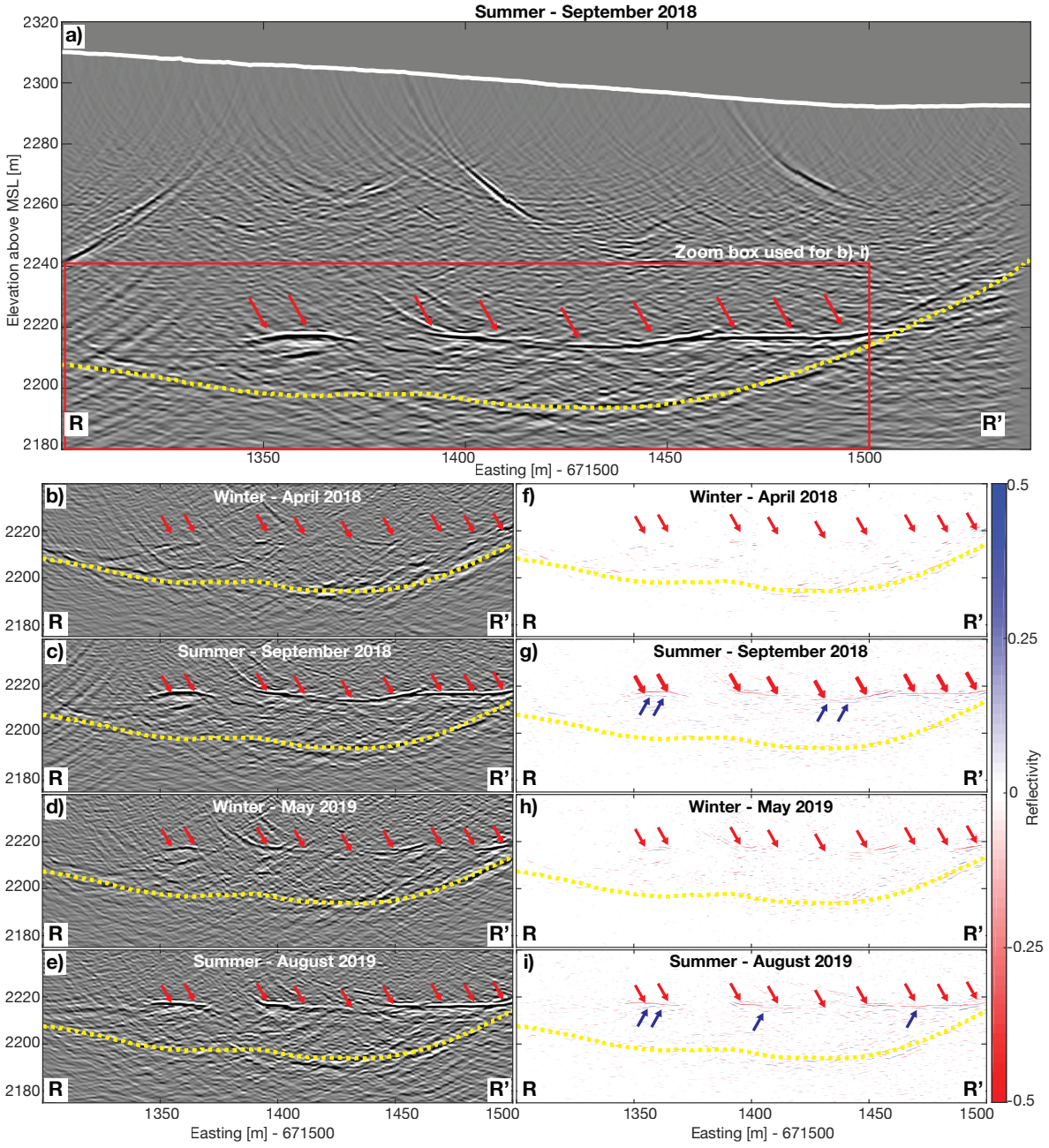

Figure 3. a) GPR imaging results over a single repeated GPR profile (R-R' in Fig. 1) in 2018. The yellow line represents the ice-bedrock interface, white line represents the glacier surface, and the red box is the zoom box for GPR imaging and reflectivity results b)-i). b)-e) are seasonal GPR imaging results and f)-i) are the seasonal GPR reflectivity results from b)-e). The red arrows represent the top of the englacial conduit network and the blue arrows represent the bottom of the englacial conduit network (g & i).

little topography variation. Furthermore, prior to picking the velocities, the CMPs were backshifted by a quarter wavelength, as suggested by Booth et al. (2010).

The velocities were picked on the englacial reflection using a second order normal moveout correction. The EM wave propagation velocity for the EM wave-propagation velocity for the winter CMP measurement (Fig. 4a) was picked on the semblance to be between 0.16 and 0.17 to be 0.165 $\pm$0.05 m ns^{-1} (Fig. 4b-c). The EM wave propagation wave-propagation velocity during the summer CMP measurement (October 2019) was between 0.165 and 0.175 picked at 0.170 $\pm$0.05 m ns^{-1}. There exist some uncertainty an uncertainty in the EM wave-propagation velocities as a result of limited transmitter-receiver offsets in comparison to the target depth (offset-depth ratio: 0.5), and the low frequency antenna with a dominant period of 15 ns create large semblance bullseyes in Figs. 4c and f. Two more CMP gathers were recorded in May and September 2019, which show a similar velocity, but with a larger uncertainty ($\pm$ 0.1 m ns^{-1}) due to poorer data quality.

The EM wave propagation velocities within ice is a function of water content, and quoted values in literature are between 0.167 and 0.169 m ns^{-1} (Fujita et al., 2000; Murray et al., 2000; Plewes and Hubbard, 2001; Reynolds, 2011; Bradford et al., 2013). As a result of the uncertainties on the propagation velocities from the CMP measurements, the migration velocity was kept constant for both summer and winter at 0.169 m ns^{-1} as used in previous temperate ice GPR studies (Glen and Paren, 1975; Rutishauser et al., 2016).

4.3 GPR Seasonal Reflectivity Results

The reflectivity from the top of the englacial reflection was extracted (red arrows highlighting the negative reflectivity event in Fig. 3g), interpolated and smoothed for each seasonal GPR acquisition over the survey area. Figure 5 highlights the seasonal spatial reflectivity over 16 months from May 2018 until August 2019. The white lines in Fig. 5 correspond to isolines with reflectivity of -0.11, which correlates to the boundary between dry and wet glacial reflection environments (Table 3). During the summer months, when the englacial conduit is active and transporting melt water through the glacier's body we observe large negative reflectivities (<-0.2). The spatial extent of the englacial network is clearly visible in the summer months acquisition.

The reflectivity during the winter months (Fig. 5a-c & g-h) is around zero indicating that the channel is not a wet environment. Whereas, during there is a lack of a reflection, and the conduit is neither filled with air, water, nor wet sand. During the summer months (Fig. 5d-f & i) the reflectivity varies between -0.2 and -0.6, corresponding to the wet reflectivity scenarios in Table 3either an ice-wet sand interface or an ice-water interface (Table 3). At the beginning of the melt season in July 2018 (Fig. 5d), the englacial conduit network does not appear to be fully developed and connected throughout the survey site, while in September and October 2018 (Fig. 5e & f), the conduit is connected across the survey site. Furthermore, in August 2019 (Fig. 5i), we observe wet-environment reflectivities in an identical reflectivities between -0.2 and -0.6 in a similar location as in summer 2018.

4.4 GPR Conduit Thickness Results

In addition to the seasonal reflectivity results, the conduit thickness was calculated for those surveys, where the top and bottom reflections could be identifiedclearly. The travel time differences between the top and bottom reflections was converted to

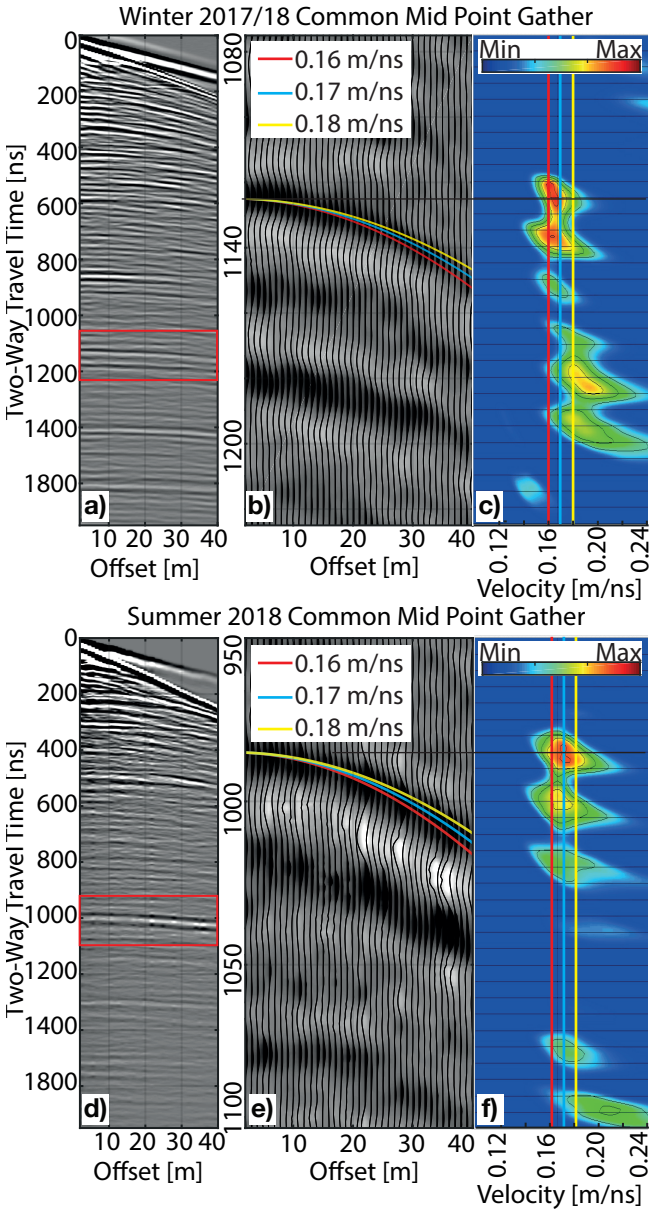

Figure 4. Common mid point gather and velocity determination. Winter (April 2018): a) The raw CMP gather. b) Zoom of the raw gather over the englacial reflection with second order normal moveout (NMO) curves using 0.16, 0.17 and 0.18 m ns^{-1}. c) Semblance display using second order NMO for the zoom section from b). Summer (October 2018): d)-f) as per winter a)-c).

250 thickness using the velocity of an EM wave travelling through water (0.0333 m ns^{-1}). Figure 3g and i shows a negative reflectivity for the top of the conduit (red arrows) and a positive reflectivity for the bottom of the conduit (blue arrows). Upon extraction of the conduit thickness, the spatial extent of the conduit thickness was determined by interpolating between the

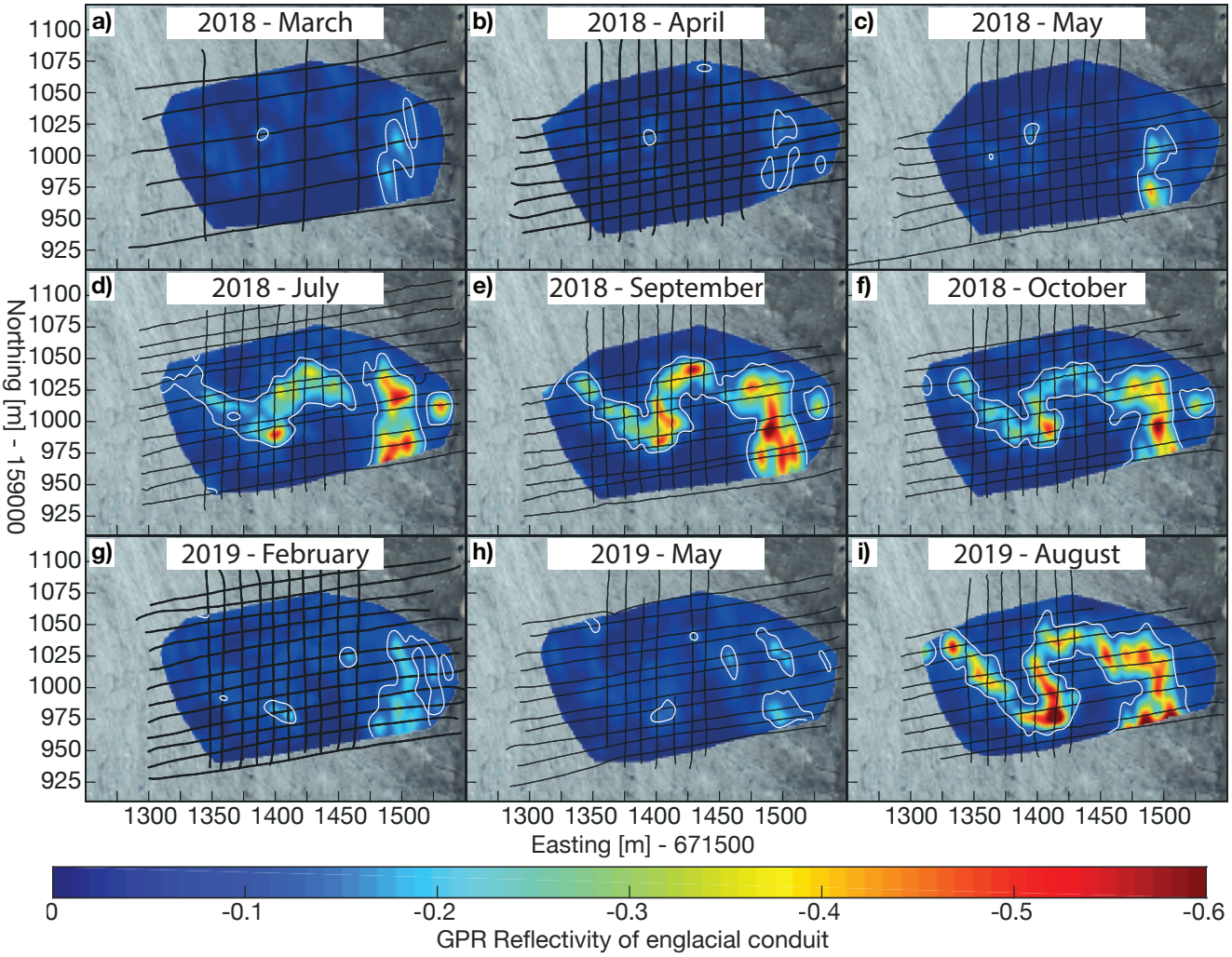

Figure 5. Seasonal GPR reflectivity from the top of the englacial channel reflection. The black grid lines represent the GPR acquisition profiles acquired for each month respectively. The white contour represents the reflectivity at ~~-0.11~~-0.1 providing an approximate outline of the englacial conduit.

GPR profiles and smoothing (Fig. 6). The conduit thickness is between 0.2 and 0.5 m throughout the melt season (Fig. 6), and there is little variability in the conduit thickness throughout the summer. We performed a thin-layer forward modelling investigation, with which we tried to appraise the reliability and robustness of the thickness estimates.

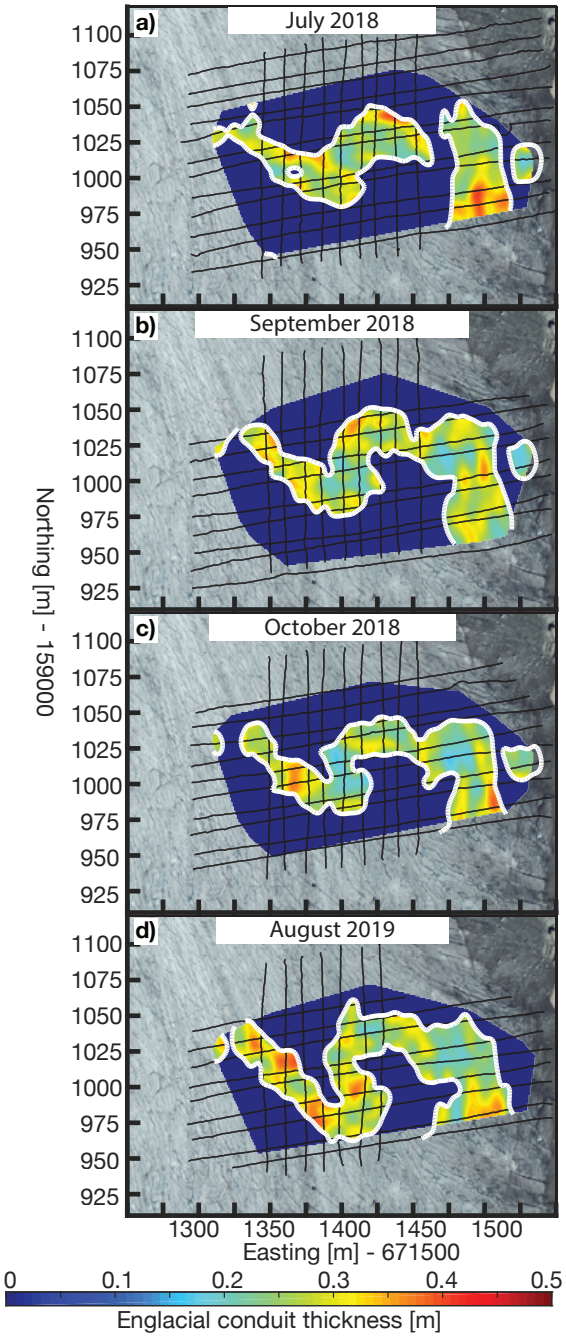

Figure 6. Estimated englacial conduit thickness during the summer months of (a-c) 2018 and (d) 2019.The white contour represents the englacial conduit reflectivity at 0.1, same contour as displayed in Fig. 5.

5 Numerical Modelling: Thin Channel Water Layer GPR Forward Modelling

5.1 Thin Channel Water Layer GPR Forward Modelling Methodology

Reynolds (2011) states that, in theory, the vertical resolution of a GPR signal is a quarter wavelength, assuming the source wavelet is two half cycles. This theory is based upon the seismic wave propagation theory as described by Widess (1973). In reality the GPR source wavelet is typically longer than a single wavelength, with this being the case, the vertical resolution is reduced as a result of the complex nature of the transmitted GPR source wavelet (Reynolds, 2011). For an EM wave propagating within a water-filled conduit the wavelength of a 25 MHz system is 1.333 m, and therefore the theoretical vertical resolution ($\lambda/4$) for a conduit filled with water using 25 MHz antennas is 0.33 m. The true conduit thickness can be determined from the reflectivity inversion if the thickness of the conduit is larger than the theoretical vertical resolution. The thicknesses shown in Fig. 5 are thus within proximity of the theoretical vertical resolution limit. ~~Therefore, we performed a thin-layer forward modelling investigation, with which we tried to appraise the reliability and robustness of the thickness estimates.~~

~~Estimated englacial conduit thickness during the summer months of (a-c) 2018 and (d) 2019.The white contour represents the englacial conduit reflectivity at 0.1, same contour as displayed in Fig. 5.~~

5.2 ~~Thin Channel Water Layer GPR Forward Modelling Results~~

A forward modelling approach was adopted in order to investigate how a thin water filled channel layer, below the theoretical vertical resolution, affects the ~~observed~~ thickness and reflectivity that we recover from the processing workflow described in Table 2. From this point the thickness and reflectivity derived from the modelled GPR data is known as the apparent thickness and reflectivity, whereas the known model thickness and known ice-water reflectivity is known as the true thickness and reflectivity. We generated synthetic radargrams using the open source software gprMax (Warren et al., 2016). This is a finite-difference time-domain solver for EM wave propagation. We employed a simple 3D model, as sketched in Fig. 7a. It includes a single thin water filled conduit that is invariable in the third dimension. The associated material parameters are summarised in Table 4. All four boundaries of the model had absorbing boundary conditions in order to prevent multiple energy interfering with the top and bottom reflection from the conduit. The synthetic GPR data (Fig. 7b) were modelled using transmitting and receiving antennas separated by 2 m, and they were moved from 2 until 18 m along the x axis in Fig. 7a at 0.5 m increments. The model space did not contain a free surface in order to have a clear interpretation of the top and bottom conduit reflector without any multiple energy being present. The numerical simulations and thickness extraction procedures were repeated with a range of conduit thicknesses between 0.05 and 2 m.

~~The synthetic GPR data,~~ Noise free simulations were initially performed, but for uncertainty analysis coherent noise was added prior to migration. The coherent noise was extracted from the GPR field data acquired in July 2018 and it was added directly to the synthetic data. The synthetic GPR with coherent real noise can be directly compared with the field data in order to make conduit thicknesses and reflection strength deductions. In order to determine how the the coherent noise effects the apparent reflectivities and thickness, we used 48 different noise types and performed statistical analysis to determine uncertainties.

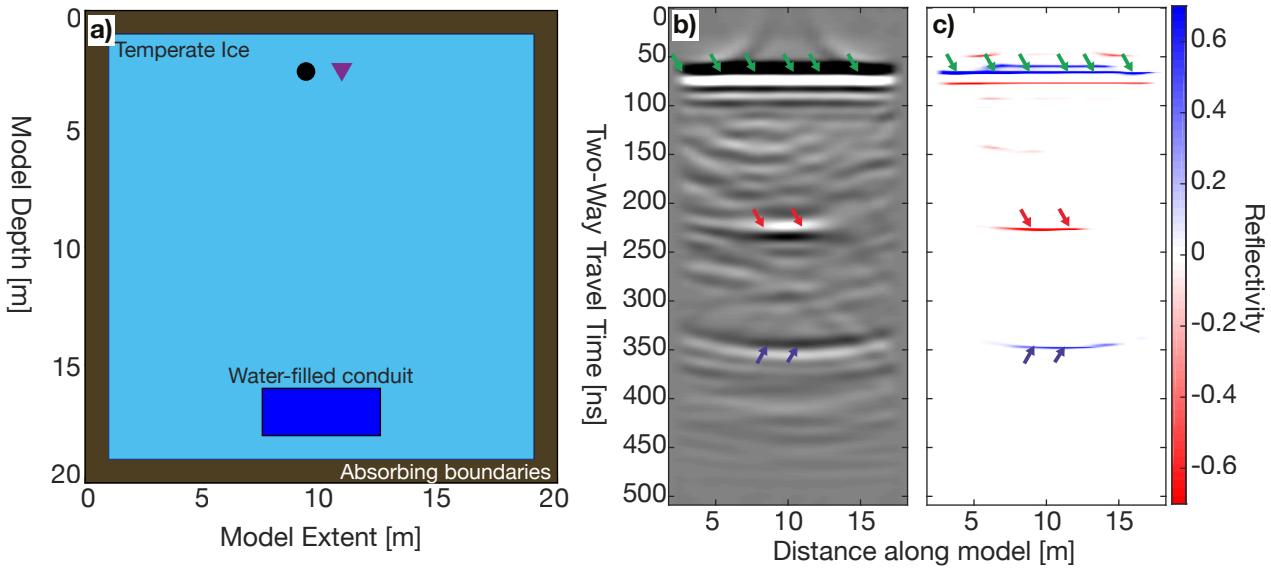

Figure 7. Forward modelling results. a) Geometry model for gprMax forward modelling with temperate ice, 2 m thick water-filled conduit and absorbing boundaries labelled. The circle and the triangle represent the transmitting and receiving antenna. b) The processed synthetic data generated from the model in a) after step 10 in Table 2. c) The reflectivity from the data b) after processing through the entire workflow described in Table 2. The green arrows represent the direct arrival, the red and blue represent the top and bottom reflection from the englacial conduit respectively.

5.2 Thin Channel Water Layer GPR Forward Modelling Results

The synthetic GPR data with an example of coherent noise added, shown in Fig. 7b, were generated with a 2 m thick water-filled englacial conduit, and the red and blue arrows represent the reflection from the top and bottom conduit respectively. There ~~is clear~~ exist a 120 ns separation between the top and bottom reflections (red and blue arrows in Fig. 7) from the conduit using a 2 m thick englacial conduit model, but, as shown in Figure 8, these two reflectors interfere with each other, when the conduit thickness reaches the vertical resolution (0.3 m in Fig. 8). The horizontal width of the water-filled conduit remained at 5 m for all tests and is below the horizontal resolution after migration. In order to extract the reflectivity (Fig. 7c and Fig. 8b) from the synthetic GPR data, the data were processed using an identical processing workflow, as applied to the field data.

The ~~numerical simulations and thickness extraction procedures were repeated with a range of conduit thicknesses between 0.05 and 2 m. The results~~ results on the apparent channel thickness as a function of the true model channel thickness are shown in Fig. 9a. We were able to ~~determine the correct conduit thickness~~ resolve the true conduit thickness of the conduit from the GPR data, when the true thickness was greater than 0.4 m (0.3λ). However, when a water filled conduit was less than 0.4 m thick, the ~~observed~~ apparent thickness from the inversion was within ± 0.15 m (yellow shaded area in Fig. 9a). In the summer, the majority of the Rhonegletscher imaged englacial conduit network is less than 0.4 m (Fig. 6) and therefore, the conduit thickness from Rhonegletscher does not represent the true thickness but the ~~calculated~~ apparent thickness is within ± 0.15 m

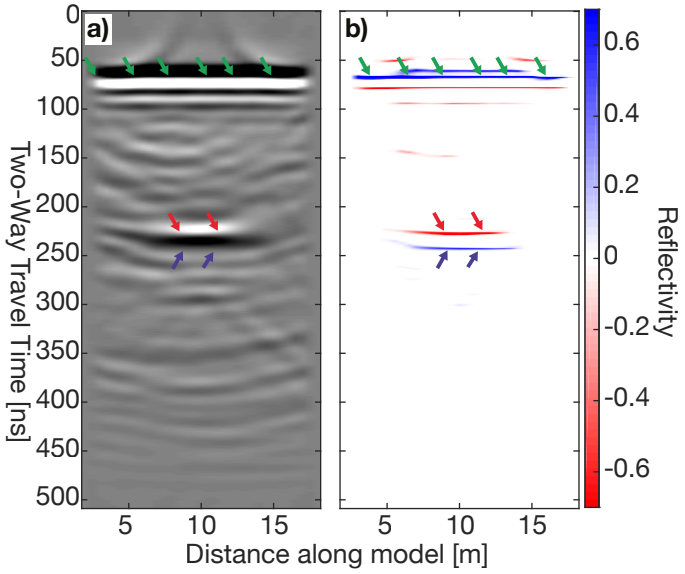

Figure 8. Forward modelling results for 0.3 m water-filled conduit. a) The processed synthetic data after step 10 in Table 2. c) The reflectivity from the data a) after processing through the entire workflow described in Table 2. The green arrows represent the direct arrival, the red and blue represent the interfering top and bottom reflection from the englacial conduit respectively.

of the ~~actual~~ true conduit thickness. The error bars show the effect of the coherent noise added into the model. There is little effect on the thickness estimation with coherent noise added to the model.

In addition to the discrepancies between ~~observed~~ apparent channel thickness and true channel thickness (Fig. 9a), the GPR zero-offset reflectivity can be analysed as a function of channel thickness (Fig. 9b). The solution for an ice-water reflection is -0.67 and is represented by the pink line in Fig. 9b. For the noise free data the apparent reflectivity is represented by the red line in Fig. 9b. In order for the channel to have an ice-water reflectivity of -0.67 (Table 3), using noise-free data, the conduit must be greater than 0.6 m thick (0.45λ), as represented by the green shaded area in Fig. 9b. With the addition of coherent noise in the simulations, the uncertainty for true thicknesses above 0.6 m is $\pm$ 0.1. When the conduit is between 0.1 and 0.6 m thick (0.07λ - 0.45λ), the ~~calculated~~ noise free apparent reflectivity is equal to the true reflectivity $\pm$ 0.1 (shaded yellow area in Fig. 9b). With the addition of the coherent noise to the simulations the uncertainty doubles to $\pm$ 0.2. When the conduit is thinner than 0.1 m, the ~~calculated~~ apparent reflectivity is below 0.5 (shaded red area in Fig. 9b). From these results, a likely explanation for the low reflectivities observed from the conduit (Fig. 5) could be the result of the conduit being below the vertical resolution.

Table 4. Material properties for the forward modelling, taken from (Plewes and Hubbard, 2001; Reynolds, 2011; Langhammer et al., 2017). The values within the brackets represent the range of uncertainty.

Material	Relative permittivity ϵ	Conductivity σ [S/m]	Relative permeability μ	~~Magnetic Loss Ω/mσ~~ EM wave-propagating Velocity [m
Temperate ice	3.2 (3-3.3)	$5e^{-8}$ ($5e^{-7}$-$5e^{-8}$)	1	~~0~~ 0.1689
Fresh water	80 (80-81)	0.0005	1	~~0~~ 0.033

6 Discussion

6.1 Uncertainties

6.1.1 EM wave-propagation velocities

The EM wave-propagation velocity for the four CMP's had a maximum uncertainty of ± 0.1 m ns^{-1} and the mean EM wave-propagating velocity was 0.1675 m ns^{-1}. The EM wave propagation velocities within ice is a function of water content, and quoted values in literature are between 0.167 and 0.169 m ns^{-1} (Fujita et al., 2000; Murray et al., 2000; Plewes and Hubbard, 2001; Re therefore the EM wave-propagation velocity was kept constant for all GPR migrations at 0.1689 m ns^{-1} and time-to-depth conversions.

6.1.2 Conduit Reflectivity

In order to evaluate the reflectivity uncertainty of the field GPR data we acquired four coincident profiles in a single day in July 2018 and compared their reflectivity results from the GPR processing flow. There exists some natural variation in the englacial reflectivity that is likely caused by a combination of minor changes in the walking path leading to different imaging points, and differences in the coherent noise. From these repeated measurements the variability has been quantified to be $\pm$ 0.15 (Fig. S3).

In addition to the field data, an estimate of the channel reflectivity uncertainty has was additionally completed using the synthetic testing, when adding coherent noise. The uncertainty on the reflectivity using coherent noise within the numerical modelling is $\pm$ 0.2 independent of the conduit thickness (grey shaded area in 9). Both of these errors provide similar uncertainty ranges and therefore, the uncertainty on the apparent reflectivty is estimated to be $\pm$ 0.2.

GPR reflection coefficients are a function of the incidence angles. As the GPR antennas were constantly separated by 4 m, and the target was around 80-100 m below the glacier surface, the angle of incidence is less than 1 degree, and vertically incident waves were therefore assumed for all reflectivity analysis.

6.1.3 Conduit Thickness

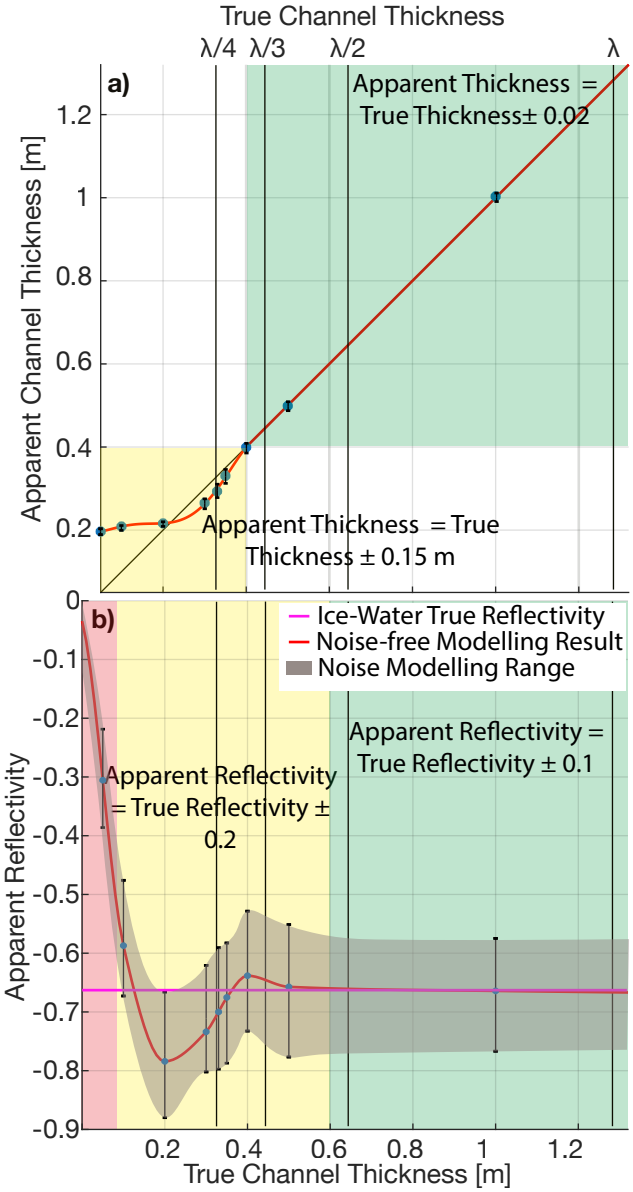

Figure 9. Forward modelling apparent thickness and reflectivity results plotted against the true model conduit thickness. a) The ~~observed~~ apparent thickness in the GPR inversion processing as a function of the true channel thickness in the model (Fig. 7a using 25 MHz antennas). b) The ~~calculated~~ apparent reflectivity from the ~~channel~~ englacial conduit top as a function of the true channel thickness. The error bars represent the two standard deviations around 48 different noise records added to the synthetic.

The uncertainty in the true channel thickness is a function of the picked two-way time, the EM wave-propagation velocity through the conduit filling material and the apparent thickness. Our borehole camera observations provided evidence that

the filling material is water (see supplement video), and there exists small amounts of loose sediments. Therefore, a EM wave-propagation velocity of fresh water (0.0333 m ns^{-1}) was employed for the time-to-thickness conversion. The small quantity of sediment could potentially increase the EM-propagation velocity. As far as we are aware, there are no studies providing the EM wave velocity through water with a small quantity of sediment. A fully saturated till layer within the conduit would alter the propagation velocity to be within 0.05-0.06 m ns^{-1} (Reynolds, 2011). Given the borehole observations, it can be assumed safely that the EM-propagating velocities are between 0.033 and 0.05 m ns^{-1}. Therefore, we have attributed a lower bound uncertainty of 50% to the apparent thickness related to the time-to-thickness conversion velocity. An upper bound of 0% exist for the velocity error as the lowest potential velocity within an englacial conduit is the EM-wave propagation velocity through water.

The picking error is within a sample (1 ns) as a result of picking the reflectivity (Fig. 3g) and not the actual GPR wavelet (Fig. 3c). This small picking error in time equates to only a 1.5 cm error in the conduit thickness and is therefore not a large source of uncertainty and can be neglected.

The GPR forward modelling exercise provided evidence that when the true channel thicknesses was below 0.4 m the apparent thickness does not represent the true conduit thickness (Fig. 9a). For true conduit thickness less than 0.4 m the apparent thickness is within 0.15 m of the true model (40% error). Whereas, for apparent thickness above 0.4 m represent the true model and therefore there is no significant error.

Compounding the conduit thickness uncertainties for apparent conduit thickness below 0.4 m, we have large errors (lower bound: -90%, upper bound: +40%). Whereas, for apparent conduit thickness greater than 0.4 m the uncertainty is only a function of the filling EM-propagating velocity (lower bound: -50%, upper bound: apparent conduit thickness). Despite these relatively large errors we are able to confidently state the englacial conduit on Rhonegletscher is still a thin-layer and below the wavelength of the GPR signal.

6.1.4 Horizontal Resolution

The first Fresnel zone defines the horizontal resolution (the ability to distinguish two closely laterally separated reflectors) for GPR. The first Fresnel zone is approximately 17 m for the geometry of our reflector (90 m depth) with a 25 MHz GPR system and the EM wave-propagation velocity through ice (0.1689 m ns^{-1}). The GPR data have been migrated using a 2D Kirchhoff migration algorithm and therefore within the profile the first Fresnel zone is reduced to the bin size (0.5 m). However, the Fresnel zone out of the GPR plane remains 17 m. The acquisition of the GPR was set-up to have profiles along and perpendicular to the glacier flow. Acquiring profiles in these orientations ensured that we have a horizontal resolution of 0.5 m in both directions in order to delineate the englacial conduit network. There exists an uncertainty of the spatial extent as a result of the linear interpolation of the reflectivities. The spacing between profiles are approximately 12 m, and therefore we would estimate that the uncertainty to be around half the profile spacing (6 m).

6.2 Conduit ~~Extension~~Geometry

6.2.1 Conduit Extension

During the melt season (July-October), when the englacial conduit is active, the conduit is around 250 m ± 0.6 m in length and between 20-45 m ± 0.6 m wide. During all the summer acquisitions, the englacial conduit thickness was estimated to be between 0.2 and 0.4 m exhibiting little variability (Fig. 6). Therefore, the conduit was far wider than thick and it does not follow the typical cylindrical englacial conduit cross-sectional shape, as observed in other GPR surveys (Stuart, 2003), or as described by englacial conduit theory (Shreve, 1972; Roethlisberger, 1972).

6.3 ~~Conduit Inclination~~

6.2.1 Conduit Inclination

There is a ten metre global elevation difference in the conduit's topography (Fig. 10) across the entire imaged englacial conduit network, thereby indicating that the conduit has a low inclination (approximately 2°). ~~It~~ The inclination is similar to englacial conduits drainage networks found on a cold-ice glacier in Svalbard (Stuart, 2003; Hansen et al., 2020). Such a small dip provides evidence that the movement of englacial water is not related with the hydraulic gradients and therefore, does not supports the englacial conduit formation models described by Shreve (1972), which postulates englacial conduits formation through upward branching of an arborescent network.

6.3 ~~Conduit Shape~~

6.2.1 Conduit Shape

The shape of the englacial conduit shows a meandering and sinusoidal outline that runs perpendicular to the ice flow direction. The outline (white contour in Fig. 6) has similar geometry to sub-sections of englacial conduits that have been mapped using speleology within cold glaciers (Gulley et al., 2009a), which have been formed as a result of the cut-and-closure mechanism. A cut-and-closure englacial conduit forms as a result of surface streams or streams within crevasses incising towards the glacier bed and subsequently becoming isolated from the surface as the ice flows due to ice creep (Fountain and Walder, 1998). Similarly, a sinusoidal shape could result from turbulent water flowing englacially. To the best of our knowledge this is the first example of a temperate glacier to have an active englacial system surveyed using geophysical techniques and showing a sinusoidal shape.

6.3 Conduit Formation

The conduit's sinusoidal shape provides some evidence that this englacial drainage system could be the result of a cut-and-closure drainage system. However this hypothesis can be ruled out, as no large visible supraglacial stream has been observed on Rhonegletscher within the proximity of the englacial conduit in previous years. Moreover, comparing the conduit's profile

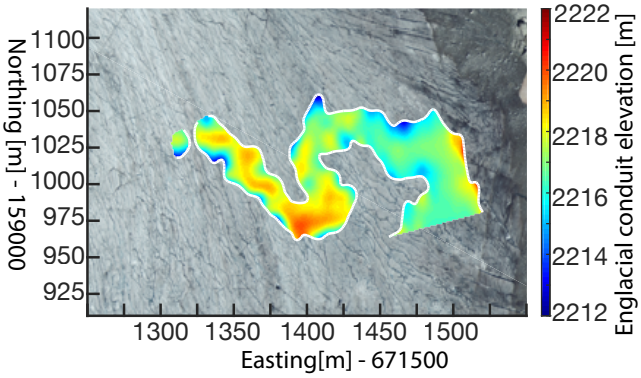

Figure 10. Elevation above mean sea level from the top of the englacial conduit network in August 2019.

and cross sections with those described by Gulley et al. (2009a) and summarised in Fig. 2 in their publication, the likely formation mechanism is extensional hydrofracturing. Hydrofracturing on extensional stressed glacial ice provides a horizontal profile (shallow dip) and an englacial conduit cross-section that is thin and wide. Such extensional stresses may result from the ~~turning of the Rhonegletscher~~ ice flow turning at the survey site towards the proglacial lake. As discussed in Church et al. (2019), the drainage network is likely fed from numerous streams running along the glacier margin and from the surrounding moraine. Additionally, the hydrofracturing can be supported by the fact that periods of high water pressure was observed as a result of the borehole expelling water 3-4 m above the glacier surface in August ~~2018.~~ 2018 (Fig. S5).

We were unable to determine the englacial water flow direction from either the GPR data or from the borehole camera. Tracer studies might be an option (Hooke and Pohjola, 1994; Hock et al., 1999). Unfortunately, this would be difficult, as the studied englacial network is expected to flow into the proglacial lake, and therefore monitoring the tracer quantity would require samples to be taken directly from a borehole instead of an outflow stream from the glacier's tongue.

6.4 Conduit's Seasonal Variations

The conduit morphology alters throughout the year as a result of the varying discharge from the glacier. ~~For~~ Theory states that a steady-state englacial conduit, where the conduits opening rates equals the conduits closure rate, the size and shape of the conduit remains constant ~~. Changes~~ (Cuffey and Paterson, 2010) and changes in water supply can alter the opening and closure rates and thereby alter the conduit's morphology. Englacial conduits can shrink and disappear, when discharge quantities are low, whereas high discharge rates can cause a conduit to expand. Runoff and discharge data are available at a gauging station in Gletsch (1800 m a.s.l), 2 km downstream from Rhonegletscher ~~.~~ (Fig. S4). The peak discharge occurs annually between 24th July and 17th August. The end of the peak discharge correlates with the time of the year, where the conduit was well developed in 2019 (Fig. 6d). We can speculate that during August, when there ~~are exist a large diurnal dischargefluctuations through the englacial conduit~~is peak discharge, the englacial network is ~~fully developed. The timing further correlates with observations~~

from other alpine glaciers, where subglacial drainage networks often switch from a distributed system to a channelised system in the peak of the melt season (Seaberg et al., 1988; Nienow et al., 1996). at its maximum observed extent.

There exists a winter shut-down of the englacial conduit network between 2018 and 2019, indicated by a near-zero reflectivity (Fig. 5e). Remnants of the englacial conduit is are detectable on the winter reflectivity, when restricting the colour scale from -0.05 to -0.15 (Fig. 11, grey line). If the conduit is fully open (thickness > 0.5 m), then it is neither water or air filled during the winter as a large negative reflectivity (ice-water: -0.67) or positive reflectivity (ice-air: +0.3) is not observed. During August 2018, we were able to make direct borehole measurements using a borehole camera and observed sediment being transported along the base of the conduit (see video supplement S1). Therefore, as a result of the lower reflectivity and the lower discharge, we speculate that during winter the conduit either physically closes or becomes very thin (< 0.1 m) and remains water filled. If the conduit physically closes, the sediments lying within the closed conduit are likely the cause of the low winter reflectivity, and the reflectivity values around -0.1 indicate a dry glacial environment (Table 3)would indicate an englacial environment without the presence of water. Whereas, if the conduit thinned to less than 0.1 m and remained water filled the reflectivity values are around -0.1 (red area in Fig. 9b). The repeated GPR summer measurements in 2018 and 2019 provided evidence that the conduit networks reopens in an identical location. In order for the conduit to be reactivated during the 2019 melt season, either the sediments lying within the closed during the winter months provided a potential permeable flow path in 2019, or the englacial conduit remained connected after becoming a very thin water-filled (<0.1 m) conduit during the winter. Furthermore, we speculate that the hydraulic potential is similar during both melt seasons as the englacial conduit is reactivated in an identical position after the winter shutdown.

The GPR wavelet character from the conduit's top remains a constant negative high amplitude reflector over the three melt season (2017, 2018 and 2019), which indicates the presence of water within the system during our GPR summer acquisitions. From the GPR data, we are able to determine that the englacial conduit network is at or above atmospheric pressure. If the system would be below at atmospheric pressure, the top reflector would be an interface between ice and air and result in a positive amplitude reflector. Such an unpressurised englacial network was observed by Stuart (2003), where the conduit's top reflection was a high positive amplitude reflector. The fact that the conduit is at or above atmospheric pressure is additionally supported by our borehole camera observations, where the borehole water level that was 1-2 m above the englacial network during observations, suggesting that the water pressure was slightly above atmospheric pressure.

6.5 General Applicability and Limitations of GPR to Characterise Englacial Conduits

So far, there exist a few studies, where englacial conduits have been characterised using a combination of GPR with speleology or borehole observations (Moorman and Michel, 2000; Stuart, 2003; Catania et al., 2008; Temminghoff et al., 2019; Schaap et al., 2019). In these studies, englacial conduits were imaged as point diffractors. Without speleology or boreholes, the interpretation of these point diffractors is typically ambiguous. In the Rhonegletscher case study, the interpretation is unambiguous with the ground-truth borehole observations, because the englacial conduit appears as a single specular reflection.

For future studies investigating englacial conduits, the GPR reflectivity workflow can be used to identify englacial conduits and conditions on the glacier's bed, but it is essential to calibrate the observed apparent reflectivities with known reflectivi-

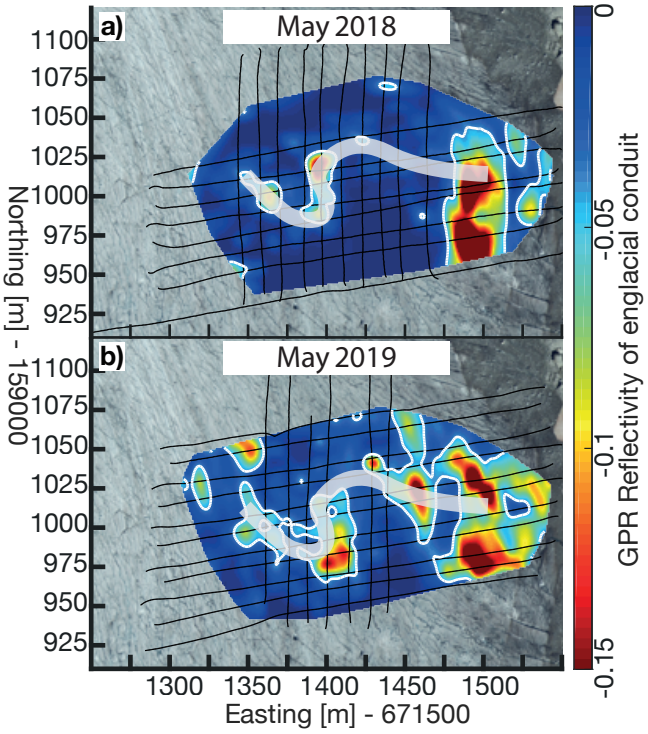

Figure 11. Winter GPR reflectivity from the top of the englacial channel reflection plotted between 0 and -0.15 reflectivity values, highlighting remnants of the englacial conduit network that exist during the winter months. The grey line represents the summer englacial conduit shape. The black grid lines represent the GPR acquisition profiles acquired for each month respectively. The white contour represents the reflectivity at -0.05.

ties on site. As far as we are aware, there does not exist such reflectivity analysis for glacial drainage networks on temperate glaciers. For the Rhonegletscher data, this was obtained from borehole observations. However, for others studies, a known reflectivity point may not be available in order to calibrate the reflectivity, and therefore by plotting the uncalibrated reflectivity of an englacial reflector potential flow paths could be delineated, however the filling material would remain unknown. Such an approach was adopted in Bælum and Benn (2011) (plotting the reflection normalised amplitude of the glacier's bed). The workflow could be extended to specular glacier basement reflectors in order to detect subglacial conduit networks. However, the GPR processing workflow does not correct for the anisotropic GPR radiation pattern. In this case, dipping specular reflectors will have amplitudes dependent on both the radiation pattern and the angle dependent reflection coefficient. Therefore an extension of the workflow needs to be made and a migration accounting for GPR antenna radiation pattern needs to be implemented prior to the impedance inversion in order to extract the reflectivity coefficient.

This study has also provided evidence that the glacier's bed needs to be interpreted with care. The Rhonegletscher case study has identified an englacial conduit as a specular reflector 10-15 m above the glacier's bed during the melt season. If a single GPR profile would have been acquired during the melt season (e.g. August 2019, Fig. 3e), the englacial conduit may

have been mis-interpreted as the glacier bed. Therefore, it is essential to understand the hydrological conditions of the glacier, when designing GPR surveys in order to successfully interpret the GPR data. For GPR surveys, where the ice thickness is the objective on temperate alpine glaciers, then GPR acquisition should be undertaken during winter in order to minimise the englacial water storage limiting penetration depth. On the contrary, for GPR surveys investigating the glacier's hydrological conditions it is intuitive that acquisition should take place during summer.

From the forward modelling, the vertical resolution for GPR was found to be 0.3λ. If two interfaces are spaced less than $0.3\ \lambda$ metres vertically apart, then there exists interference between the two reflectors which leads to an erroneous thickness interpretation (Fig. 9). This GPR vertical resolution is larger than seismic vertical resolution found through forward modelling on ice-water reflectivities (King et al., 2004), as a result of the complex nature of the GPR source wavelet.

7 Conclusions

By using repeated GPR measurements and processing the data with an impedance inversion to extract the reflectivity, we have mapped the changing spatial extent and thickness of an active and dynamic englacial conduit network on a temperate glacier. The repeated seasonal GPR measurements in 2018 and 2019 and the reflection coefficient analysis of the englacial conduit provided an insight into the evolution of an active englacial hydrological network.

In summer the englacial conduit was ~~active~~transporting water through the glacier, leading to large negative reflectivity values (<-0.2). The Rhonegletscher's englacial network followed a meandering and sinusoidal shape throughout the melt season. The conduit is 15-20 m wide and between 0.2 and 0.4 m thick. Such a conduit cross section (wide and thin) can occur as a result of hydraulic fracturing with extensional stresses acting on the ice, based upon the englacial conduit shape review by Gulley et al. (2009a). Furthermore, water flowing through the englacial conduit during the melt season feeds the subglacial drainage network, which likely increases subglacial water pressure and facilitates basal sliding.

The englacial conduit was found to ~~be inactive~~ have reduced in thickness and was not transporting water during the winter period, with reflectivity values between -0.05 and -0.15. Therefore, we speculate that during the winter the conduit network either physically closes or is very thin (<0.1 m). Either, sediments that were being transported within the conduit in the summer or water within a thin-layer conduit are likely responsible for the reflectivity visible during the winter GPR acquisition. The englacial conduit became active in an identical location after a winter shut down. The conduit's shape remained similar in the winter compared to the summer.

Difficulties arise when interpreting a series of reflectors that are separated by the vertical resolution. The forward modelling has shown that two horizons are perfectly distinguishable when they are separated by more than 0.3λ. Whereas, the amplitude or reflectivity of the top interface is only resolved when the thickness is greater than 0.45λ. We conclude that care must be taken when inferring material properties from a reflectivity processing workflow with the presence of thin layers that approach the vertical resolution of the GPR source wavelet.

Video supplement. Movie S1 https://doi.org/10.3929/ethz-b-000406689 shows the borehole camera observations made directly into the active englacial conduit on 24th July 2018.

Author contributions. GC, MG, AB and HM designed the GPR experiments, which were carried out by GC and MG. GC processed the data with help from CS and all authors analysed the data. GC interpreted the data with help from all co-authors. GC wrote the manuscript with contributions from all co-authors.

Competing interests. The authors declare that they have no conflict of interest.

Acknowledgements. The Swiss National Science Foundation financed the project (SNF Grant 200021_169329/1). Data acquisition has been provided by the Exploration and Environment Geophysics (EEG) group and the Laboratory of Hydraulics, Hydrology and Glaciology (VAW) of ETH Zurich. The authors gratefully acknowledge the Landmark Graphics Corporation for providing data processing software through the Landmark University Grant Program. The authors wish to acknowledge all volunteers for their valuable help in participating the fieldwork.

References

Arcone, S. A. and Yankielun, N. E.: 1.4 GHz radar penetration and evidence of drainage structures in temperate ice: Black Rapids Glacier, Alaska, U.S.A., Journal of Glaciology, 46, 477–490, https://doi.org/10.3189/172756500781833133, 2000.

Arcone, S. A., Lawson, D. E., and Delaney, A. J.: Short-pulse radar wavelet recovery and resolution of dielectric contrasts within englacial and basal ice of Matanuska Glacier, Alaska, U.S.A., Journal of Glaciology, 41, 68–86, https://doi.org/10.1017/S0022143000017779, 1995.

Bælum, K. and Benn, D. I.: Thermal structure and drainage system of a small valley glacier (Tellbreen, Svalbard), investigated by ground penetrating radar, The Cryosphere, 5, 139–149, https://doi.org/10.5194/tc-5-139-2011, 2011.

Bartholomaus, T. C., Amundson, J. M., Walter, J. I., O'Neel, S., West, M. E., and Larsen, C. F.: Subglacial discharge at tidewater glaciers revealed by seismic tremor, Geophysical Research Letters, 42, 6391–6398, https://doi.org/10.1002/2015GL064590, http://doi.wiley.com/10.1002/2015GL064590, 2015.

Benn, D., Gulley, J., Luckman, A., Adamek, A., and Glowacki, P. S.: Englacial drainage systems formed by hydrologically driven crevasse propagation, Journal of Glaciology, 55, 513–523, https://doi.org/10.3189/002214309788816669, 2009.

Bingham, R. G., Nienow, P. W., Sharp, M. J., and Boon, S.: Subglacial drainage processes at a High Arctic polythermal valley glacier, Journal of Glaciology, 51, 15–24, https://doi.org/10.3189/172756505781829520, 2005.

Bingham, R. G., Hubbard, A. L., Nienow, P. W., and Sharp, M. J.: An investigation into the mechanisms controlling seasonal speedup events at a High Arctic glacier, Journal of Geophysical Research: Earth Surface, 113, 1–13, https://doi.org/10.1029/2007JF000832, 2008.

Boon, S. and Sharp, M.: The role of hydrologically-driven ice fracture in drainage system evolution on an Arctic glacier, Geophysical Research Letters, 30, 3–6, https://doi.org/10.1029/2003GL018034, 2003.

Booth, A. D., Clark, R., and Murray, T.: Semblance response to a ground-penetrating radar wavelet and resulting errors in velocity analysis, Near Surface Geophysics, 8, 235–246, https://doi.org/10.3997/1873-0604.2010008, 2010.

Bradford, J. H., Nichols, J., Harper, J. T., and Meierbachtol, T.: Compressional and EM wave velocity anisotropy in a temperate glacier due to basal crevasses, and implications for water content estimation, Annals of Glaciology, 54, 168–178, https://doi.org/10.3189/2013AoG64A206, 2013.

Catania, G. A. and Neumann, T. A.: Persistent englacial drainage features in the Greenland Ice Sheet, Geophysical Research Letters, 37, 1–5, https://doi.org/10.1029/2009GL041108, 2010.

Catania, G. A., Neumann, T. A., and Price, S. F.: Characterizing englacial drainage in the ablation zone of the Greenland ice sheet, Journal of Glaciology, 54, 567–578, https://doi.org/10.3189/002214308786570854, 2008.

Christianson, K., Jacobel, R. W., Horgan, H. J., Alley, R. B., Anandakrishnan, S., Holland, D. M., and DallaSanta, K. J.: Basal conditions at the grounding zone of Whillans Ice Stream, West Antarctica, from ice-penetrating radar, Journal of Geophysical Research: Earth Surface, 121, 1954–1983, https://doi.org/10.1002/2015JF003806, 2016.

Church, G., Bauder, A., Grab, M., Rabenstein, L., Singh, S., and Maurer, H.: Detecting and characterising an englacial conduit network within a temperate Swiss glacier using active seismic, ground penetrating radar and borehole analysis, Annals of Glaciology, 60, 193–205, https://doi.org/10.1017/aog.2019.19, 2019.

Church, G. J., Bauder, A., Grab, M., Hellmann, S., and Maurer, H.: High-resolution helicopter-borne ground penetrating radar survey to determine glacier base topography and the outlook of a proglacial lake, in: 2018 17th International Conference on Ground Penetrating Radar (GPR), pp. 1–4, IEEE, https://doi.org/10.1109/ICGPR.2018.8441598, 2018.

Cuffey, K. M. and Paterson, W. S. B.: The Physics of Glaciers, Fourth Edition, Academic Press, fourth edi edn., 2010.

Farinotti, D., Huss, M., Bauder, A., and Funk, M.: An estimate of the glacier ice volume in the Swiss Alps, Global and Planetary Change, 68, 225–231, https://doi.org/10.1016/j.gloplacha.2009.05.004, 2009.

Fountain, A. G. and Walder, J. S.: Water flow through temperate glaciers, Reviews of Geophysics, 36, 299–328, https://doi.org/10.1029/97RG03579, 1998.

Fountain, A. G., Jacobel, R. W., Schlichting, R., and Jansson, P.: Fractures as the main pathways of water flow in temperate glaciers, Nature, 433, 618–621, https://doi.org/10.1038/nature03296, 2005.

Fujita, S., Matsuoka, T., Ishida, T., Matsuoka, K., and Mae, S.: A summary of the complex dielectric permittivity of ice in the megahertz range and its applications for radar sounding of polar ice sheets, Physics of Ice Core Records, pp. 185–212, 2000.

Gimbert, F., Tsai, V. C., Amundson, J. M., Bartholomaus, T. C., and Walter, J. I.: Subseasonal changes observed in subglacial channel pressure, size, and sediment transport, Geophysical Research Letters, 43, 3786–3794, https://doi.org/10.1002/2016GL068337, 2016.

Glen, J. W. and Paren, J. G.: The Electrical Properties of Snow and Ice, Journal of Glaciology, 15, 15–38, https://doi.org/10.3189/S0022143000034249, 1975.

Grab, M., Bauder, A., Ammann, F., Langhammer, L., Hellmann, S., Church, G., Schmid, L., Rabenstein, L., and Maurer, H.: Ice volume estimates of Swiss glaciers using helicopter-borne GPR an example from the Glacier de la Plaine Morte, in: 2018 17th International Conference on Ground Penetrating Radar (GPR), pp. 1–4, IEEE, https://doi.org/10.1109/ICGPR.2018.8441613, 2018.

Gulley, J.: Structural control of englacial conduits in the temperate Matanuska Glacier, Alaska, USA, Journal of Glaciology, 55, 681–690, https://doi.org/10.3189/002214309789470860, 2009.

Gulley, J. and Benn, D. I.: Structural control of englacial drainage systems in Himalayan debris-covered glaciers, Journal of Glaciology, 53, 399–412, https://doi.org/10.3189/002214307783258378, 2007.

Gulley, J., Benn, D., Müller, D., and Luckman, A.: A cut-and-closure origin for englacial conduits in uncrevassed regions of polythermal glaciers, Journal of Glaciology, 55, 66–80, https://doi.org/10.3189/002214309788608930, 2009a.

Gulley, J., Benn, D., Screaton, E., and Martin, J.: Mechanisms of englacial conduit formation and their implications for subglacial recharge, Quaternary Science Reviews, 28, 1984–1999, https://doi.org/10.1016/j.quascirev.2009.04.002, 2009b.

Guo, L., Chen, J., and Lin, H.: Subsurface lateral preferential flow network revealed by time-lapse ground-penetrating radar in a hillslope, Water Resources Research, 50, 9127–9147, https://doi.org/10.1002/2013WR014603, http://doi.wiley.com/10.1002/2013WR014603, 2014.

Hansen, L. U., Piotrowski, J. A., Benn, D. I., and Sevestre, H.: A cross-validated three-dimensional model of an englacial and subglacial drainage system in a High-Arctic glacier, Journal of Glaciology, pp. 1–13, https://doi.org/10.1017/jog.2020.1, 2020.

Hart, J. K., Rose, K. C., Clayton, A., and Martinez, K.: Englacial and subglacial water flow at Skálafellsjökull, Iceland derived from ground penetrating radar, in situ Glacsweb probe and borehole water level measurements, Earth Surface Processes and Landforms, 40, 2071–2083, https://doi.org/10.1002/esp.3783, 2015.

Hewitt, I. J.: Seasonal changes in ice sheet motion due to melt water lubrication, Earth and Planetary Science Letters, 371-372, 16–25, https://doi.org/10.1016/j.epsl.2013.04.022, http://dx.doi.org/10.1016/j.epsl.2013.04.022, 2013.

Hock, R., Iken, L., and Wangler, A.: Tracer experiments and borehole observations in the over-deepening of Aletschgletscher, Switzerland, Annals of Glaciology, 28, 253–260, https://doi.org/10.3189/172756499781821742, 1999.

Hooke, R. L. and Pohjola, V. A.: Hydrology of a segment of a glacier situated in an overdeepening, Storglaciaren, Sweden, Journal of Glaciology, 40, 140–148, 1994.

Huss, M. and Farinotti, D.: Distributed ice thickness and volume of all glaciers around the globe, Journal of Geophysical Research: Earth Surface, 117, 1–10, https://doi.org/10.1029/2012JF002523, 2012.

Iken, A. and Bindschadler, R. A.: Combined measurements of Subglacial Water Pressure and Surface Velocity of Findelengletscher, Switzerland: Conclusions about Drainage System and Sliding Mechanism, Journal of Glaciology, 32, 101–119, https://doi.org/10.3189/S0022143000006936, 1986.

Iken, A., Fabri, K., and Funk, M.: Water storage and subglacial drainage conditions inferred from borehole measurements on Gornergletscher, Valais, Switzerland, Journal of Glaciology, 42, 233–245, 1996.

Irvine-Fynn, T. D. L., Moorman, B. J., Williams, J. L. M., and Walter, F. S. A.: Seasonal changes in ground-penetrating radar signature observed at a polythermal glacier, Bylot Island, Canada, Earth Surface Processes and Landforms, 31, 892–909, https://doi.org/10.1002/esp.1299, http://doi.wiley.com/10.1002/esp.1299, 2006.

King, E. C., Woodward, J., and Smith, A. M.: Seismic evidence for a water-filled canal in deforming till beneath Rutford Ice Stream, West Antarctica, Geophysical Research Letters, 31, 4–7, https://doi.org/10.1029/2004GL020379, 2004.

Langhammer, L., Rabenstein, L., Bauder, A., and Maurer, H.: Ground-penetrating radar antenna orientation effects on temperate mountain glaciers, Geophysics, 82, H15–H24, https://doi.org/10.1190/geo2016-0341.1, 2017.

Lindner, F., Walter, F., Laske, G., and Gimbert, F.: Glaciohydraulic seismic tremors on an Alpine glacier, The Cryosphere Discussions, pp. 1–32, https://doi.org/10.5194/tc-2019-155, 2019.

Lliboutry, L.: Permeability, Brine Content and Temperature of Temperate Ice, Journal of Glaciology, 10, 15–29, https://doi.org/10.1017/S002214300001296X, 1971.

Macgregor, J. A., Anandakrishnan, S., Catania, G. A., and Winebrenner, D. P.: The grounding zone of the Ross Ice Shelf, West Antarctica, from ice-penetrating radar, Journal of Glaciology, 57, 917–928, https://doi.org/10.3189/002214311798043780, 2011.

Mercanton, P.: Vermessungen am Rhonegletscher/ Mensuration au glacier du Rhone: 1874-1915., vol. 52, Zürcher & Furrer, 1916.

Moorman, B. J. and Michel, F. a.: Glacial hydrological system characterization using ground-penetrating radar, Hydrological Processes, 14, 2645–2667, https://doi.org/10.1002/1099-1085(20001030)14:15<2645::AID-HYP84>3.0.CO;2-2, 2000.

Murray, T., Stuart, G. W., Gamble, N. H., and Crabtree, M. D.: Englacial water distribution in a temperature glacier from surface and borehole radar velocity analysis, Journal of Glaciology, 46, 389–398, https://doi.org/10.3189/172756500781833188, 2000.

Naegeli, K., Lovell, H., Zemp, M., and Benn, D. I.: Dendritic subglacial drainage systems in cold glaciers formed by cut-and-closure processes, Geografiska Annaler, Series A: Physical Geography, 96, 591–608, https://doi.org/10.1111/geoa.12059, 2014.

Nanni, U., Gimbert, F., Vincent, C., Gräff, D., Walter, F., Piard, L., and Moreau, L.: Quantification of seasonal and diurnal dynamics of subglacial channels using seismic observations on an Alpine glacier, Cryosphere, 14, 1475–1496, https://doi.org/10.5194/tc-14-1475-2020, 2020.

Nienow, P., Sharp, M., and Willis, I.: Temporal Switching Between Englacial and Subglacial Drainage Pathways: Dye Tracer Evidence from the Haut Glacier D'arolla, Switzerland, Geografiska Annaler: Series A, Physical Geography, 78, 51–60, https://doi.org/10.1080/04353676.1996.11880451, 1996.

Nienow, P., Sharp, M., and Willis, I.: Seasonal changes in the morphology of the subglacial drainage system, Haut Glacier d'Arolla, Switzerland, Earth Surface Processes and Landforms, 23, 825–843, https://doi.org/10.1002/(SICI)1096-9837(199809)23:9<825::AID-ESP893>3.0.CO;2-2, 1998.

Pettersson, R., Jansson, P., and Holmlund, P.: Cold surface layer thinning on Storglaciären, Sweden, observed by repeated ground penetrating radar surveys, Journal of Geophysical Research: Earth Surface, 108, n/a–n/a, https://doi.org/10.1029/2003JF000024, 2003.

Plewes, L. A. and Hubbard, B.: A review of the use of radio-echo sounding in glaciology, Progress in Physical Geography, 25, 203–236, https://doi.org/10.1177/030913330102500203, 2001.

Reynolds, J. M.: An Introduction to Applied and Environmental Geophysics, John Wiley & Sons, 2011.

Roethlisberger, H.: Seismic Exploration in Cold Regions, 1972.

Röthlisberger, H.: Water Pressure in Intra- and Subglacial Channels, Journal of Glaciology, 11, 177–203, https://doi.org/10.1017/S0022143000022188, 1972.

Russell, B. H.: Introduction to Seismic Inversion Methods, Society of Exploration Geophysicists, https://doi.org/10.1190/1.9781560802303, 1988.

Rutishauser, A., Maurer, H., and Bauder, A.: Helicopter-borne ground-penetrating radar investigations on temperate alpine glaciers: A comparison of different systems and their abilities for bedrock mapping, GEOPHYSICS, 81, WA119–WA129, https://doi.org/10.1190/geo2015-0144.1, 2016.

Sacchi, M. D.: Reweighting strategies in seismic deconvolution, Geophysical Journal International, 129, 651–656, https://doi.org/10.1111/j.1365-246X.1997.tb04500.x, 1997.

Schaap, T., Roach, M. J., Peters, L. E., Cook, S., Kulessa, B., and Schoof, C.: Englacial drainage structures in an East Antarctic outlet glacier, Journal of Glaciology, https://doi.org/10.1017/jog.2019.92, 2019.

Schmelzbach, C. and Huber, E.: Efficient deconvolution of ground-penetrating radar data, IEEE Transactions on Geoscience and Remote Sensing, 53, 5209–5217, https://doi.org/10.1109/TGRS.2015.2419235, 2015.

Schmelzbach, C., Tronicke, J., and Dietrich, P.: High-resolution water content estimation from surface-based ground-penetrating radar reflection data by impedance inversion, Water Resources Research, 48, 1–16, https://doi.org/10.1029/2012WR011955, 2012.

Seaberg, S. Z., Seaberg, J. Z., Hooke, R. L., and Wiberg, D. W.: Character of the Englacial and Subglacial Drainage System in the Lower Part of the Ablation Area of Storglaciären, Sweden, as Revealed by Dye-Trace Studies, Journal of Glaciology, 34, 217–227, https://doi.org/10.3189/S0022143000032263, 1988.

Shreve, R. L.: Movement of Water in Glaciers, Journal of Glaciology, 11, 205–214, https://doi.org/10.3189/S002214300002219X, 1972.

Stuart, G.: Characterization of englacial channels by ground-penetrating radar: An example from austre Brøggerbreen, Svalbard, Journal of Geophysical Research, 108, 2525, https://doi.org/10.1029/2003JB002435, 2003.

Temminghoff, M., Benn, D. I., Gulley, J. D., and Sevestre, H.: Characterization of the englacial and subglacial drainage system in a high Arctic cold glacier by speleological mapping and ground-penetrating radar, Geografiska Annaler, Series A: Physical Geography, 101, 98–117, https://doi.org/10.1080/04353676.2018.1545120, 2019.

Truss, S., Grasmueck, M., Vega, S., and Viggiano, D. A.: Imaging rainfall drainage within the Miami oolitic limestone using high-resolution time-lapse ground-penetrating radar, Water Resources Research, 43, 1–15, https://doi.org/10.1029/2005WR004395, http://doi.wiley.com/10.1029/2005WR004395, 2007.

Tsutaki, S., Sugiyama, S., Nishimura, D., and Funk, M.: Acceleration and flotation of a glacier terminus during formation of a proglacial lake in Rhonegletscher, Switzerland, Journal of Glaciology, 59, 559–570, https://doi.org/10.3189/2013JoG12J107, 2013.

van der Veen, C. J.: Fracture propagation as means of rapidly transferring surface meltwater to the base of glaciers, Geophysical Research Letters, 34, 1–5, https://doi.org/10.1029/2006GL028385, 2007.

Vatne, G.: Geometry of englacial water conduits, Austre Brøggerbreen, Svalbard, Norsk Geografisk Tidsskrift, 55, 85–93, https://doi.org/10.1080/713786833, 2001.

Velis, D. R.: Stochastic sparse-spike deconvolution, Geophysics, 73, R1–R9, https://doi.org/10.1190/1.2790584, 2008.

Vore, M. E., Bartholomaus, T. C., Winberry, J. P., Walter, J. I., and Amundson, J. M.: Seismic Tremor Reveals Spatial Organization and Temporal Changes of Subglacial Water System, Journal of Geophysical Research: Earth Surface, 124, 427–446, https://doi.org/10.1029/2018JF004819, 2019.

Warren, C., Giannopoulos, A., and Giannakis, I.: gprMax: Open source software to simulate electromagnetic wave propagation for Ground Penetrating Radar, Computer Physics Communications, 209, 163–170, https://doi.org/10.1016/j.cpc.2016.08.020, http://dx.doi.org/10.1016/j.cpc.2016.08.020, 2016.

Widess, M. B.: How thin is a bed?, Geophysics, 38, 1176–1180, https://doi.org/10.1190/1.1440403, 1973.

Zwally, H. J., Abdalati, W., Herring, T., Larson, K., Saba, J., and Steffen, K.: Surface melt-induced acceleration of Greenland ice-sheet flow, Science, 297, 218–222, https://doi.org/10.1126/science.1072708, 2002.

Supplement Figures: Monitoring the seasonal changes of an englacial conduit network using repeated ground penetrating radar measurements

Gregory Church[1,2], Melchior Grab[1,2], Cédric Schmelzbach[2], Andreas Bauder[1], and Hansruedi Maurer[2]

[1]Laboratory of Hydraulics, Hydrology and Glaciology (VAW), ETH Zurich, Zurich, Switzerland
[2]Institute of Geophysics, ETH Zurich, Zurich, Switzerland

Correspondence: Gregory Church (church@vaw.baug.ethz.ch)

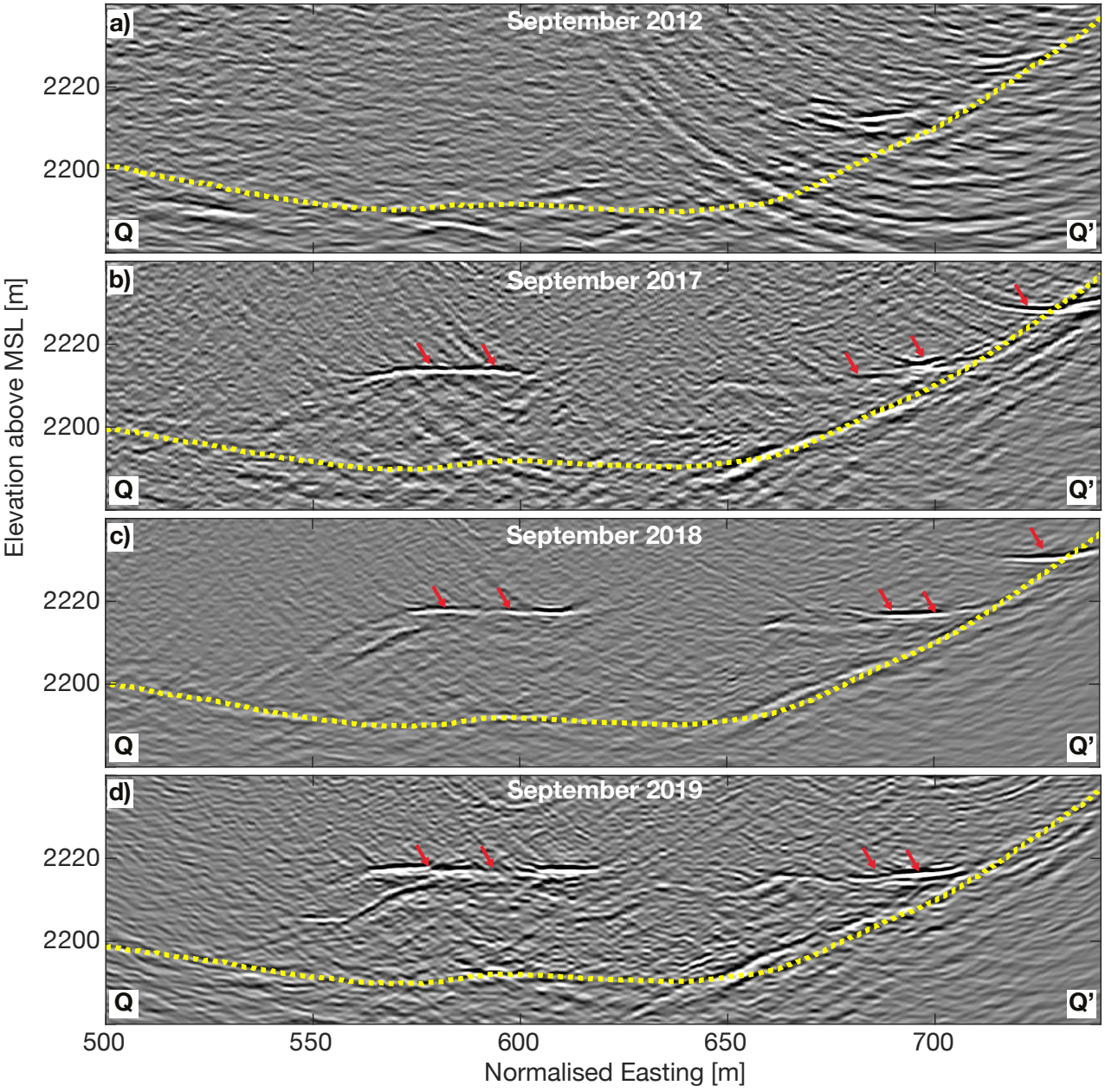

Figure S1. GPR imaging results from a repeated profile over a single line after migration from 2012 until 2019 showing zoomed in area of englacial conduit reflection. The yellow line represents the ice-bedrock interface and the red arrows represent the englacial conduit network reflection appearing from summer 2017.

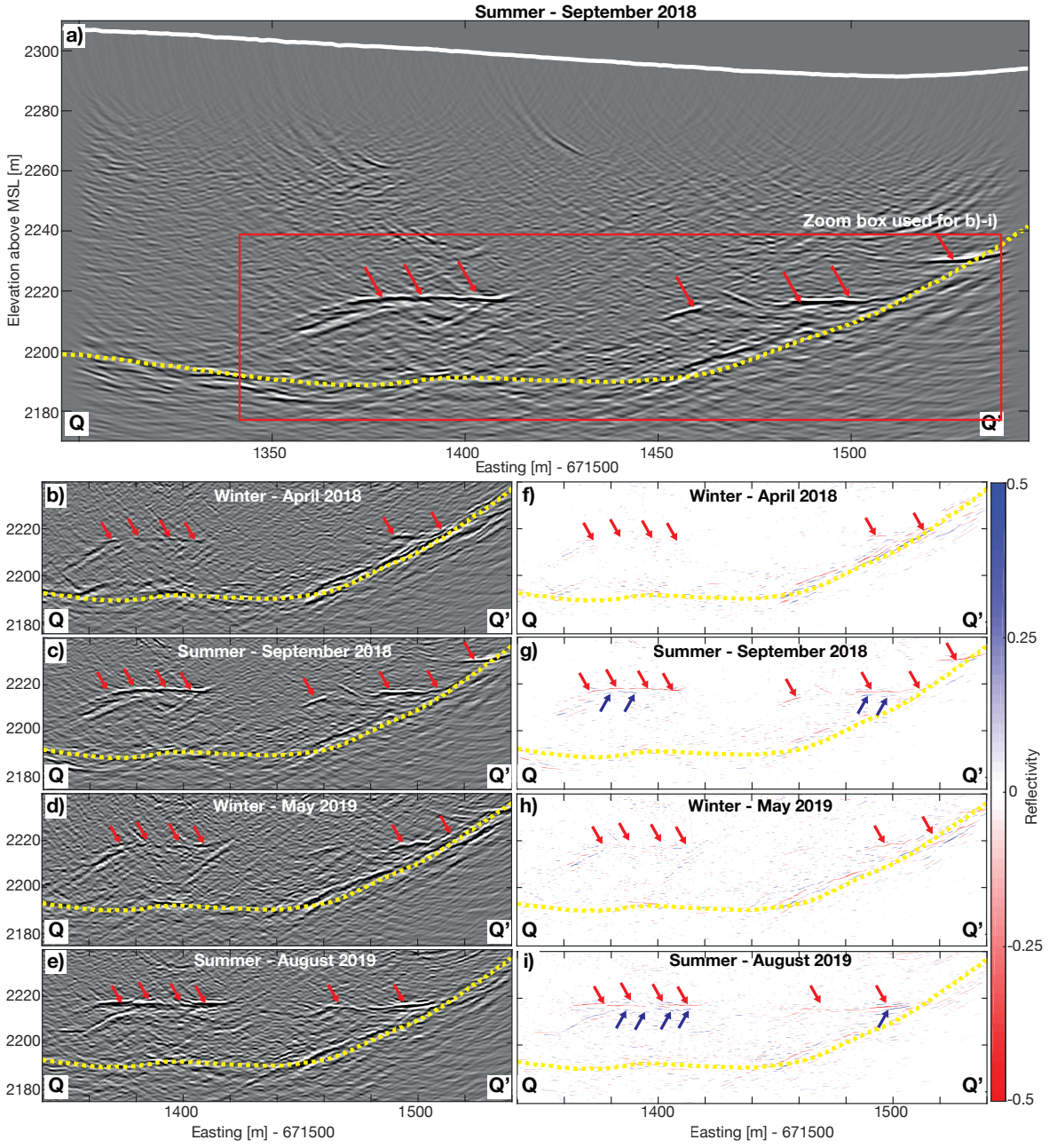

Figure S2. a) GPR imaging results over a single repeated GPR profile (Q-Q' in Fig. 1) in 2018. The yellow line represents the ice-bedrock interface, white line represents the glacier surface, and the red box is the zoom box for GPR imaging and reflectivity results b)-i). b)-e) are seasonal GPR imaging results and f)-i) are the seasonal GPR reflectivity results from b)-e). The red arrows represent the top of the englacial conduit network and the blue arrows represent the bottom of the englacial conduit network (g & i).

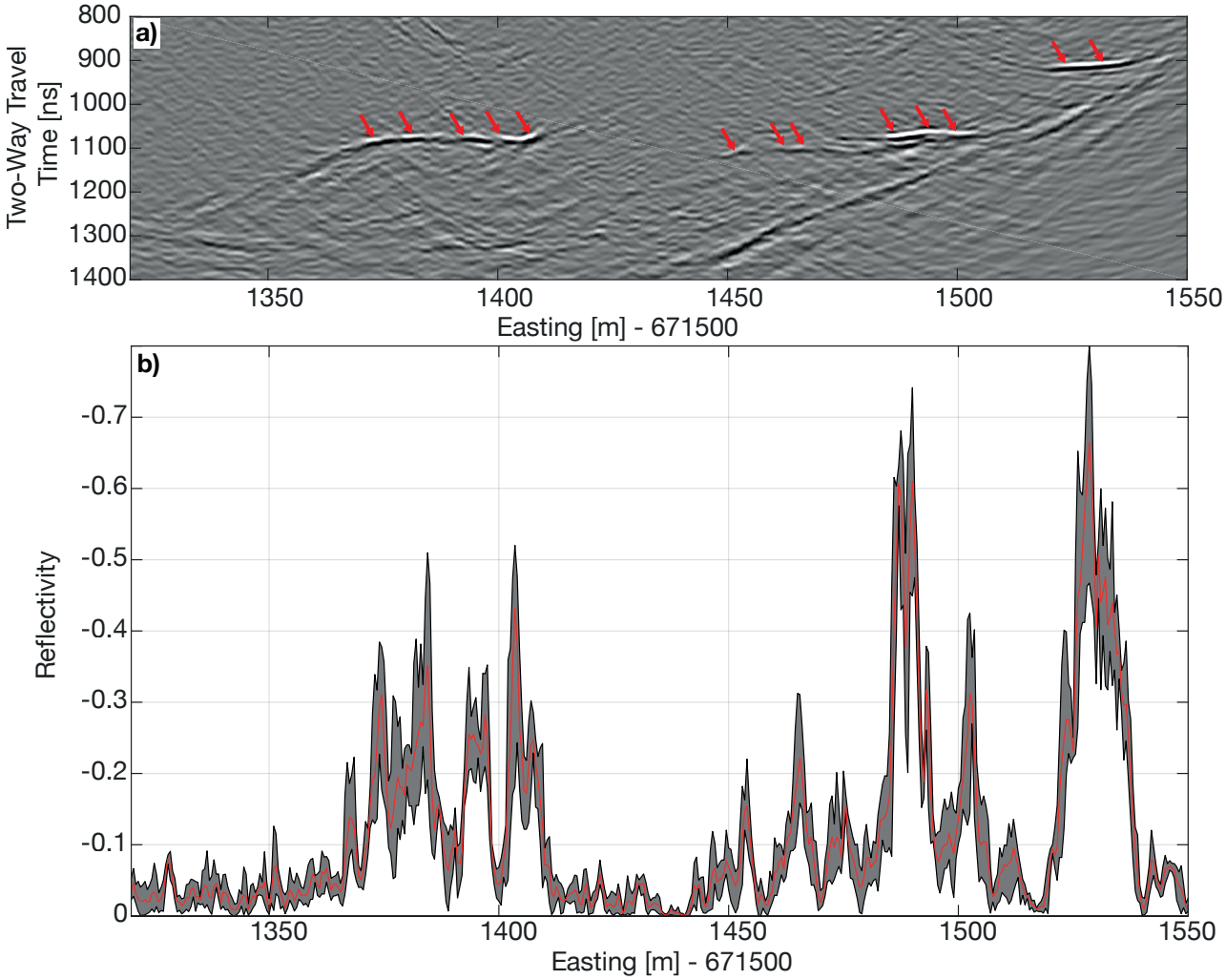

Figure S3. Uncertainty results from repeated GPR profiles undertaken in July 2018. a) GPR imaging result for repeated profile. b) Apparent reflectivity extracted from the GPR field data. The grey filled area represents the minimum and maximum reflectivity range from the four repeated profiles. The red line is the mean of the four profiles.

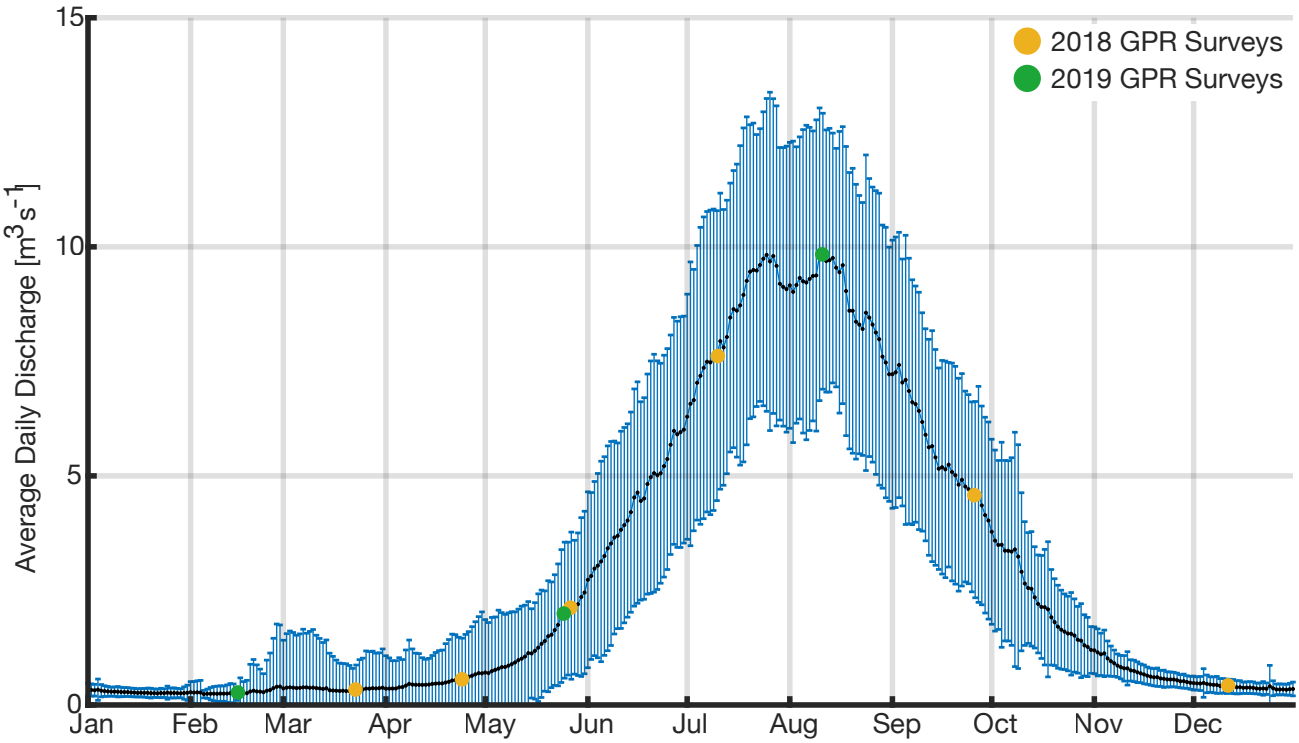

Figure S4. Average daily discharge measured in Gletsch (2 km downstream of Rhonegletscher) between 1957 and 2017. The error bars represent two standard deviations. The yellow and green dots represent the GPR survey dates for 2018 and 2019 respectively.

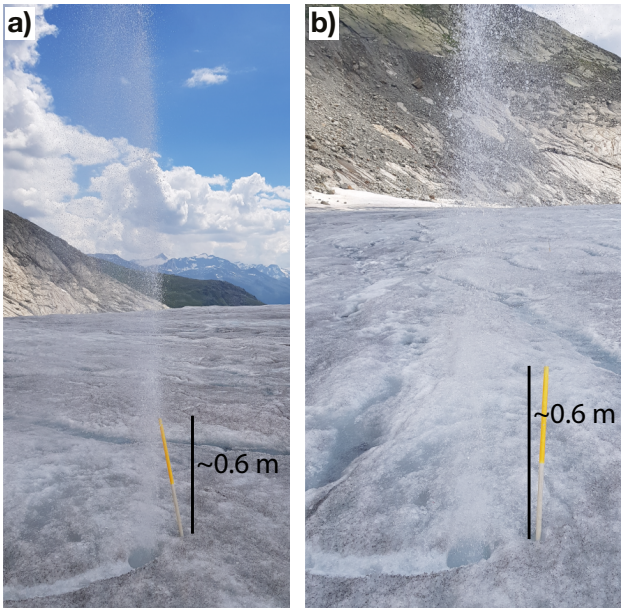

Figure S5. Borehole surface observations taken on 24th July 2018 showing water being forcibly spouted from the borehole head upto a height of approximately 4 m. Such observations were also recorded on 3rd August 2018.

Monitoring the seasonal changes of an englacial conduit network using repeated ground penetrating radar measurements

Gregory Church[1,2], Melchior Grab[1,2], Cédric Schmelzbach[2], Andreas Bauder[1], and Hansruedi Maurer[2]

[1]Laboratory of Hydraulics, Hydrology and Glaciology (VAW), ETH Zurich, Zurich, Switzerland
[2]Institute of Geophysics, ETH Zurich, Zurich, Switzerland

Correspondence: Gregory Church (church@vaw.baug.ethz.ch)

Abstract. Between 2012 and 2019, repeated 25 MHz ground penetrating radar (GPR) surveys were carried out over an active englacial conduit network within the ablation area of the temperate Rhonegletscher, Switzerland. In 2018 and 2019 the repetition survey rate was increased to monitor seasonal variations. The resulting GPR data were processed using an impedance inversion workflow to compute GPR reflection coefficients and layer impedances, which are indicative of the conduit's infill material. The spatial and temporal evolution of the reflection coefficients also provided insights into the morphology of the Rhonegletscher's englacial conduit network. During the summer melt seasons, we observed an active, water-filled, sediment-transporting englacial conduit network that yielded large negative GPR reflection coefficients (<-0.2). For all the GPR surveys conducted during the summer, the englacial conduit was 15-20 m wide, ~0.4 m thick, ~250 m long with a shallow inclination (2°) and having a sinusoidal shape. We speculate that such a geometry is likely the result of extensional hydraulic fracturing. Synthetic GPR waveform modelling using a thin water-filled conduit showed that a conduit thickness larger than 0.4 m (0.3 × minimum wavelength) thick can be correctly identified using 25 MHz GPR data. During the winter periods, the englacial conduit shuts down and either physically closed or becomes very thin (<0.1 m), thereby producing small negative reflection coefficients that are caused by either sediments lying within the closed conduit or water within the very thin conduit. Furthermore, the englacial conduit reactivated during the following melt season at an identical position as in the previous year.

1 Introduction

Surface meltwater is routed through the glacier's interior by englacial drainage systems, before it reaches subglacial drainage systems (Fountain and Walder, 1998; Cuffey and Paterson, 2010). Subglacial drainage systems play an important role on the dynamics of glaciers (Iken et al., 1996; Bingham et al., 2008). For example, high subglacial water pressure can lubricate the ice-bed interface, which may result in a faster sliding velocity (Iken and Bindschadler, 1986; Zwally et al., 2002). The subglacial water pressure can dramatically increase, when the drainage system does not adapt quickly enough, while surface meltwater is routed rapidly through the englacial drainage system. There is often a short time lag between the surface meltwater being present and the increase in glacier velocity (Bingham et al., 2005). Therefore, studying the seasonal evolution of an englacial drainage system throughout the melt season is key to understanding how and when they transport water to the subglacial drainage system.

Depending on the temperature of the ice, there exist different mechanisms for developing englacial drainage networks. Ice below the pressure melting point (cold ice) is impermeable and until recently it was assumed that surface melt water has limited penetration within cold-ice glaciers. However, recent research has provided evidence that surface-to-bed drainage networks are present in cold ice glaciers and they are formed by three distinct mechanisms (Benn et al., 2009; Gulley, 2009). The first mechanism includes surface melt water that creates incisions on the glacier's surface, and these surface streams can become englacial, if their upper levels becomes blocked or closes due to ice creep. Such englacial streams are known as 'cut-and-closure' conduits (Gulley et al., 2009a). The second mechanism for the formation of englacial conduits within cold ice, is hydraulically assisted fracture propagation (Boon and Sharp, 2003; van der Veen, 2007). Englacial conduits can develop from water filled crevasses where stressed ice and the water pressure within the fracture is large enough to overcome the fracture toughness of the surrounding ice. The third mechanism is related to the exploitation of permeable structures within the body of the glacier (Gulley et al., 2009a).

The englacial drainage network theory was originally developed for ice at the pressure melting point (temperate ice) (Shreve, 1972; Röthlisberger, 1972). Temperate ice was assumed to be permeable and this led to the theoretical model that englacial conduits form from water flowing between ice crystal boundaries within connected veins. As a result of theoretical challenges by Lliboutry (1971) and field observations by Gulley et al. (2009b) the formation mechanisms of englacial conduits within temperate ice has been questioned. As within cold ice, englacial conduits seem to form as a result of hydraulically assisted fracture propagation in temperate ice (Gulley, 2009). Additionally, englacial conduits can form from the exploitation of pre-existing fractures (Fountain et al., 2005; Gulley et al., 2009a).

There exist only a limited number of studies investigating englacial conduit conditions on temperate ice. Studies of glacier's drainage systems are based primarily on dye tracer experiments, speleology, borehole studies, geophysical measurements or a combination of these techniques. Englacial drainage systems have been interpreted from dye testing on temperate glaciers (Nienow et al., 1996, 1998; Hock et al., 1999), but difficulties arose, since tracer tests do not offer direct observations of englacial drainage networks. Direct observations have been made into inactive englacial channels using speleology techniques (Gulley, 2009; Naegeli et al., 2014; Temminghoff et al., 2019), but they were obviously conducted, only when the drainage system was dry and inactive.

Geophysical experiments can provide observations on active englacial conduit networks covering a large spatial distribution, and they can be repeated, thereby providing information on the temporal evolution. Ground-penetrating-radar (GPR) has been used to detect englacial drainage systems on cold ice (Moorman and Michel, 2000; Stuart, 2003; Catania et al., 2008; Catania and Neumann, 2010; Schaap et al., 2019; Hansen et al., 2020) and temperate ice (Arcone and Yankielun, 2000; Hart et al., 2015). Across several years, GPR measurements were performed by Bælum and Benn (2011) over a small cold-ice valley glacier to investigate the glacier's thermal regime. Pettersson et al. (2003) used time-lapse GPR, separated by 12 years, to detect changes to the cold-temperate ice transition surface and Irvine-Fynn et al. (2006) used repeated GPR measurements to investigate hydrological seasonal changes on a polythermal glacier. However, for these studies the GPR profiles were not repeated several times during a year and across a number of years. Therefore, very limited information is available on the seasonal evolution of englacial drainage systems on temperate glaciers.

In this study, we use a comprehensive GPR dataset that includes annual measurements from 2012, 2016, 2017 and seasonal measurements during 2018 and 2019. This facilitates studying the temporal and spatial changes of an englacial conduit network on a temperate glacier. By repeating GPR measurements several times throughout the melt seasons, we can gain insights into how an englacial network changes and evolves. Additionally, by performing GPR measurements across subsequent melt seasons, we can check, if these englacial networks were reactivated after the winter period in a similar location, or if they close down and become inactive the following melt season. We detect these seasonal and annual changes by extracting the GPR reflection strength (reflectivity) using a GPR impedance inversion scheme (Schmelzbach et al., 2012). The spatial extent of the reflectivity patterns allows potential englacial flow paths to be imaged. In brief, there are three main objectives of this research, namely

1. to implement a GPR processing routine to extract GPR reflection coefficients related to englacial structures,
2. to interpret the spatial reflection coefficients in order to gain an understanding of the temporal conduit morphology, and
3. to correlate the englacial conduit's dimensions to previous studies in order to understand the conduit's formation mechanisms.

Furthermore, using a GPR modelling algorithm, we are able to quantify the spatial dimensions of an active englacial conduit network.

2 Study Site

This englacial network monitoring case study was conducted on the Rhonegletscher (Fig. 1), where an englacial conduit network was previously detected using active seismic reflection data (Church et al., 2019). The Rhonegletscher is the sixth largest glacier in the Swiss Alps (Farinotti et al., 2009), and it is the source of the Rhone river. The glacier has been well studied and documented due to the ease of access from the nearby Furka pass, with the first measurements from the beginning of the 17th century (Mercanton, 1916). The glacier flows southwards from 3600 down to 2200 m above sea level (asl) with a surface area of approximately 16 km^2 (Huss and Farinotti, 2012). In recent years, a proglacial lake formed as a result of the glacier retreating (Tsutaki et al., 2013; Church et al., 2018). This proglacial lake is dammed by a granite riegel, and there is likely a hydraulic interaction between the lake and the glacier's drainage network. The survey site was located within the lower ablation area between 2280 m and 2350 m asl, where the ice thickness in 2017 was approximately 100 m (Fig. 1).

3 Methods

3.1 GPR Data Acquisition

To investigate seasonal englacial conduit variations, we performed several GPR field campaigns from 2012 until 2019 (Table 1). Three GPR surveys, that covered a single profile across the survey site (Q-Q' in Fig. 1), were conducted over three different

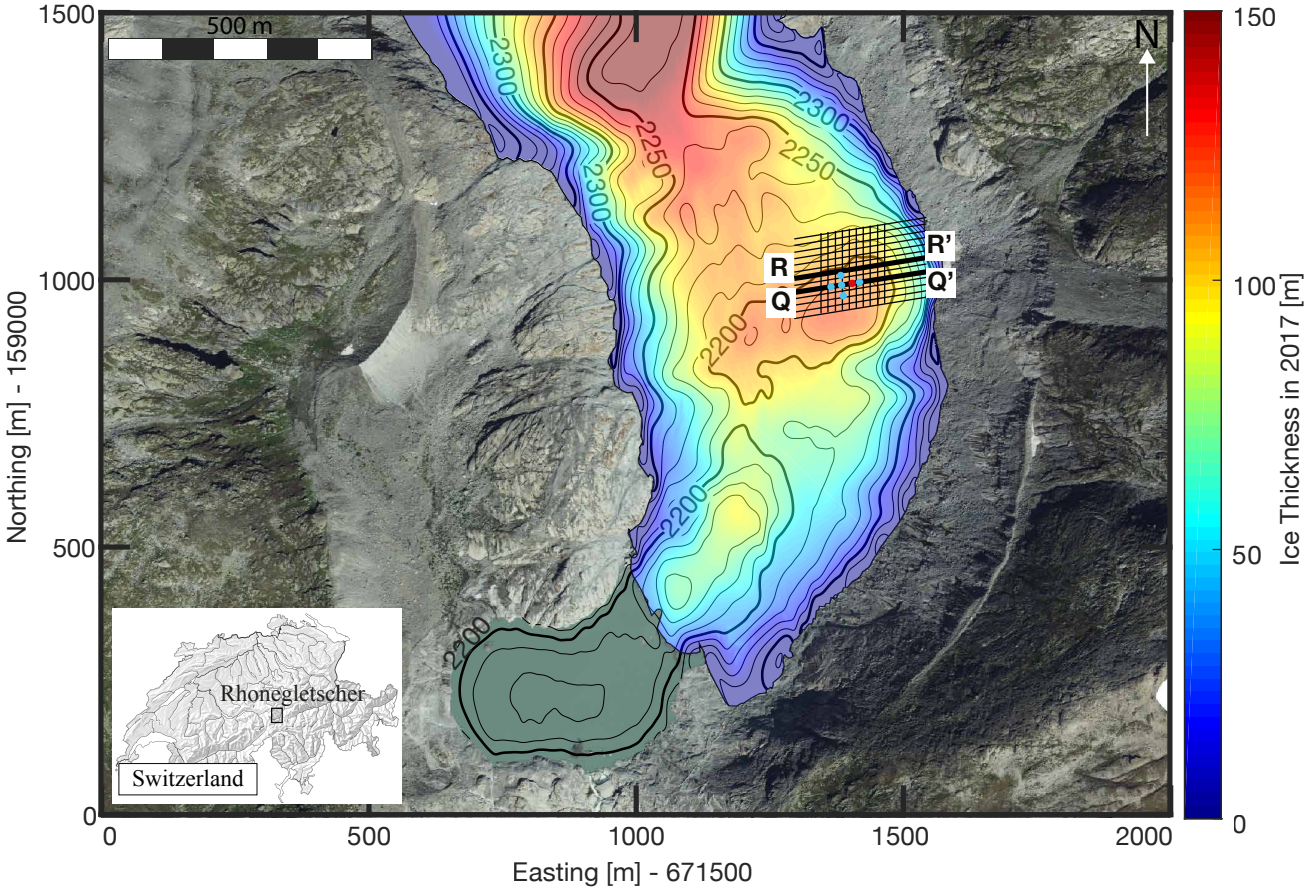

Figure 1. Map of the Rhonegletscher's lower ablation area, ice thickness (colour-coding), basal topography (black contour lines) updated from Church et al. (2018) and GPR repeated survey site (black grid). The two thicker GPR profile lines (R-R' and Q-Q') are displayed in Fig. 3 and Fig. 4. Five boreholes were drilled in August 2018 to provide ground-truths on the conduit and are marked as blue and red dots. The red dot represents the borehole where the borehole camera acquired a video.

years (2012, 2016 and 2017) . Upon detection of the englacial conduit network in 2017 (Church et al., 2019), we performed a dense GPR grid at different times of the year in 2018 and 2019 over the englacial conduit network (grids of black lines in Fig. 1). The GPR grid includes 13 profiles oriented east-west (average length: 250 m) and 10 profiles oriented north-south (average length: 150 m), with a spacing of 13 m between adjacent profiles.

All field measurements were conducted as common offset (CO) surveys using a Sensor & Software pulseEKKO Pro GPR system with 25 MHz antennas. The GPR antennas were carried by hand during summer month acquisitions (snow-free, June-October) and during winter month acquisitions (snow covered, November-May), they were mounted and pulled on pulk sleds. The GPR antennas were positioned in a transverse electric (TE) broadside configuration and kept at a constant offset of 4 m between transmitting and receiving antennas. Additionally, the orientation of the antennas were perpendicular to the

Table 1. Overview of the GPR surveys acquired over the englacial conduit network. Survey months in italic and bold represent winter (snow covered) and summer (snow free) acquisition respectively and the asterisk marks the months where common midpoint measurements were additionally acquired.

Year	No. of surveys	Time of Year	Survey Type
2012	1	**Sep**	Single Profile
2016	1	*Apr*	Single Profile
2017	1	**Sep**	Single Profile
2018	7	*Mar*, *Apr**, *May**, **Jul**, **Sep***, **Oct***, *Dec*	Grid
2019	3	*Feb*, *May*, **Aug**	Grid

walking direction. For all GPR lines, a high precision global navigation satellite system (GNSS) continuously recorded the GPR antennas mid-point and the accuracy given by the GNSS was generally below 0.05 m.

In addition to the CO profiles, we acquired common midpoint (CMP) data in order to evaluate the electromagnetic (EM) wave velocity of the glacial ice. These CMP measurements were performed in April, May, September and October 2018 over the englacial conduit in order to detect any seasonal changes to the EM-wave velocities.

3.2 Borehole Data Acquisition

In 2018, six boreholes were drilled around the englacial conduit network (Fig. 1) using a hot water drill. Two boreholes were drilled directly into the conduit network, and we were able to lower a borehole camera (GeoVISION^{TM} Dual-Scan) within these boreholes to make direct observations within the englacial conduit network.

3.3 GPR Data Processing

The raw CO GPR data were processed using a combination of an in-house MATLAB based toolbox (GPRglaz Rutishauser et al. (2016); Langhammer et al. (2017); Grab et al. (2018)) and Seismic Unix. The processing scheme aims to recover the GPR reflection coefficients from the englacial conduit reflections by means of an impedance inversion scheme. This inversion scheme is based upon the seismic impedance inversion developed in the late 1970s and 1980s (Russell, 1988). The reflectivity is recovered by the inversion on pre-conditioned GPR data using the underlying assumption that the GPR reflectivity is represented by a series of sparsely distributed spikes, this inversion is known as a sparse-spiking deconvolution (Velis, 2008). The aim of the sparse-spiking deconvolution operator is to find the smallest number of spikes that, after convolution with the GPR source wavelet, matches the pre-conditioned GPR data within a small error. Within a glaciological setting, the spikes from the deconvolution would represent englacial reflectors or the glacier base. The workflow implemented was based upon the processing described in Schmelzbach et al. (2012).

Table 2. Common offset GPR processing workflow

	Processing Step	Comments
1.	Merge GPR and GNSS data	
2.	Set time zero and record length	2000 ns (~170 m depth of penetration in ice)
3.	Interpolate clipped GPR data	
4.	Butterworth bandpass filter	10-75 MHz
5.	Trace Binning along profile	Binned to 0.5 m spacing
6.	Elevation static correction	
7.	Amplitude corrections	Summer α = 0.0007, winter α = 0.0004 (see Schmelzbach et al. (2012) for details)
8.	GPR deconvolution	Schmelzbach and Huber (2015)
9.	Phase Shift Migration	Seismic Unix migration and constant velocity of 0.1689 m ns^{-1}
10.	Amplitude matching between all GPR datasets	
11.	Sparse deconvolution to recover reflectivity	Described in Sacchi (1997)
12.	Calibrate the reflectivity	Setting the reflectivity to be the ice-water reflectivity at the borehole site in 2018
13.	Time to depth conversion	Constant velocity 0.1689 m ns^{-1}

An outline of the GPR CO processing is described in Table 2. It consists of the following major steps: (1-6) pre-processing by assigning the GNSS data with the GPR data, setting time zero and the record length, interpolating clipped data, bandpass filtering to remove noise, trace binning to account for varying walking speeds, elevation static correction, (7) deterministic amplitude correction to compensate for the amplitude decay due to gemoetrical spreading, absorption and transmission losses, (8) GPR deconvolution to remove the GPR source wavelet and increase the vertical resolution (Schmelzbach and Huber, 2015), (9) an amplitude preserving migration to re-position the reflections in their correct location and to increase the horizontal resolution, (10) identifying an amplitude matching scalar in order to match the amplitudes across all GPR surveys, (11-13) sparse-spike deconvolution to recover the reflectivity (Sacchi, 1997) and to calibrate the reflectivity and stretch the reflectivity to depth below glacier surface. In order to calibrate the reflectivity, ground truth data were used. The reflectivity within the vicinity of the borehole was calibrated to be the ice-water reflectivity as direct observations provided a flowing water-filled conduit (Church et al., 2019). The outcome of this workflow after migration (9) is shown in Fig. 2 and Fig. 3a-e. The final output (13), including the reflection coefficients, are displayed in Fig. 3f-i.

The spatial and temporal distribution of the reflection coefficients is the primary outcome of the processing workflow. The reflection coefficient explains the proportions of energy that are reflected from a given interface. Its values range between -1 and 1. Their magnitudes and polarities are indicative for the electrical material properties adjacent to an interface. Bælum and Benn (2011) divided the zero-offset (vertical incidence) reflection coefficients for glaciological environments into dry and wet groups (Table 3).

Table 3. GPR reflection coefficients from typical glaciological environments using zero-offset measurements (Bælum and Benn, 2011). Wet and dry environments are highlighted by dark grey and light grey cell shading respectively.

		Upper Medium	
		Ice	Water
Lower Medium	Ice	-	+0.67
	Air	+0.28	-
	Granite	-0.11	+0.6
	Wet Sand	-0.47	-
	Water	-0.67	-

The GPR reflection coefficient has previously been used in order to determine the presence of water or bed conditions on Matanuska Glacier in Alaska, USA (Arcone et al., 1995). In the Rhonegletscher case study, we will make use of the reflection coefficient for imaging the spatial extent and the temporal evolution of the englacial conduit, and it will also provide information, as to whether the conduit is dry or wet. Since the GPR antennas were constantly separated by 4 m, and the target was around 80-100 m below the glacier surface, the angle of incidence is less than 1 degree, and vertically incident waves can be assumed.

The CMP measurements were also processed using GPRglaz, but SeisSpace ProMAX 2-D was used for the velocity analysis. The pre-processing included assigning the geometry and amplitude correction for geometrical spreading. As described by Booth et al. (2010), we applied a static shift prior to picking the velocities in ProMAX in order to remove the systematic error in semblance analysis of GPR CMP data. The velocity determined from the CMP measurements (Fig. 4a and d) were used for the migration velocity in the workflow indicated in Table 2.

4 Results

4.1 GPR Imaging Results

For studying the general evolution of the englacial conduit network we analysed all GPR profiles, however we consider profile Q-Q' (Fig. 1) as an example for the annual evolution. In Fig. 2, the GPR sections acquired during the summer months are displayed. Due to the increased presence of water during the summer melt season, the signature of a potential englacial conduit is expected to be most pronounced during this time of the year. As shown in Fig. 2a, there is no clear englacial reflection visible in September 2012, but in September 2017, we observe a conspicuous reflection pattern at about 2210 m asl (Fig. 2b). This feature is also visible in the GPR sections acquired in summer 2018 and 2019 (Figs. 2c and 2d), although its shape and strengths exhibits some minor variations. From these observations we conclude that this englacial feature is recent, and it must have formed between 2012 and 2017.

Besides the general appearance of this englacial feature, it is also interesting to study its seasonal variability. We analysed all GPR profiles within the grid between 2018 and 2019, however, we consider profile R-R' (Fig. 1) as an example for the seasonal imaging results. In Fig. 3, the GPR sections, acquired in 2018 and 2019, are displayed. Additionally, the spatial distribution of the reflectivity (reflection coefficients) is provided. The single continuous englacial reflector is present across the majority of the acquired profile during the summer months (Fig. 3c and e), whereas in April 2018 (winter) it is almost absent (Fig. 3b), and its reflection strength is also reduced in May 2019 (winter) (Fig. 3d). The reflectivity (Fig. 3f-i) emphasises the contrasting englacial environment between summer and winter. Similar observations were also made in profile Q-Q' (not shown) and across the majority of GPR profiles acquired, but in profile R-R' they are slightly more pronounced.

4.2 GPR Common Midpoint Results

The CMPs were acquired in order to determine the EM wave propagation velocity through glacial ice for the CO phase shift migrations and to determine, if any seasonal variation exist. Four CMPs were acquired at different times of the year (Table 1), and the velocities were picked using semblance analysis from SeisSpace ProMAX 2-D. The location of the CMPs was directly over the englacial conduit (marked by the green line in Fig. 2c), where the conduit was a specular reflector showing little topography variation. Furthermore, prior to picking the velocities, the CMPs were backshifted by a quarter wavelength, as suggested by Booth et al. (2010).

The velocities were picked on the englacial reflection using a second order normal moveout correction. The EM wave propagation velocity for the winter CMP measurement (Fig. 4a) was picked on the semblance to be between 0.16 and 0.17 m ns^{-1} (Fig. 4b-c). The EM wave propagation velocity during the summer CMP measurement (October 2019) was between 0.165 and 0.175 m ns^{-1}. There exist some uncertainty as a result of limited transmitter-receiver offsets in comparison to the target depth (offset-depth ratio: 0.5), and the low frequency antenna with a dominant period of 15 ns create large semblance bullseyes in Figs. 4c and f. Two more CMP gathers were recorded in May and September 2019, which show a similar velocity, but with a larger uncertainty due to poorer data quality.

The EM wave propagation velocities within ice is a function of water content, and quoted values in literature are between 0.167 and 0.169 m ns^{-1} (Fujita et al., 2000; Murray et al., 2000; Plewes and Hubbard, 2001; Reynolds, 2011; Bradford et al., 2013). As a result of the uncertainties on the propagation velocities from the CMP measurements, the migration velocity was kept constant for both summer and winter at 0.169 m ns^{-1} as used in previous temperate ice GPR studies (Glen and Paren, 1975; Rutishauser et al., 2016).

4.3 GPR Seasonal Reflectivity Results

The reflectivity from the top of the englacial reflection was extracted (red arrows highlighting the negative reflectivity event in Fig. 3g), interpolated and smoothed for each seasonal GPR acquisition over the survey area. Figure 5 highlights the seasonal spatial reflectivity over 16 months from May 2018 until August 2019. The white lines in Fig. 5 correspond to isolines with reflectivity of -0.11, which correlates to the boundary between dry and wet glacial reflection environments (Table 3). During the

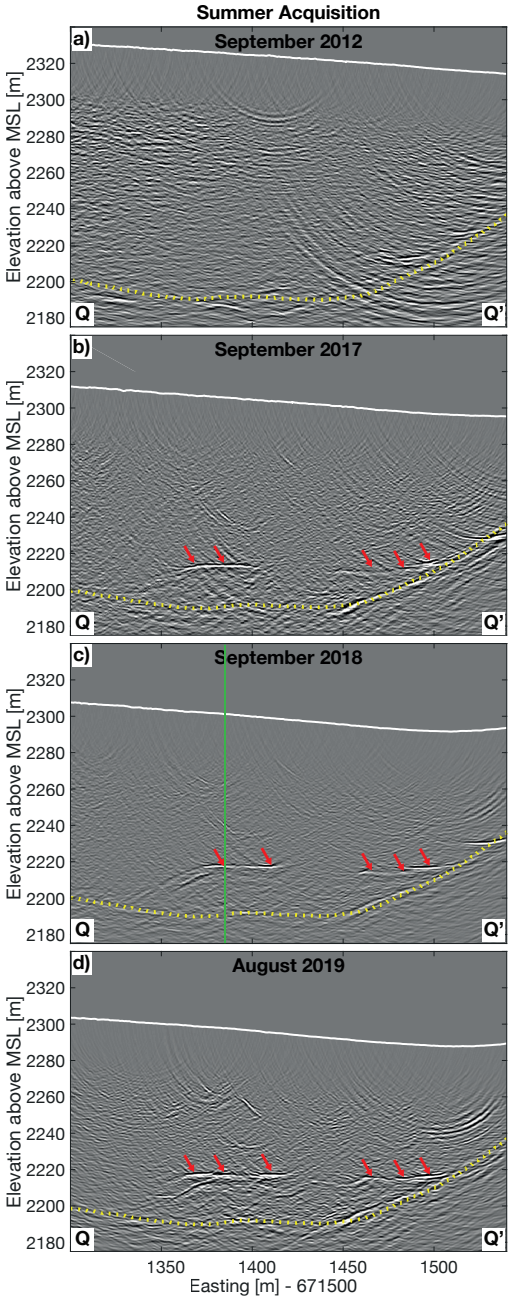

Figure 2. GPR imaging results from a repeated profile (Q-Q' in Fig. 1) over a single line after migration from 2012 until 2019. The yellow line represents the ice-bedrock interface and the red arrows represent the englacial conduit network reflection appearing from summer 2017. The green line in c) marks the location of the CMP acquired

f

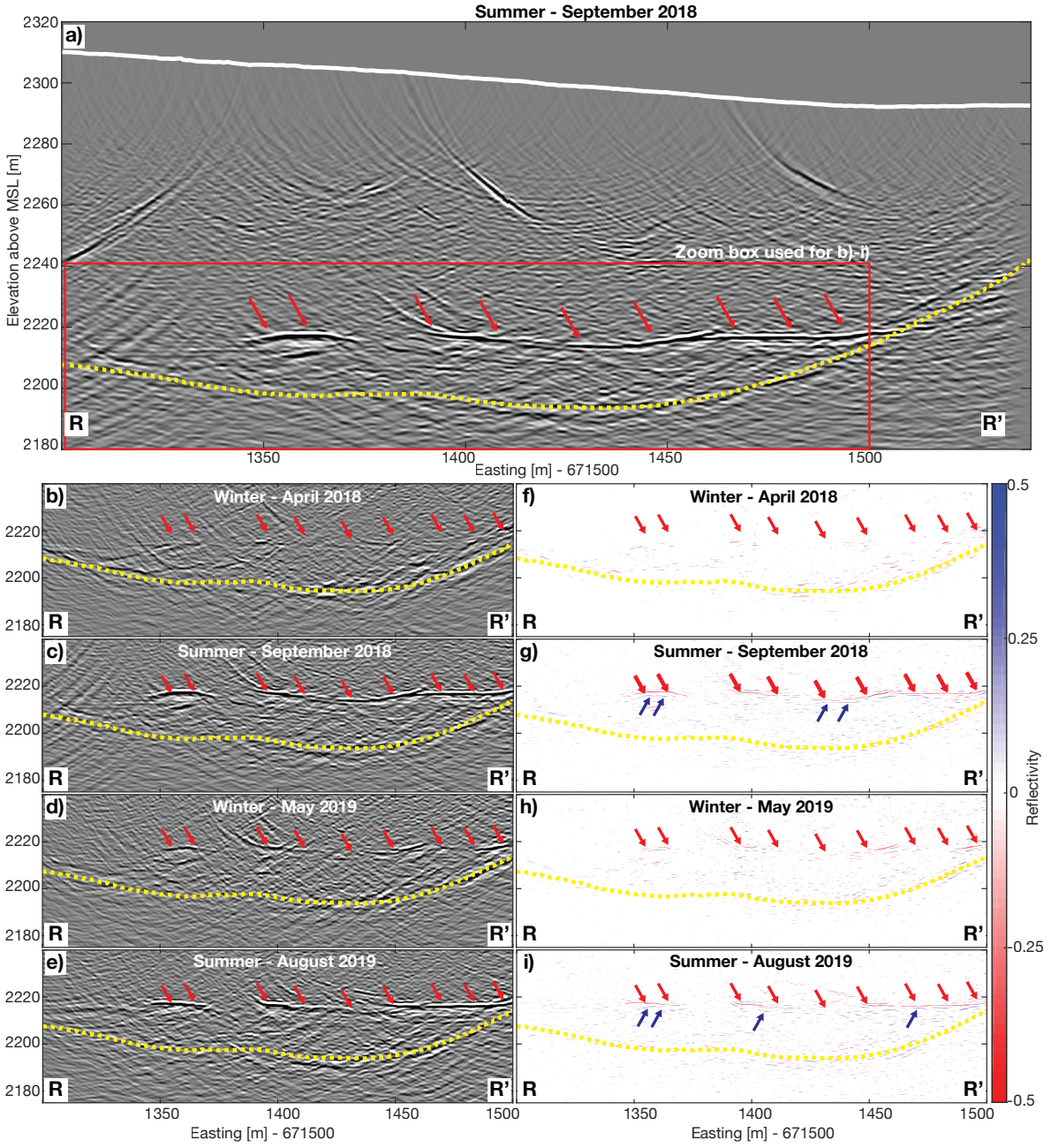

Figure 3. a) GPR imaging results over a single repeated GPR profile (R-R' in Fig. 1) in 2018. The yellow line represents the ice-bedrock interface, white line represents the glacier surface, and the red box is the zoom box for GPR imaging and reflectivity results b)-i). b)-e) are seasonal GPR imaging results and f)-i) are the seasonal GPR reflectivity results from b)-e). The red arrows represent the top of the englacial conduit network and the blue arrows represent the bottom of the englacial conduit network (g & i).

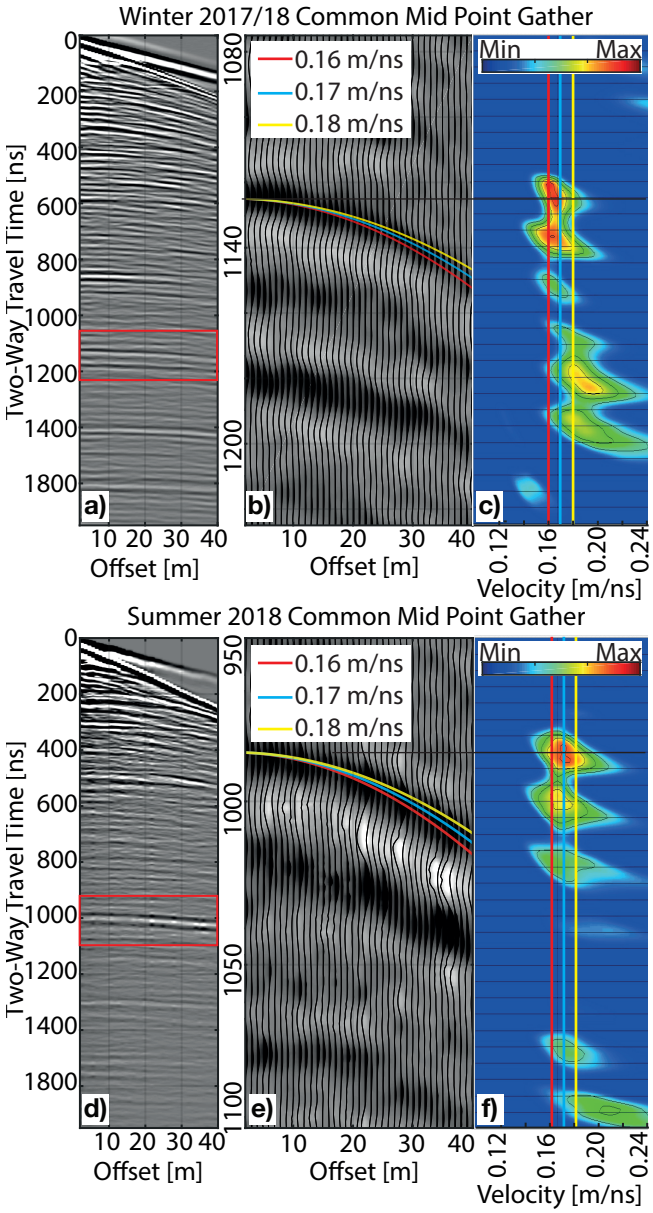

Figure 4. Common mid point gather and velocity determination. Winter (April 2018): a) The raw CMP gather. b) Zoom of the raw gather over the englacial reflection with second order normal moveout (NMO) curves using 0.16, 0.17 and 0.18 m ns^{-1}. c) Semblance display using second order NMO for the zoom section from b). Summer (October 2018): d)-f) as per winter a)-c).

summer months, when the englacial conduit is active and transporting melt water through the glacier's body we observe large negative reflectivities (<-0.2). The spatial extent of the englacial network is clearly visible in the summer months acquisition.

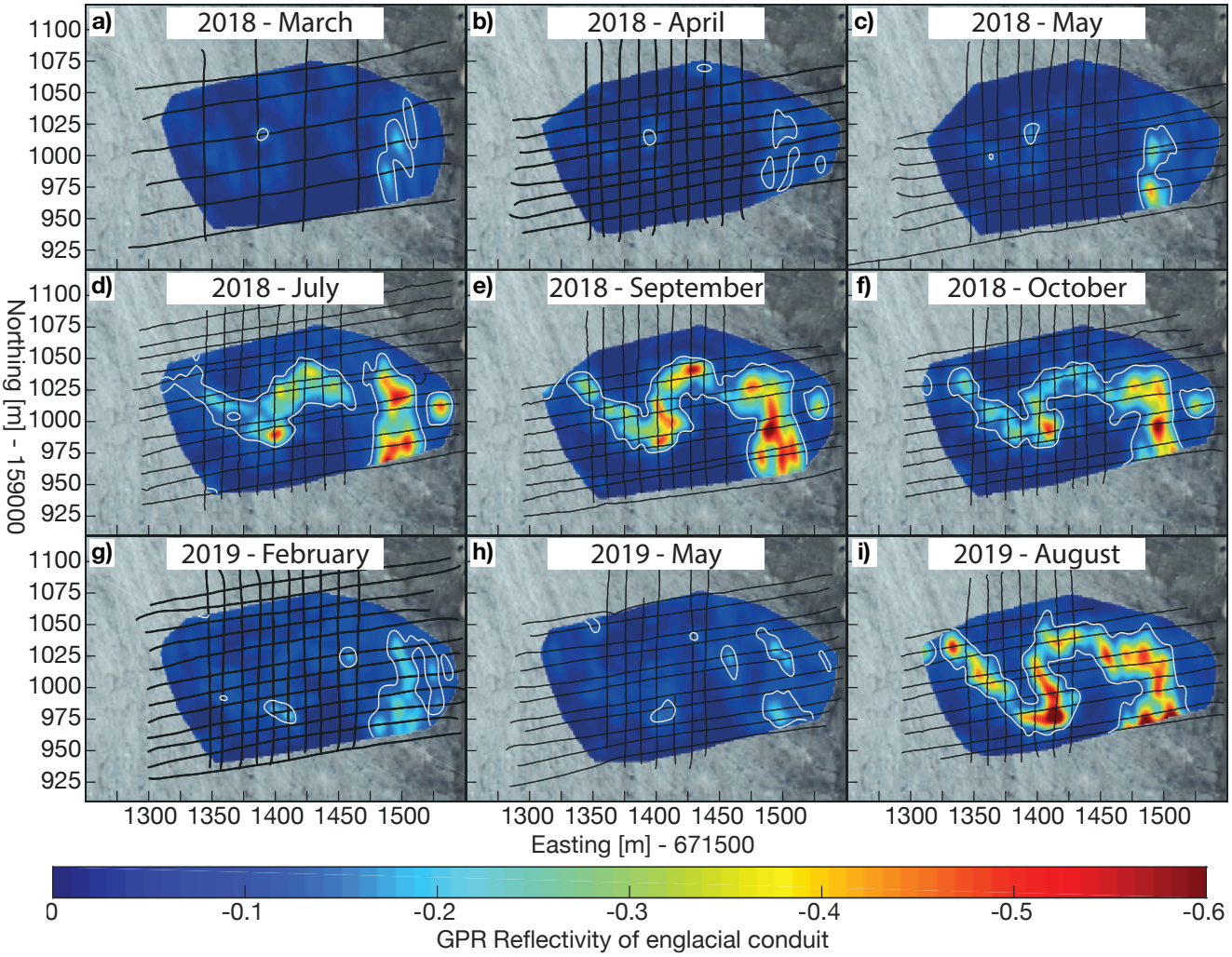

Figure 5. Seasonal GPR reflectivity from the top of the englacial channel reflection. The black grid lines represent the GPR acquisition profiles acquired for each month respectively. The white contour represents the reflectivity at -0.11.

The reflectivity during the winter months (Fig. 5a-c & g-h) is around zero indicating that the channel is not a wet environment. Whereas, during the summer months (Fig. 5d-f & i) the reflectivity varies between -0.2 and -0.6, corresponding to the wet reflectivity scenarios in Table 3. At the beginning of the melt season in July 2018 (Fig. 5d), the englacial conduit network does not appear to be fully developed and connected throughout the survey site, while in September and October 2018 (Fig. 5e & f), the conduit is connected across the survey site. Furthermore, in August 2019 (Fig. 5i), we observe wet-environment reflectivities in an identical location as in summer 2018.

4.4 GPR Conduit Thickness Results

In addition to the seasonal reflectivity results, the conduit thickness was calculated for those surveys, where top and bottom reflections could be identified clearly. The travel time differences between the top and bottom reflections was converted to thickness using the velocity of an EM wave travelling through water (0.0333 m ns^{-1}). Figure 3g and i shows a negative reflectivity for the top of the conduit (red arrows) and a positive reflectivity for the bottom of the conduit (blue arrows). Upon extraction of the conduit thickness, the spatial extent of the conduit thickness was determined by interpolating between the GPR profiles and smoothing (Fig. 6). The conduit thickness is between 0.2 and 0.5 m throughout the melt season (Fig. 6), and there is little variability in the conduit thickness throughout the summer.

Reynolds (2011) states that, in theory, the vertical resolution of a GPR signal is a quarter wavelength, assuming the source wavelet is two half cycles. This theory is based upon the seismic wave propagation theory as described by Widess (1973). In reality the GPR source wavelet is typically longer than a single wavelength, with this being the case, the vertical resolution is reduced as a result of the complex nature of the transmitted GPR source wavelet (Reynolds, 2011). For an EM wave propagating within a water-filled conduit the wavelength of a 25 MHz system is 1.333 m, and therefore the theoretical vertical resolution ($\lambda/4$) for a conduit filled with water using 25 MHz antennas is 0.33 m. The true conduit thickness can be determined from the reflectivity inversion if the thickness of the conduit is larger than the theoretical vertical resolution. The thicknesses shown in Fig. 5 are thus within proximity of the theoretical vertical resolution limit. Therefore, we performed a thin-layer forward modelling investigation, with which we tried to appraise the reliability and robustness of the thickness estimates.

4.5 Thin Channel Water Layer GPR Forward Modelling Results

A forward modelling approach was adopted in order to investigate how a thin water filled channel layer, below the theoretical vertical resolution, affects the observed thickness and reflectivity that we recover from the processing workflow described in Table 2. We generated synthetic radargrams using the open source software gprMax (Warren et al., 2016). This is a finite-difference time-domain solver for EM wave propagation. We employed a simple 3D model, as sketched in Fig. 7a. It includes a single thin water filled conduit that is invariable in the third dimension. The associated material parameters are summarised in Table 4. All four boundaries of the model had absorbing boundary conditions in order to prevent multiple energy interfering with the top and bottom reflection from the conduit. The synthetic GPR data (Fig. 7b) were modelled using transmitting and receiving antennas separated by 2 m, and they were moved from 2 until 18 m along the x axis in Fig. 7a at 0.5 m increments. The model space did not contain a free surface in order to have a clear interpretation of the top and bottom conduit reflector without any multiple energy being present.

The synthetic GPR data, shown in Fig. 7b, were generated with a 2 m thick water-filled englacial conduit, and the red and blue arrows represent the reflection from the top and bottom conduit respectively. There is clear separation between the top and bottom reflections from the conduit using a 2 m thick englacial conduit model, but, as shown in Figure 8, these two reflectors interfere with each other, when the conduit thickness reaches the vertical resolution (0.3 m in Fig. 8). The horizontal width of the water-filled conduit remained at 5 m for all tests and is below the horizontal resolution after migration. In order to

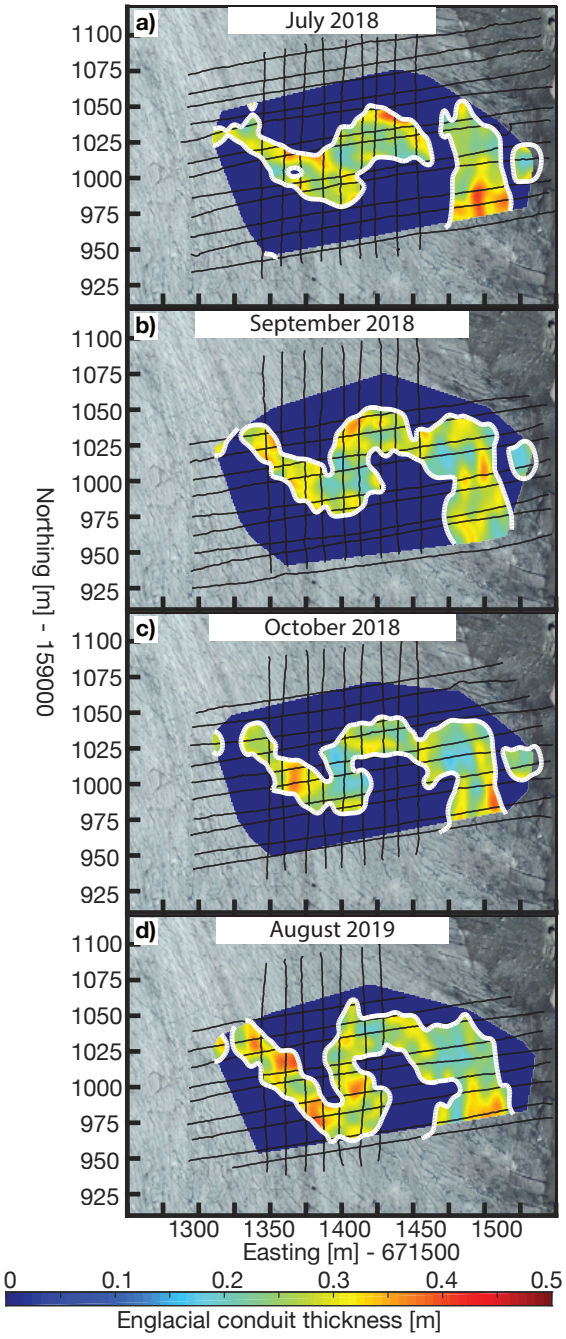

Figure 6. Estimated englacial conduit thickness during the summer months of (a-c) 2018 and (d) 2019.The white contour represents the englacial conduit reflectivity at 0.1, same contour as displayed in Fig. 5.

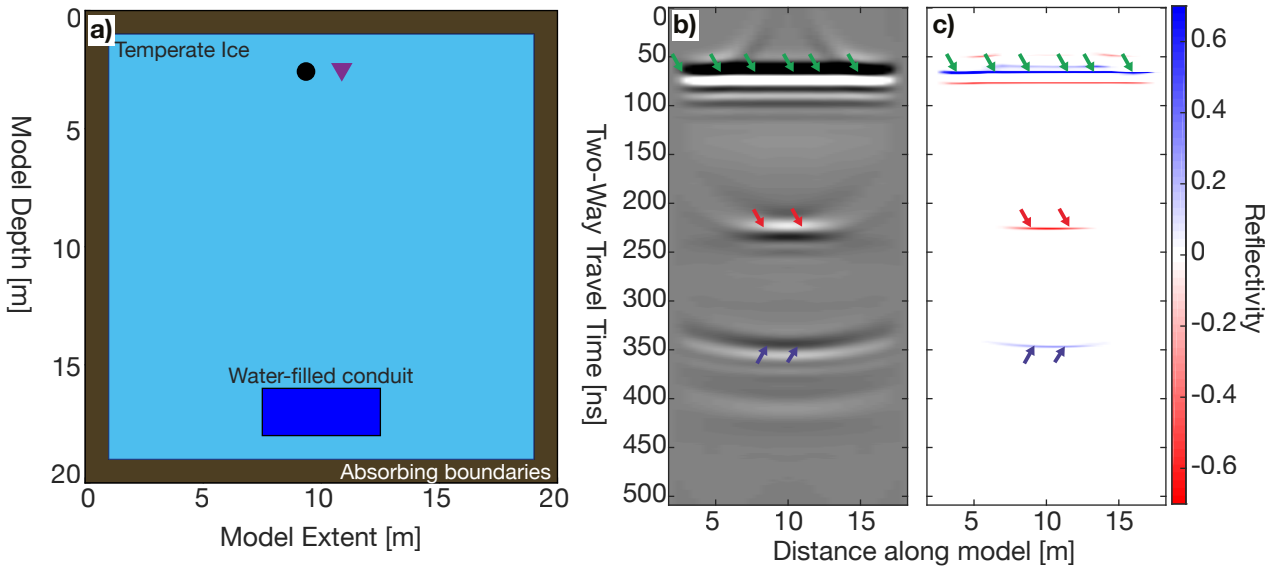

Figure 7. Forward modelling results. a) Geometry model for gprMax forward modelling with temperate ice, 2 m thick water-filled conduit and absorbing boundaries labelled. The circle and the triangle represent the transmitting and receiving antenna. b) The processed synthetic data generated from the model in a) after step 10 in Table 2. c) The reflectivity from the data b) after processing through the entire workflow described in Table 2. The green arrows represent the direct arrival, the red and blue represent the top and bottom reflection from the englacial conduit respectively.

extract the reflectivity (Fig. 7c and Fig. 8b) from the synthetic GPR data, the data were processed using an identical processing workflow, as applied to the field data.

The numerical simulations and thickness extraction procedures were repeated with a range of conduit thicknesses between 0.05 and 2 m. The results are shown in Fig. 9a. We were able to determine the correct conduit thickness, when the true thickness was greater than 0.4 m (0.3λ). However, when a water filled conduit was less than 0.4 m thick, the observed thickness from the inversion was within $\pm$0.15 m (yellow shaded area in Fig. 9a). In the summer, the majority of the Rhonegletscher imaged englacial conduit network is less than 0.4 m (Fig. 6) and therefore, the conduit thickness does not represent the true thickness but the calculated thickness is within $\pm$0.15 m of the actual conduit thickness.

In addition to the discrepancies between observed channel thickness and true channel thickness (Fig. 9a), the GPR zero-offset reflectivity can be analysed as a function of channel thickness (Fig. 9b). In order for the channel to have an ice-water reflectivity of -0.67 (Table 3) the conduit must be greater than 0.6 m thick (0.45λ), as represented by the green shaded area in Fig. 9b. When the conduit is between 0.1 and 0.6 m thick (0.07λ - 0.45λ), the calculated reflectivity is equal to the true reflectivity $\pm$ 0.1 (shaded yellow area in Fig. 9b). When the conduit is thinner than 0.1 m, the calculated reflectivity is below 0.5 (shaded red area in Fig. 9b). From these results, a likely explanation for the low reflectivities observed from the conduit (Fig. 5) could be the result of the conduit being below the vertical resolution.

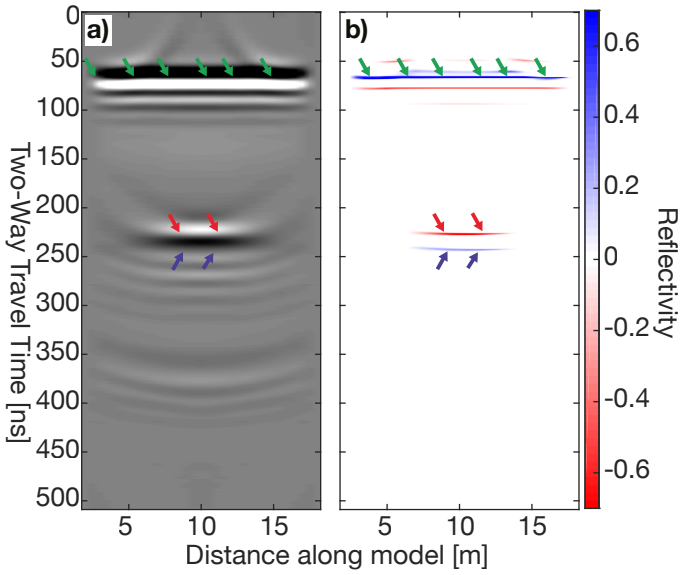

Figure 8. Forward modelling results for 0.3 m water-filled conduit. a) The processed synthetic data after step 10 in Table 2. c) The reflectivity from the data a) after processing through the entire workflow described in Table 2. The green arrows represent the direct arrival, the red and blue represent the interfering top and bottom reflection from the englacial conduit respectively.

Table 4. Material properties for the forward modelling, taken from (Plewes and Hubbard, 2001; Reynolds, 2011; Langhammer et al., 2017)

Material	Relative permittivity ϵ	Conductivity σ [S/m]	Relative permeability μ	Magnetic Loss [Ω/m] σ	Velocity [m/ns]
Temperate ice	3.2	$5e^{-8}$	1	0	0.1689
Fresh water	80	0.0005	1	0	0.033

5 Discussion

5.1 Conduit Extension

During the melt season (July-October), when the englacial conduit is active, the conduit is around 250 m in length and between 20-45 m wide. During all the summer acquisitions, the englacial conduit thickness was estimated to be between 0.2 and 0.4 m exhibiting little variability (Fig. 6). Therefore, the conduit was far wider than thick and it does not follow the typical cylindrical englacial conduit cross-sectional shape, as observed in other GPR surveys (Stuart, 2003), or as described by theory (Shreve, 1972; Roethlisberger, 1972).

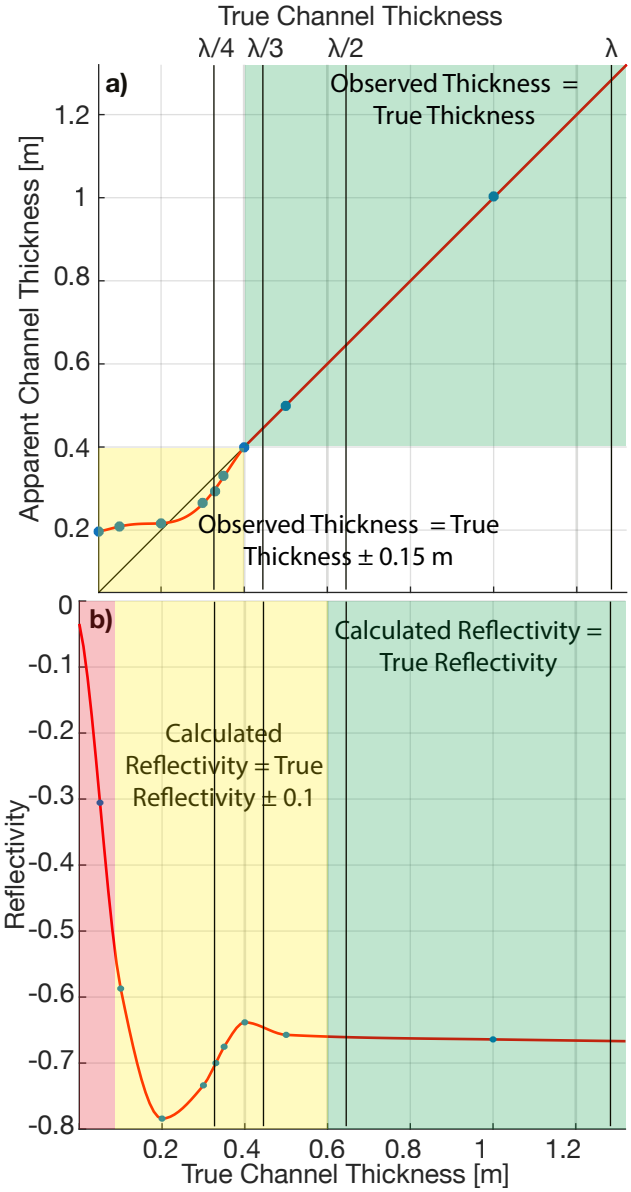

Figure 9. Forward modelling thickness and reflectivity results plotted against model conduit thickness. a) The observed thickness in the GPR inversion processing as a function of the true channel thickness in the model (Fig. 7a using 25 MHz antennas). b) The calculated reflectivity from the channel top as a function of the true channel thickness.

5.2 Conduit Inclination

There is a ten metre elevation difference in the conduit's topography (Fig. 10) across the entire imaged englacial conduit network, thereby indicating that the conduit has a low inclination (approximately 2°). It is similar to englacial conduits drainage networks found on a cold-ice glacier in Svalbard (Stuart, 2003; Hansen et al., 2020). Such a small dip provides evidence that the movement of englacial water is not related with the hydraulic gradients and therefore, does not supports the englacial conduit formation models described by Shreve (1972), which postulates englacial conduits formation through upward branching of an arborescent network.

5.3 Conduit Shape

The shape of the englacial conduit shows a sinusoidal outline that runs perpendicular to the ice flow direction. The outline (white contour in Fig. 6) has similar geometry to sub-sections of englacial conduits that have been mapped using speleology within cold glaciers (Gulley et al., 2009a), which have been formed as a result of the cut-and-closure mechanism. Similarly, a sinusoidal shape could result from turbulent water flowing englacially. To the best of our knowledge this is the first example of a temperate glacier to have an active englacial system surveyed using geophysical techniques and showing a sinusoidal shape.

5.4 Conduit Formation

The conduit's sinusoidal shape provides some evidence that this englacial drainage system could be the result of a cut-and-closure drainage system. However this hypothesis can be ruled out, as no large visible supraglacial stream has been observed on Rhonegletscher within the proximity of the englacial conduit in previous years. Moreover, comparing the conduit's profile and cross sections with those described by Gulley et al. (2009a) and summarised in Fig. 2 in their publication, the likely formation mechanism is extensional hydrofracturing. Hydrofracturing on extensional stressed glacial ice provides a horizontal profile (shallow dip) and an englacial conduit cross-section that is thin and wide. Such extensional stresses may result from the turning of the Rhonegletscher at the survey site towards the proglacial lake. As discussed in Church et al. (2019), the drainage network is likely fed from numerous streams running along the glacier margin and from the surrounding moraine. Additionally, the hydrofracturing can be supported by the fact that periods of high water pressure was observed as a result of the borehole expelling water 3-4 m above the glacier surface in August 2018.

We were unable to determine the flow direction from either the GPR data or from the borehole camera. Tracer studies might be an option (Hooke and Pohjola, 1994; Hock et al., 1999). Unfortunately, this would be difficult, as the studied englacial network is expected to flow into the proglacial lake, and therefore monitoring the tracer quantity would require samples to be taken directly from a borehole instead of an outflow stream from the glacier's tongue.

5.5 Conduit's Seasonal Variations

The conduit morphology alters throughout the year as a result of the varying discharge from the glacier. For a steady-state englacial conduit, where the conduits opening rates equals the conduits closure rate, the size and shape of the conduit re-

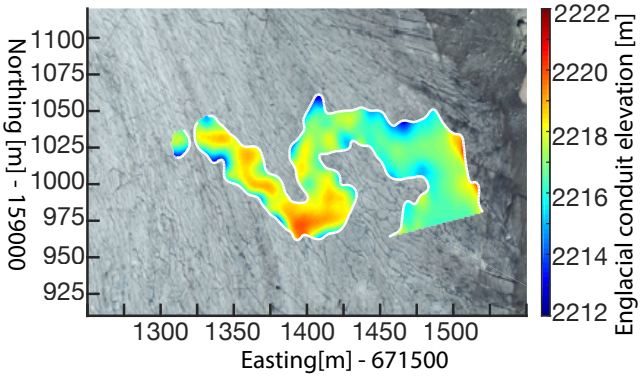

Figure 10. Elevation above mean sea level from the top of the englacial conduit network in August 2019.

mains constant. Changes in water supply can alter the opening and closure rates and thereby alter the conduit's morphology. Englacial conduits can shrink and disappear, when discharge quantities are low, whereas high discharge rates can cause a conduit to expand. Runoff and discharge data are available at a gauging station in Gletsch (1800 m a.s.l), 2 km downstream from Rhonegletscher. The peak discharge occurs annually between 24th July and 17th August. The end of the peak discharge correlates with the time of the year, where the conduit was well developed in 2019 (Fig. 6d). We can speculate that during August, when there are exist a large diurnal discharge fluctuations through the englacial conduit, the englacial network is fully developed. The timing further correlates with observations from other alpine glaciers, where subglacial drainage networks often switch from a distributed system to a channelised system in the peak of the melt season (Seaberg et al., 1988; Nienow et al., 1996).

There exists a winter shut-down of the englacial conduit network between 2018 and 2019, indicated by a near-zero reflectivity (Fig. 5e). Remnants of the englacial conduit is detectable on the winter reflectivity, when restricting the colour scale from -0.05 to -0.15 (Fig. 11, grey line). If the conduit is fully open (thickness > 0.5 m), then it is neither water or air filled during the winter as a large negative reflectivity (ice-water: -0.67) or positive reflectivity (ice-air: +0.3) is not observed. During August 2018, we were able to make direct borehole measurements using a borehole camera and observed sediment being transported along the base of the conduit (see video supplement). Therefore, as a result of the lower reflectivity and the lower discharge, we speculate that during winter the conduit either physically closes or becomes very thin (< 0.1 m) and remains water filled. If the conduit physically closes, the sediments lying within the closed conduit are likely the cause of the low winter reflectivity, and the reflectivity values around -0.1 indicate a dry glacial environment (Table 3). Whereas, if the conduit thinned to less than 0.1 m and remained water filled the reflectivity values are around -0.1 (red area in Fig. 9b). The repeated GPR summer measurements in 2018 and 2019 provided evidence that the conduit networks reopens in an identical location. In order for the conduit to be reactivated during the 2019 melt season, either the sediments lying within the closed during the winter months provided a potential permeable flow path in 2019, or the englacial conduit remained connected after becoming a very thin

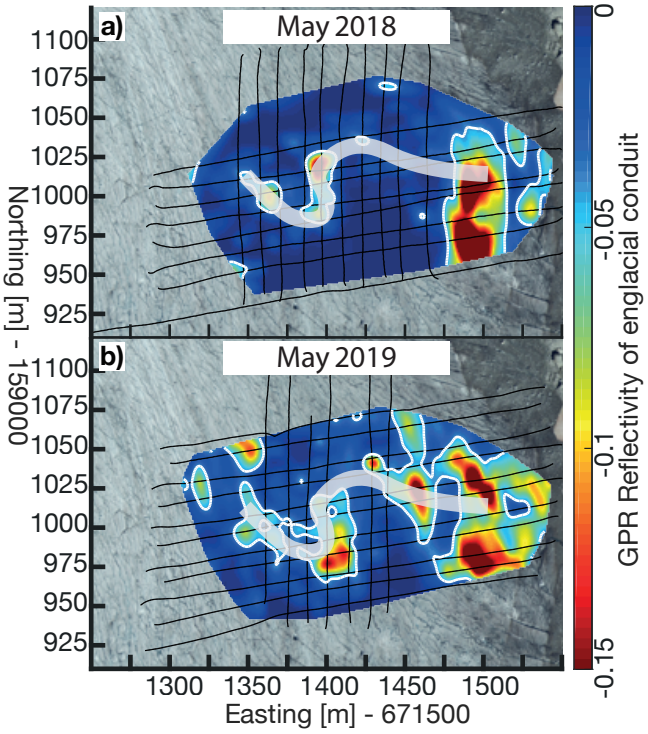

Figure 11. Winter GPR reflectivity from the top of the englacial channel reflection plotted between 0 and -0.15 reflectivity values, highlighting remnants of the englacial conduit network that exist during the winter months. The grey line represents the summer englacial conduit shape. The black grid lines represent the GPR acquisition profiles acquired for each month respectively. The white contour represents the reflectivity at -0.05.

water-filled (<0.1 m) conduit during the winter. Furthermore, we speculate that the hydraulic potential is similar during both melt seasons as the englacial conduit is reactivated in an identical position after the winter shutdown.

The GPR wavelet character from the conduit's top remains a constant negative high amplitude reflector over the three melt season (2017, 2018 and 2019), which indicates the presence of water within the system during our GPR summer acquisitions. From the GPR data, we are able to determine that the englacial conduit network is at or above atmospheric pressure. If the system would be below atmospheric pressure, the top reflector would be an interface between ice and air and result in a positive amplitude reflector. Such an unpressurised englacial network was observed by Stuart (2003), where the conduit's top reflection was a high positive amplitude reflector. The fact that the conduit is at or above atmospheric pressure is additionally supported by our borehole camera observations, where the borehole water level that was 1-2 m above the englacial network during observations, suggesting that the water pressure was slightly above atmospheric pressure.

5.6 General Applicability and Limitations of GPR to Characterise Englacial Conduits

So far, there exist a few studies, where englacial conduits have been characterised using a combination of GPR with speleology or borehole observations (Moorman and Michel, 2000; Stuart, 2003; Catania et al., 2008; Temminghoff et al., 2019; Schaap et al., 2019). In these studies, englacial conduits were imaged as point diffractors. Without speleology or boreholes, the interpretation of these point diffractors is typically ambiguous. In the Rhonegletscher case study, the interpretation is unambiguous with the ground-truth borehole observations, because the englacial conduit appears a single specular reflection.

For future studies investigating englacial conduits, the GPR reflectivity workflow can be used to identify englacial conduits and conditions on the glacier's bed, but it is essential to calibrate the observed reflectivities with known reflectivities on site. For the Rhonegletscher data, this was obtained from borehole observations. However, for others studies, a known reflectivity point may not be available in order to calibrate the reflectivity, and therefore by plotting the uncalibrated reflectivity of an englacial reflector potential flow paths could be delineated, however the filling material would remain unknown. Such an approach was adopted in Bælum and Benn (2011) (plotting the reflection normalised amplitude of the glacier's bed). The workflow could be extended to specular glacier basement reflectors in order to detect subglacial conduit networks. However, the GPR processing workflow does not correct for the anisotropic GPR radiation pattern. In this case, dipping specular reflectors will have amplitudes dependent on both the radiation pattern and the angle dependent reflection coefficient. Therefore an extension of the workflow needs to be made and a migration accounting for GPR antenna radiation pattern needs to be implemented prior to the impedance inversion in order to extract the reflectivity coefficient.

This study has also provided evidence that the glacier's bed needs to be interpreted with care. The Rhonegletscher case study has identified an englacial conduit as a specular reflector 10-15 m above the glacier's bed during the melt season. If a single GPR profile would have been acquired during the melt season (e.g. August 2019, Fig. 3e), the englacial conduit may have been mis-interpreted as the glacier bed. Therefore, it is essential to understand the hydrological conditions of the glacier, when designing GPR surveys in order to successfully interpret the GPR data. For GPR surveys, where the ice thickness is the objective on temperate alpine glaciers, then GPR acquisition should be undertaken during winter in order to minimise the englacial water storage limiting penetration depth. On the contrary, for GPR surveys investigating the glacier's hydrological conditions it is intuitive that acquisition should take place during summer.

From the forward modelling, the vertical resolution for GPR was found to be 0.3λ. If two interfaces are spaced less than $0.3\ \lambda$ metres vertically apart, then there exists interference between the two reflectors which leads to an erroneous thickness interpretation (Fig. 9). This GPR vertical resolution is larger than seismic vertical resolution found through forward modelling on ice-water reflectivities (King et al., 2004), as a result of the complex nature of the GPR source wavelet.

6 Conclusions

By using repeated GPR measurements and processing the data with an impedance inversion to extract the reflectivity, we have mapped the changing spatial extent and thickness of an active and dynamic englacial conduit network on a temperate glacier.

The repeated seasonal GPR measurements in 2018 and 2019 and the reflection coefficient analysis of the englacial conduit provided an insight into the evolution of an active englacial hydrological network.

In summer the englacial conduit was active, leading to large negative reflectivity values (<-0.2). The Rhonegletscher's englacial network followed a sinusoidal shape throughout the melt season. The conduit is 15-20 m wide and between 0.2 and 0.4 m thick. Such a conduit cross section (wide and thin) can occur as a result of hydraulic fracturing with extensional stresses acting on the ice, based upon the englacial conduit shape review by Gulley et al. (2009a). Furthermore, water flowing through the englacial conduit during the melt season feeds the subglacial drainage network, which likely increases subglacial water pressure and facilitates basal sliding.

The englacial conduit was found to be inactive during the winter period, with reflectivity values between -0.05 and -0.15. Therefore, we speculate that during the winter the conduit network either physically closes or is very thin (<0.1 m). Either, sediments that were being transported within the conduit in the summer or water within a thin-layer conduit are likely responsible for the reflectivity visible during the winter GPR acquisition. The englacial conduit became active in an identical location after a winter shut down. The conduit's shape remained similar in the winter compared to the summer.

Difficulties arise when interpreting a series of reflectors that are separated by the vertical resolution. The forward modelling has shown that two horizons are perfectly distinguishable when they are separated by more than 0.3λ. Whereas, the amplitude or reflectivity of the top interface is only resolved when the thickness is greater than 0.45λ. We conclude that care must be taken when inferring material properties from a reflectivity processing workflow with the presence of thin layers that approach the vertical resolution of the GPR source wavelet.

Video supplement. Movie S1 https://doi.org/10.3929/ethz-b-000406689 shows the borehole camera observations made directly into the active englacial conduit on 24th July 2018.

Author contributions. GC, MG, AB and HM designed the GPR experiments, which were carried out by GC and MG. GC processed the data with help from CS and all authors analysed the data. GC interpreted the data with help from all co-authors. GC wrote the manuscript with contributions from all co-authors.

Competing interests. The authors declare that they have no conflict of interest.

Acknowledgements. The Swiss National Science Foundation financed the project (SNF Grant 200021_169329/1). Data acquisition has been provided by the Exploration and Environment Geophysics (EEG) group and the Laboratory of Hydraulics, Hydrology and Glaciology (VAW) of ETH Zurich. The authors gratefully acknowledge the Landmark Graphics Corporation for providing data processing software through the Landmark University Grant Program. The authors wish to acknowledge all volunteers for their valuable help in participating the fieldwork.

References

Arcone, S. A. and Yankielun, N. E.: 1.4 GHz radar penetration and evidence of drainage structures in temperate ice: Black Rapids Glacier, Alaska, U.S.A., Journal of Glaciology, 46, 477–490, https://doi.org/10.3189/172756500781833133, 2000.

Arcone, S. A., Lawson, D. E., and Delaney, A. J.: Short-pulse radar wavelet recovery and resolution of dielectric contrasts within englacial and basal ice of Matanuska Glacier, Alaska, U.S.A., Journal of Glaciology, 41, 68–86, https://doi.org/10.1017/S0022143000017779, 1995.

Bælum, K. and Benn, D. I.: Thermal structure and drainage system of a small valley glacier (Tellbreen, Svalbard), investigated by ground penetrating radar, The Cryosphere, 5, 139–149, https://doi.org/10.5194/tc-5-139-2011, 2011.

Benn, D., Gulley, J., Luckman, A., Adamek, A., and Glowacki, P. S.: Englacial drainage systems formed by hydrologically driven crevasse propagation, Journal of Glaciology, 55, 513–523, https://doi.org/10.3189/002214309788816669, 2009.

Bingham, R. G., Nienow, P. W., Sharp, M. J., and Boon, S.: Subglacial drainage processes at a High Arctic polythermal valley glacier, Journal of Glaciology, 51, 15–24, https://doi.org/10.3189/172756505781829520, 2005.

Bingham, R. G., Hubbard, A. L., Nienow, P. W., and Sharp, M. J.: An investigation into the mechanisms controlling seasonal speedup events at a High Arctic glacier, Journal of Geophysical Research: Earth Surface, 113, 1–13, https://doi.org/10.1029/2007JF000832, 2008.

Boon, S. and Sharp, M.: The role of hydrologically-driven ice fracture in drainage system evolution on an Arctic glacier, Geophysical Research Letters, 30, 3–6, https://doi.org/10.1029/2003GL018034, 2003.

Booth, A. D., Clark, R., and Murray, T.: Semblance response to a ground-penetrating radar wavelet and resulting errors in velocity analysis, Near Surface Geophysics, 8, 235–246, https://doi.org/10.3997/1873-0604.2010008, 2010.

Bradford, J. H., Nichols, J., Harper, J. T., and Meierbachtol, T.: Compressional and EM wave velocity anisotropy in a temperate glacier due to basal crevasses, and implications for water content estimation, Annals of Glaciology, 54, 168–178, https://doi.org/10.3189/2013AoG64A206, 2013.

Catania, G. A. and Neumann, T. A.: Persistent englacial drainage features in the Greenland Ice Sheet, Geophysical Research Letters, 37, 1–5, https://doi.org/10.1029/2009GL041108, 2010.

Catania, G. A., Neumann, T. A., and Price, S. F.: Characterizing englacial drainage in the ablation zone of the Greenland ice sheet, Journal of Glaciology, 54, 567–578, https://doi.org/10.3189/002214308786570854, 2008.

Church, G., Bauder, A., Grab, M., Rabenstein, L., Singh, S., and Maurer, H.: Detecting and characterising an englacial conduit network within a temperate Swiss glacier using active seismic, ground penetrating radar and borehole analysis, Annals of Glaciology, 60, 193–205, https://doi.org/10.1017/aog.2019.19, 2019.

Church, G. J., Bauder, A., Grab, M., Hellmann, S., and Maurer, H.: High-resolution helicopter-borne ground penetrating radar survey to determine glacier base topography and the outlook of a proglacial lake, in: 2018 17th International Conference on Ground Penetrating Radar (GPR), pp. 1–4, IEEE, https://doi.org/10.1109/ICGPR.2018.8441598, 2018.

Cuffey, K. M. and Paterson, W. S. B.: The Physics of Glaciers, Fourth Edition, Academic Press, fourth edi edn., 2010.

Farinotti, D., Huss, M., Bauder, A., and Funk, M.: An estimate of the glacier ice volume in the Swiss Alps, Global and Planetary Change, 68, 225–231, https://doi.org/10.1016/j.gloplacha.2009.05.004, 2009.

Fountain, A. G. and Walder, J. S.: Water flow through temperate glaciers, Reviews of Geophysics, 36, 299–328, https://doi.org/10.1029/97RG03579, 1998.

Fountain, A. G., Jacobel, R. W., Schlichting, R., and Jansson, P.: Fractures as the main pathways of water flow in temperate glaciers, Nature, 433, 618–621, https://doi.org/10.1038/nature03296, 2005.

Fujita, S., Matsuoka, T., Ishida, T., Matsuoka, K., and Mae, S.: A summary of the complex dielectric permittivity of ice in the megahertz range and its applications for radar sounding of polar ice sheets, Physics of Ice Core Records, pp. 185–212, 2000.

Glen, J. W. and Paren, J. G.: The Electrical Properties of Snow and Ice, Journal of Glaciology, 15, 15–38, https://doi.org/10.3189/S0022143000034249, 1975.

Grab, M., Bauder, A., Ammann, F., Langhammer, L., Hellmann, S., Church, G., Schmid, L., Rabenstein, L., and Maurer, H.: Ice volume estimates of Swiss glaciers using helicopter-borne GPR an example from the Glacier de la Plaine Morte, in: 2018 17th International Conference on Ground Penetrating Radar (GPR), pp. 1–4, IEEE, https://doi.org/10.1109/ICGPR.2018.8441613, 2018.

Gulley, J.: Structural control of englacial conduits in the temperate Matanuska Glacier, Alaska, USA, Journal of Glaciology, 55, 681–690, https://doi.org/10.3189/002214309789470860, 2009.

Gulley, J., Benn, D., Müller, D., and Luckman, A.: A cut-and-closure origin for englacial conduits in uncrevassed regions of polythermal glaciers, Journal of Glaciology, 55, 66–80, https://doi.org/10.3189/002214309788608930, 2009a.

Gulley, J., Benn, D., Screaton, E., and Martin, J.: Mechanisms of englacial conduit formation and their implications for subglacial recharge, Quaternary Science Reviews, 28, 1984–1999, https://doi.org/10.1016/j.quascirev.2009.04.002, 2009b.

Hansen, L. U., Piotrowski, J. A., Benn, D. I., and Sevestre, H.: A cross-validated three-dimensional model of an englacial and subglacial drainage system in a High-Arctic glacier, Journal of Glaciology, pp. 1–13, https://doi.org/10.1017/jog.2020.1, 2020.

Hart, J. K., Rose, K. C., Clayton, A., and Martinez, K.: Englacial and subglacial water flow at Skálafellsjökull, Iceland derived from ground penetrating radar, in situ Glacsweb probe and borehole water level measurements, Earth Surface Processes and Landforms, 40, 2071–2083, https://doi.org/10.1002/esp.3783, 2015.

Hock, R., Iken, L., and Wangler, A.: Tracer experiments and borehole observations in the over-deepening of Aletschgletscher, Switzerland, Annals of Glaciology, 28, 253–260, https://doi.org/10.3189/172756499781821742, 1999.

Hooke, R. L. and Pohjola, V. A.: Hydrology of a segment of a glacier situated in an overdeepening, Storglaciaren, Sweden, Journal of Glaciology, 40, 140–148, 1994.

Huss, M. and Farinotti, D.: Distributed ice thickness and volume of all glaciers around the globe, Journal of Geophysical Research: Earth Surface, 117, 1–10, https://doi.org/10.1029/2012JF002523, 2012.

Iken, A. and Bindschadler, R. A.: Combined measurements of Subglacial Water Pressure and Surface Velocity of Findelengletscher, Switzerland: Conclusions about Drainage System and Sliding Mechanism, Journal of Glaciology, 32, 101–119, https://doi.org/10.3189/S0022143000006936, 1986.

Iken, A., Fabri, K., and Funk, M.: Water storage and subglacial drainage conditions inferred from borehole measurements on Gornergletscher, Valais, Switzerland, Journal of Glaciology, 42, 233–245, 1996.

Irvine-Fynn, T. D. L., Moorman, B. J., Williams, J. L. M., and Walter, F. S. A.: Seasonal changes in ground-penetrating radar signature observed at a polythermal glacier, Bylot Island, Canada, Earth Surface Processes and Landforms, 31, 892–909, https://doi.org/10.1002/esp.1299, http://doi.wiley.com/10.1002/esp.1299, 2006.

King, E. C., Woodward, J., and Smith, A. M.: Seismic evidence for a water-filled canal in deforming till beneath Rutford Ice Stream, West Antarctica, Geophysical Research Letters, 31, 4–7, https://doi.org/10.1029/2004GL020379, 2004.

Langhammer, L., Rabenstein, L., Bauder, A., and Maurer, H.: Ground-penetrating radar antenna orientation effects on temperate mountain glaciers, Geophysics, 82, H15–H24, https://doi.org/10.1190/geo2016-0341.1, 2017.

Lliboutry, L.: Permeability, Brine Content and Temperature of Temperate Ice, Journal of Glaciology, 10, 15–29, https://doi.org/10.1017/S002214300001296X, 1971.

Mercanton, P.: Vermessungen am Rhonegletscher/ Mensuration au glacier du Rhone: 1874-1915., vol. 52, Zürcher & Furrer, 1916.

Moorman, B. J. and Michel, F. a.: Glacial hydrological system characterization using ground-penetrating radar, Hydrological Processes, 14, 2645–2667, https://doi.org/10.1002/1099-1085(20001030)14:15<2645::AID-HYP84>3.0.CO;2-2, 2000.

Murray, T., Stuart, G. W., Gamble, N. H., and Crabtree, M. D.: Englacial water distribution in a temperature glacier from surface and borehole radar velocity analysis, Journal of Glaciology, 46, 389–398, https://doi.org/10.3189/172756500781833188, 2000.

Naegeli, K., Lovell, H., Zemp, M., and Benn, D. I.: Dendritic subglacial drainage systems in cold glaciers formed by cut-and-closure processes, Geografiska Annaler, Series A: Physical Geography, 96, 591–608, https://doi.org/10.1111/geoa.12059, 2014.

Nienow, P., Sharp, M., and Willis, I.: Temporal Switching Between Englacial and Subglacial Drainage Pathways: Dye Tracer Evidence from the Haut Glacier D'arolla, Switzerland, Geografiska Annaler: Series A, Physical Geography, 78, 51–60, https://doi.org/10.1080/04353676.1996.11880451, 1996.

Nienow, P., Sharp, M., and Willis, I.: Seasonal changes in the morphology of the subglacial drainage system, Haut Glacier d'Arolla, Switzerland, Earth Surface Processes and Landforms, 23, 825–843, https://doi.org/10.1002/(SICI)1096-9837(199809)23:9<825::AID-ESP893>3.0.CO;2-2, 1998.

Pettersson, R., Jansson, P., and Holmlund, P.: Cold surface layer thinning on Storglaciären, Sweden, observed by repeated ground penetrating radar surveys, Journal of Geophysical Research: Earth Surface, 108, n/a–n/a, https://doi.org/10.1029/2003JF000024, 2003.

Plewes, L. A. and Hubbard, B.: A review of the use of radio-echo sounding in glaciology, Progress in Physical Geography, 25, 203–236, https://doi.org/10.1177/030913330102500203, 2001.

Reynolds, J. M.: An Introduction to Applied and Environmental Geophysics, John Wiley & Sons, 2011.

Roethlisberger, H.: Seismic Exploration in Cold Regions, 1972.

Röthlisberger, H.: Water Pressure in Intra- and Subglacial Channels, Journal of Glaciology, 11, 177–203, https://doi.org/10.1017/S0022143000022188, 1972.

Russell, B. H.: Introduction to Seismic Inversion Methods, Society of Exploration Geophysicists, https://doi.org/10.1190/1.9781560802303, 1988.

Rutishauser, A., Maurer, H., and Bauder, A.: Helicopter-borne ground-penetrating radar investigations on temperate alpine glaciers: A comparison of different systems and their abilities for bedrock mapping, GEOPHYSICS, 81, WA119–WA129, https://doi.org/10.1190/geo2015-0144.1, 2016.

Sacchi, M. D.: Reweighting strategies in seismic deconvolution, Geophysical Journal International, 129, 651–656, https://doi.org/10.1111/j.1365-246X.1997.tb04500.x, 1997.

Schaap, T., Roach, M. J., Peters, L. E., Cook, S., Kulessa, B., and Schoof, C.: Englacial drainage structures in an East Antarctic outlet glacier, Journal of Glaciology, https://doi.org/10.1017/jog.2019.92, 2019.

Schmelzbach, C. and Huber, E.: Efficient deconvolution of ground-penetrating radar data, IEEE Transactions on Geoscience and Remote Sensing, 53, 5209–5217, https://doi.org/10.1109/TGRS.2015.2419235, 2015.

Schmelzbach, C., Tronicke, J., and Dietrich, P.: High-resolution water content estimation from surface-based ground-penetrating radar reflection data by impedance inversion, Water Resources Research, 48, 1–16, https://doi.org/10.1029/2012WR011955, 2012.

Seaberg, S. Z., Seaberg, J. Z., Hooke, R. L., and Wiberg, D. W.: Character of the Englacial and Subglacial Drainage System in the Lower Part of the Ablation Area of Storglaciären, Sweden, as Revealed by Dye-Trace Studies, Journal of Glaciology, 34, 217–227, https://doi.org/10.3189/S0022143000032263, 1988.

Shreve, R. L.: Movement of Water in Glaciers, Journal of Glaciology, 11, 205–214, https://doi.org/10.3189/S002214300002219X, 1972.

Stuart, G.: Characterization of englacial channels by ground-penetrating radar: An example from austre Brøggerbreen, Svalbard, Journal of Geophysical Research, 108, 2525, https://doi.org/10.1029/2003JB002435, 2003.

Temminghoff, M., Benn, D. I., Gulley, J. D., and Sevestre, H.: Characterization of the englacial and subglacial drainage system in a high Arctic cold glacier by speleological mapping and ground-penetrating radar, Geografiska Annaler, Series A: Physical Geography, 101, 98–117, https://doi.org/10.1080/04353676.2018.1545120, 2019.

Tsutaki, S., Sugiyama, S., Nishimura, D., and Funk, M.: Acceleration and flotation of a glacier terminus during formation of a proglacial lake in Rhonegletscher, Switzerland, Journal of Glaciology, 59, 559–570, https://doi.org/10.3189/2013JoG12J107, 2013.

van der Veen, C. J.: Fracture propagation as means of rapidly transferring surface meltwater to the base of glaciers, Geophysical Research Letters, 34, 1–5, https://doi.org/10.1029/2006GL028385, 2007.

Velis, D. R.: Stochastic sparse-spike deconvolution, Geophysics, 73, R1–R9, https://doi.org/10.1190/1.2790584, 2008.

Warren, C., Giannopoulos, A., and Giannakis, I.: gprMax: Open source software to simulate electromagnetic wave propagation for Ground Penetrating Radar, Computer Physics Communications, 209, 163–170, https://doi.org/10.1016/j.cpc.2016.08.020, http://dx.doi.org/10.1016/j.cpc.2016.08.020, 2016.

Widess, M. B.: How thin is a bed?, Geophysics, 38, 1176–1180, https://doi.org/10.1190/1.1440403, 1973.

Zwally, H. J., Abdalati, W., Herring, T., Larson, K., Saba, J., and Steffen, K.: Surface melt-induced acceleration of Greenland ice-sheet flow, Science, 297, 218–222, https://doi.org/10.1126/science.1072708, 2002.